



universität  
wien

# DISSERTATION

Titel der Dissertation

„Structural and tectonic setting of Zagros fold-and-thrust  
belt, NE Kurdistan“

Verfasser

Daniel Reif, Mag.

angestrebter akademischer Grad

Doktor der Naturwissenschaften (Dr.rer.nat.)

Wien, 2011

Studienkennzahl lt. Studienblatt: A 091 426

Dissertationsgebiet lt. Studienblatt: Erdwissenschaften

Betreuerin / Betreuer: Univ. Prof. Bernhard Grasemann, Mag., Dr.

## Table of Contents

Summary .....	2
Zusammenfassung .....	4
Acknowledgements .....	6
Introduction.....	7
Importance of the study area.....	7
Regional geography and geomorphology.....	7
Geological settings .....	11
Research history .....	13
Aims of the project.....	13
Applied methods.....	14
Synthesis .....	16
References .....	25
Contribution to the published studies.....	27
Appendices (Manuscripts) .....	28
Appendix 1 .....	28
<i>Reif, D., Grasemann, B. &amp; Faber, R. H. (2011) Quantitative structural analysis using remote sensing data Kurdistan, Northeast Iraq. AAPG Journal, 2011</i>	
Appendix 2 .....	45
<i>Reif, D., Frehner, M., &amp; Grasemann, B. (under review) Mechanical versus kinematic shortening reconstructions of the Zagros High Folded Zone (Kurdistan Region of Iraq), Northeast Iraq. Tectonics</i>	
Appendix 3 .....	67
<i>Reif, D., Decker, K., Grasemann, B. and Peresson, H., (under review). Fracture patterns in the Zagros fold-and-thrust belt, Kurdistan Region of Iraq. Tectonophysics Special Issue "Into the deformation history of the folded rocks".</i>	
Curriculum Vitae .....	92

## Summary

The presented PhD thesis investigates in detail the simply folded part of Zagros Fold-and-Thrust Belt north-east of the city of Erbil in the Kurdistan Region of Iraq. The Zagros Mountains extend over 1800 kilometres in NW-SE direction and are bordered by the Central Iranian Plateau in the NE, the Taurus Mountain range in Turkey in the NW, the Oman Fault in the SE, and the Persian Gulf foreland in the SW and are one of the most promising areas for future hydrocarbon discoveries. Although parts of the Zagros have already been thoroughly studied in Iran, comparatively nothing has been published in international scientific journals from Kurdistan Region of Iraq. In this thesis, field work is combined with methods of tectonic geomorphology, remote sensing and numerical modelling. The main aim is to better understand the structural development of the study area. The thesis is divided in three parts, each part resulting in one published scientific article. The scientific articles cover the following topics:

1. Quantitative structural analysis using remote sensing data and comparing them with the field data using a newly developed software tool for interactively mapping and measuring the spatial orientation (dip angle and dip direction) of finite planar geologic structure from digital elevation models.
2. Comparison of mechanical and kinematic balancing for quantifying the amount of shortening in folded, geologic profiles: The cross-sectional fold geometry was constructed using the dip domain method. The stretch required for achieving the pre-folding geometry was estimated using two different models, one with and one without layer-parallel slip. The results obtained from these mechanical, Finite Element Method models were compared with purely kinematic models for balancing cross-sections. The mechanical model with layer-parallel slip resembles more closely the balanced profile than the model without slip.
3. Study of fracture patterns in the simply folded part of the Zagros fold-and-thrust belt, extending the previous studies in the SE (Iranian) part of the Zagros. The study is focused on fracture systems developed in the lesser investigated parts of the NW Zagros. Fracture patterns in the Zagros Mountains demonstrate the reactivation of old and the generation of new fractures during folding and are of importance for understanding the tectonic evolution. The quantitative characterization of the orientation, density and morphology of fractures delivers crucial input parameters for the modelling of hydrocarbon reservoirs.

The first results of the field and remote sensing mapping showed development of the fluvial terraces in the Foothill Zone. It was suggested that investigation of the orientation and age of the river terrace sediments (located on the limbs of the

anticlines in the High Folded Zone) can help to better constrain the rates of folding. This idea resulted in a pilot project comprising further analysis and sampling of 10 outcrops for Optically Stimulated Luminescence (OSL) dating.



## Zusammenfassung

Die vorliegende PhD Arbeit befasst sich im Detail mit einem Teil der einfach gefalteten Zone des Zagros Orogens, nordöstlich der Stadt von Erbil in der irakischen Kurdistan Region. Das Zagros Gebirge erstreckt sich über mehr als 1800 Kilometer in NW-SO Richtung und ist begrenzt von dem Zentral Iranischem Plateau vom NO, dem Taurus Gebirge in der Türkei von NW, der Oman Störung vom SO, Persischem Golf vom SW und ist einer der vielversprechendsten Regionen für künftige Kohlenwasser-Exploration und Förderung im Mittleren Osten. Obwohl gewisse Teile des Zagros-Orogens bereits ausführlich im Iran untersucht wurden, gibt es vergleichsweise wenige wissenschaftliche Studien aus der irakischen Kurdistan Region.

Diese Arbeit kombiniert strukturgeologische Geländekartierung mit Fernerkundungsmethoden, tektonischer Geomorphologie und numerischer Modellierung. Das Hauptziel ist die Schaffung besseren Verständnisses für die strukturelle Entwicklung des Untersuchungsgebietes. Die folgende Studie kann in drei Teile unterteilt werden, die sich anhand der angewandten Methoden unterscheiden. Die entsprechenden Resultate der einzelnen Teile wurden in einschlägigen wissenschaftlichen Fachzeitschriften eingereicht und publiziert. Im Folgenden werden die einzelnen Publikationen separat beschrieben:

1. Anhand von Fernerkundungsdaten und strukturgeologischer Geländedaten wurde eine quantitative Strukturanalyse durchgeführt. Anschließend wurden die Geländedaten mit den Fernerkundungsdaten verglichen und die Unterschiede statistisch ausgewertet. Die Ergebnisse wurden zur Ermittlung des bei der Anwendung von Fernerkundungsdaten entstehenden Fehlers verwendet und diskutiert. Die komplette Bearbeitung der Fernerkundungsdaten wurde mithilfe einer neu entwickelten Software durchgeführt. Diese ermöglicht die interaktive Erfassung und Berechnung der räumlichen Orientierung (Neigungswinkel und Fallrichtungswinkel) von endlichen, planaren, geologischen Strukturen, wie zum Beispiel Störungen oder sedimentären Schichtungen, aus digitalen Geländemodellen.
2. Vergleich mechanischer und kinematischer Bilanzierung zur Quantifizierung der Verkürzung in gefalteten geologischen Profilen: Die Faltungsgeometrie der Profile wurde anhand der *dip-domain* Methode konstruiert. Die für eine Prä-Faltungsgeometrie benötigte Streckung wurde mit zwei unterschiedlichen Modellen (mit oder ohne lagenparalleles Gleiten) bestimmt. Die Ergebnisse der mechanischen, Finiten Element Methode Modellen, wurden mit den Resultaten rein kinematischer Modelle für bilanzierte Profile verglichen. Die Ergebnisse des mechanischen Modells mit lagenparallelem Gleiten ähneln dem bilanzierten Profil eher als dem Modell ohne Gleiten.
3. Das Studium von Störungs- und Kluft-Systemen bezieht sich auf den bisher spärlich untersuchten, nordwestlichen Teil des Zagros Orogens. Die

Ergebnisse zeigen teilweise Ähnlichkeiten mit Resultaten aus dem Iran (südöstliches Zagros Orogen), jedoch mit merklich weniger Versatz und geringerer Störungsdichte als im Iran. Die Klüftung zeigt eine Reaktivierung von älteren Klüften und Abschiebungen durch ein späteres Faltungs- und Kompressions-Regime an. In Kombination dazu kommt es zur Entwicklung neuer Kluft-Systeme. Die quantitative Charakteristik der Orientierung und Morphologie der Kluft-Systeme stellt einen wichtigen Baustein für die Modellierung von Kohlenwasser-Reservoirien dar.

Anhand von den ersten Ergebnissen der Gelände- und Fernerkundungs-Kartierung wurden fluviatile Terrassen in der „Foothill Zone“ identifiziert. Inzwischen zeigte sich, dass die Ermittlung des Alters und Einfallwinkels der Flussterrassen, vorkommend auf den Antiklinalflanken in der „High Folded Zone“ helfen kann, die Faltungs-Raten zu bestimmen. Diese Idee entwickelte sich zu einer Pilot-Studie mit dem Ziel, 10 Aufschlüsse genauer zu untersuchen und mittels Optisch stimulierter Lumineszenz (OSL) zu datieren.

## Acknowledgements

In the first place thanks to my supervisor Bernhard Grasemann for help and support during the studies and also beyond that. My PhD thesis was financed and supported as a part of FA536005 Research Projects (2008-2011) by OMV Exploration & Production Company. I wish to thank all people working at OMV, which were very helpful and inspiring during my internship at OMV in 2007, then during the adventurous fieldwork in Iraq (2008 and 2010) and also giving me the opportunities to attend different scientific conferences as well giving comments, suggestions and reviews concerning my scientific publications and study results. I particularly want to thank my supervisors at OMV, who initiated the project in the first years: Gerhard Milan and Duncan Lockhart. For the further assistance, helpful comments and proof-reading of the published scientific articles during the later phase of the project also Gabor Tari and Herwig Peresson have to be thanked. I also wish to thank Jonathan Church, Mohammad Fallah, Florian Conradi and Utte Sattler for providing available data and accompanying discussions.

Concerning the optically stimulated luminescence (OSL) dating of river terraces, Marcus Fiebig and Johanna Lomax have to be thanked. They advised me during the selection of suitable samples, carried out the OSL-dating and also provided detailed information about sampling and various dating techniques for this particular method.

I want to thank Hugh Rice and Kateřina Schöpfer for proof-reading of all my scientific texts in English and Norbert Irnberger for helping me with the preparation and printing of the posters for all scientific conferences and presentations. Many thanks also to the company Geotest and Palacký University for inviting me to teach block courses in Brno and in Olomouc. For the huge amount of help during the preparation of the final report for the OMV Anja Peckmann and Bernhard Grasemann have to be gratefully acknowledged.

Also I want to thank all the co-authors of papers and presentations published during this project: Robert Faber, Marcel Frehner, Kurt Decker, Herwig Peresson for their help and cooperation. Many thanks to Olivier Lacombe and Stefano Tavani, who invited me to publish one of the papers in the Special Issue of Tectonophysics: "Into the deformation history of the folded rocks".

Last but not least all my colleagues and friends from the University of Vienna have to be thanked: Andreas Beidinger, Christoph Tuitz, Bernhard Bretis, Andras Zamolyi, Alex Rath, Nikolaus Bartl, Benjamin Huet, Alexander Kopecny and Jürgen Scheibz. The professors Hermann Häusler and Franz Kohlbeck (TU Wien) have to be thanked for allowing me to get acquainted with all different geophysical methods in their study area near the Lake Neusiedl in the early weeks of my PhD study.

I deeply appreciate the help and encouragement from my whole family and my girlfriend Marie during all my studies. Thank You!

## Introduction

### Importance of the study area

The Kurdistan Region is in first place very interesting for the oil companies, operating in the Middle East, as oil and gas prospection area. According to Roeder, 2010, the fold-thrust belts contain more than 700 billion barrels of oil equivalent (BBOE) of known hydrocarbon reserves. About 74% (517 of BBOE) are stored in anticlinal traps of the Zagros Fold-And-Thrust Belt. The remaining 26% (183 of BBOE) are spread over more than 30 other fold-and-thrust belts.

Such exploration potential concentrated in a single area is unique (Fig. 1) and was also the reason for receiving support for this work from OMV E&P. Within the frame of the study area, selected by OMV, we had been allowed to concentrate primarily on scientific work.

This region is also very interesting from the scientific point of view. The excellent outcrop quality and (concerning structural geology) very briefly explored area left a lot of geological features with an open structural interpretation. Therefore it offers many possibilities for application of various scientific methods and techniques.

### Regional geography and geomorphology

The Kurdistan Region of Iraq is situated in border areas between three countries and comprises parts of the three governorates of Erbil, Suleimaniah and Duhok. Its area extends over 40 063 square kilometres with population of 3.7 million. It borders Syria to the west, Iran to the east, and Turkey to the north, located where fertile plains meet the Zagros Mountains. It is traversed by the Sirwan River, the Tigris River and its tributaries, the Great Zab and the Little Zab rivers.

Kurdistan is the name of a geographic and cultural region inhabited by the Kurds including originally parts of neighbouring W Iran and S Turkey, but only the Iraqi Kurdistan has gained official recognition as a federal entity today. Our study area (Fig. 2A) is found in the Erbil Governorate, approximately 50 km NE of the ancient capital city of Erbil (also known as Hawler). Kurdistan Region, as a part of Iraq was some time ago too dangerous for oil companies to invest in exploration here because of the unstable political situation and absence of a refinery and/or pipe-line to transport hydrocarbons for further processing. Even when this situation improved, the results of the long on-going fight between the different fractions left most of the areas full of mines and other unexploded ordnance, which is still potentially dangerous for the people working in the field. Due to high erosional rates the mines can possibly move with the sediment, especially during the rain-season and appear on places declared previously as safe.

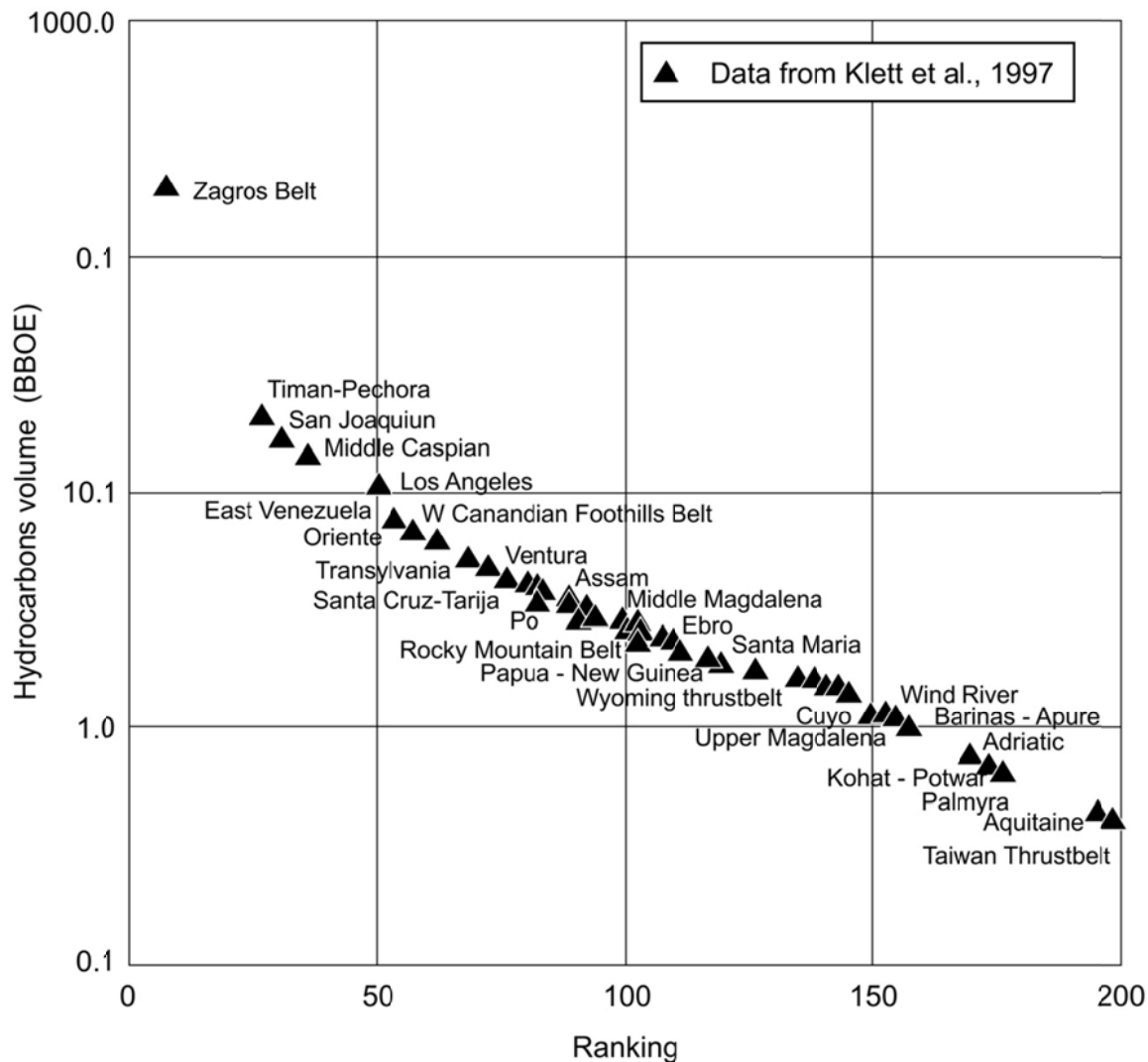


**Fig. 1: The plot showing the leading position of the Zagros Fold-And-Thrust Belt hydrocarbon volume compared to other fold-and-thrust belts hydrocarbon volumes in the world (not all names are shown; Y axis shows HC volume; X-axis shows achieved rank from all fold-and-thrust belts).**

The geomorphology (Fig. 2B) is characterised by significantly flat foreland, which is part of the Mesopotamian Basin in the south. Here the younger, Pliocene to Holocene sediments cover the deeper positioned anticlines. Further to the north of the area the simple folded anticlines of the Zagros Orogeny start to appear on the surface and the mountainous character of the area is more significant. The mountains of the Kurdistan Region have an average height of about 2,400 metres, rising to 3,000–3,300 metres in places. The highest peak, named Hasar Rost and situated in the Erbil Governorate, reaches up to 3607 meters. The highest mountain ridges contain the only forest land in the Region. Missing vegetation cover amplifies the erosional influence of harsh climatic conditions.

The studied region has semi-arid continental climate. It is very hot in the summer and bitterly cold in the winter. In summer, the region falls under the influence of

Mediterranean anticyclones, with dust storms carrying dust into the region, raising daily temperature to a maximum value of more than 45 °C. Kurdistan experiences some of the highest temperatures anywhere in the world. These scorching conditions are often accompanied by a persistent dusty, north-westerly wind, called “Shamal”. In winter, the region is invaded by cyclones from various sources, bringing an appreciable amount of rain and in higher elevations snow into the region. Precipitation rates vary between 700 and 3,000 mm a year (Fig. 2A), increasing from southwest to northeast. The annual averages range from 350mm in the Erbil area to more than 1100mm at Sherwan-Mazen in the high mountains bordering Iran (Aziz, 2003). The rainy season starts in September and usually ends by May. The annual rainfall in Kurdistan Region of Iraq is not much less than annual rainfall in Europe, but compared to the later it is not that well distributed. This causes droughts or rainstorms and flooding (example for the resulting hazards in the study area is the old bridge over the Wadi Bastoor, destroyed during the spring flooding).

All of the above mentioned factors (young mountainous landscape, missing vegetation cover, extreme temperature differences and combination of droughts and rainstorms) cause high erosion rates in the study area, exposing nicely the outcropping formations. This distinctively shows the differences in the erosional resistivity between the various lithologies and forms structures such as the “whale-back” anticlines (Fig. 2B), typical for the Zagros Fold-And-Thrust Belt.

The well-developed drainage network is very significant on the satellite imagery of the area (Fig. 2B). It is particularly evident in the mountainous landscape of the High Folded Zone (Fig. 2A), even though being dry for most of the year. The formation of the river terraces along the Greater Zab River meanders, with diameter up to 3 km, can be observed in the Foothill Zone. The formation of wind-gaps (dry river valleys) and water-gaps (river valleys), cutting through the folded sedimentary successions, was observed, even when the most of drainage network are dry wadis or streams very limited water flow.



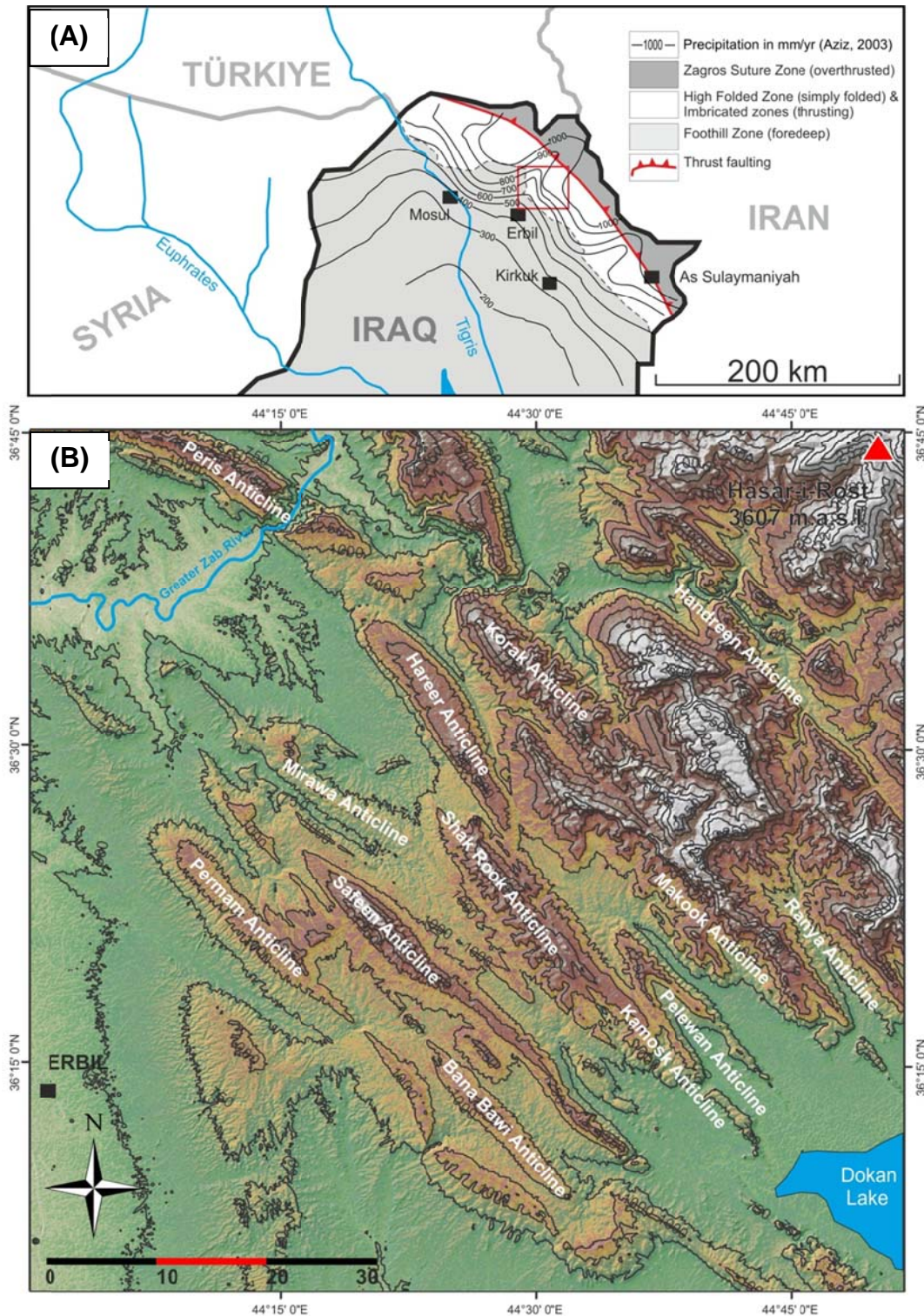


**Fig. 2: (A) Geographic position and precipitation contours (contour interval 100 m) in the study area (red rectangle). (B) Shaded relief with the topographic contours (contour interval 250 m), calculated from ASTER digital elevation model with names of the anticline structures. Note the Hasar-i-Rost, highest peak of the Kurdish Zagros in the upper right corner.**

## Geological settings

The complete Zagros mountain chain is approximately 1800 km long and stretches from Iran, through Kurdistan Region of Iraq to southern Turkey. It is directly linked to the Oman Mountains of the Arabian Peninsula to the southeast. From south to north, Zagros in Kurdistan Region can be divided in four zones (Fig. 2A), significant also by contrasting geomorphology. Firstly, there is the marginal area of the Mesopotamian Basin (continuing further to the south) and its northern edge with simply folded anticlines covered by Neogene sediments, described as the “Foothill Zone”. Further to the north the geomorphology changes distinctively as the typical “whale-back” folds are exposed on the surface, due to the elevated basement underneath (Jassim and Goff, 2006). The simple folded character of this “High Folded Zone” changes to the north and the folding is combined with surface faulting (Fig. 3A), characterising the “Imbricated Zones”. These are bounded further to the north by the Zagros main thrust, behind which the metamorphic rocks of the Zagros Suture Zone appear. These are located already on the border to Turkey and contain the two main ophiolite belts inclosing the Sanandaj-Sirjan Zone, described by Ghasemi and Talbot (2006).

The folding and thrusting of the Zagros Mountains started first in Cretaceous-Paleogene, continued during the Middle Miocene (Letouzey et al., 2003) and in Oligocene to Quaternary (Sinclair, 1997; Vrielynck, 1997). The Cretaceous-Paleogene deformation is thick-skinned and the two later deformation phases (Middle Miocene and Oligocene-Quaternary) are thin-skinned. The thin-skin deformation is better related to the geomorphology of the investigated area, which is characterised by mechanical anisotropy between the different formations. The weaker, less competent formations act as local detachments, decoupling the competent formations from each other on more depth levels.

The oil and gas potential of the Cretaceous rocks is documented by the bitumen-filling of fractures and voids in the formations. For example the Upper Cretaceous Aqra-Bekhme, a dolomitic limestone bears bitumen (tar) in otherwise with calcite filled fractures and voids (Fig. 3B). The calcite crystals in the voids and fractures seems to predate the bitumen-filling, which is bound in the centre of the voids, surrounded by the calcite mineralisation, or between the calcite layers developed in the fractures, respectively. This suggests that the oil migrated in the already existing fractures and voids later (i.e. post-dating the fracturing and to that connected deformation).



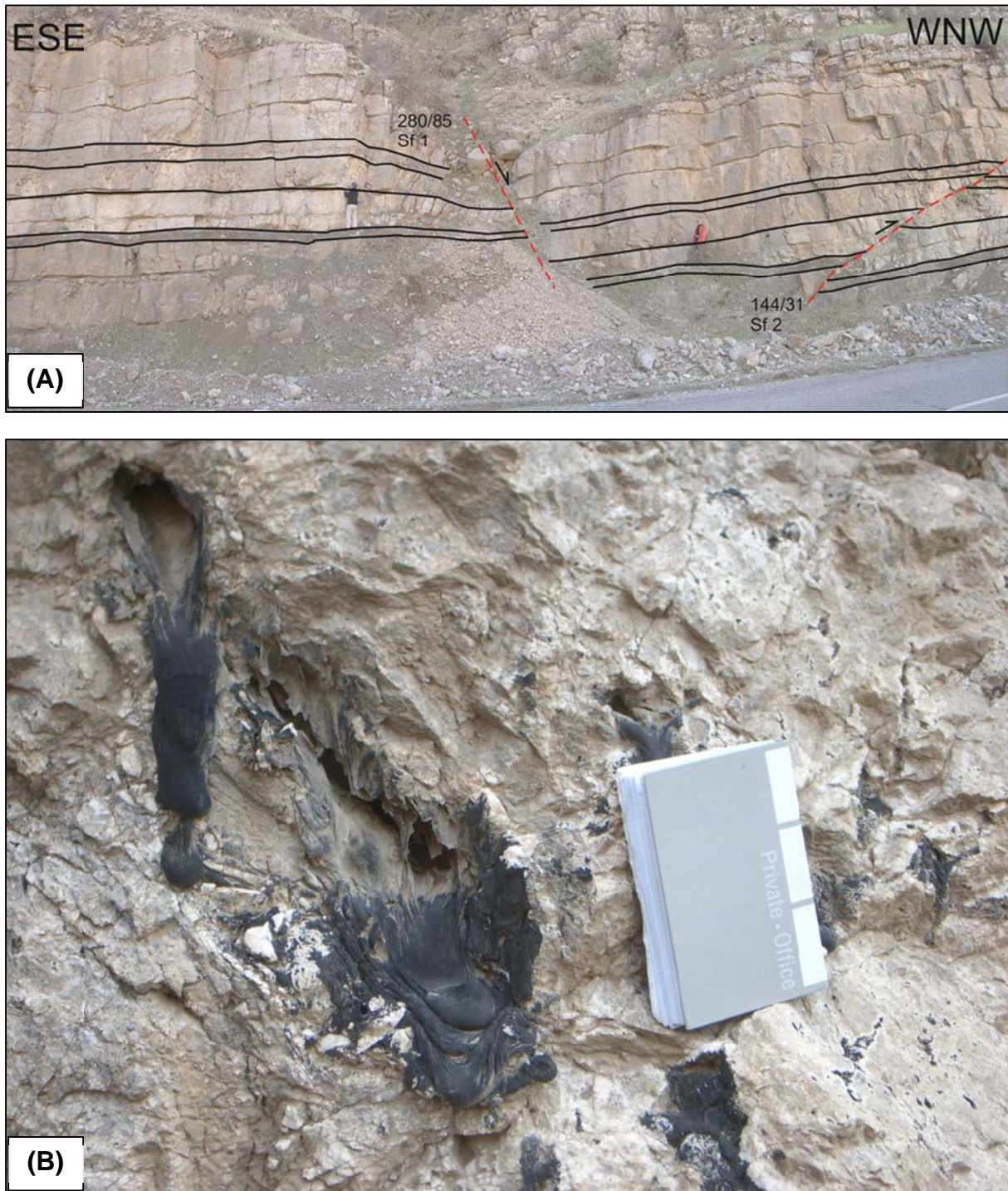


**Fig. 3: (A) Thrust fault Sf2 and normal fault Sf1 (only approximated value) in the well-bedded Qamchuqa Formation. (B) Bitumen-filled voids and fractures in the Aqra-Bekhme Formation, with the calcite crystals on the outer rims and fracture surfaces.**

## Research history

Generally, the Kurdish part of the Zagros Fold-And-Thrust Belt and its structures with the focus on the oil reservoirs, entrapment and sealing formations, were described in many books (e.g. Nemcok et al., 2005, Jassim and Goff, 2006) and studies (e.g. Dunnington, 1958, El Zarka, 1993, Alsharhan and Nairn, 1997).

In comparison to many other, more extensively described orogens, as for example the European Alps or the Iranian part of the Zagros, the Iraqi part of the Zagros High Folded Zone is much less studied in detail. Therefore most of the cited sources are publications focusing on the other parts of the Zagros, the nearest being mainly in the Iranian High Zagros, Dezful and Lorestan regions. The first two articles (Appendices 1 and 2) are more method-focused and therefore the comparison with scientific results from the same locality is not so important. The situation is quite different for the third article (Appendix 3), concerning the pre-, syn- and post-folding developed fracture systems in the study area. Here the results are correlated with scientific articles from Iran, more precisely from Bangestan Anticline (Tavani et al., 2011) and with an older study of the Pila Spi Formation (Numan, 1998) aimed on Ain Safra, Bashiga and Maqlub anticlines in Iraq, approximately 100 km W of our study area.

Concerning the OSL dating of the fluvial sediments in Kurdistan, only the regional study of terrace staircases of the Euphrates River, covering SE Turkey, northern Syria and western Iraq has been published (Demir et al., 2007). No further studies focusing on the age of river terraces of the Greater Zab River and its tributaries have been published from the study area.

## Aims of the project

The main aim of the project was to better constrain the deformation style and evolution of the anticlinal structures in the investigated area, focusing on the use of remote sensing methods as the basis for identification of problematic areas, where field mapping will be necessary. The data, resulting from the use of the remote sensing techniques, consecutive field mapping and extensive background research was summarized in an ArcGIS database, presented to OMV. According to the agreement with OMV, the results of the studies were published in relevant scientific journals.

Additional goal was proposed on the basis of the first results from the outcrop- and remote sensing- mapping, showing the development of tilted fluvial terraces in the Foothill Zone. The planned project comprised sampling and dating of the fluvial sands and mapping of the river terraces. The goal was to calculate the rates of the passive tilting of the river terraces individually and further constrain the folding activity in the investigated area.

Main research questions included:

1. Estimating the accuracy and applicability of remote sensing method using the WinGeol software for mapping finite planar elements (fault planes, sedimentary bedding planes etc.) in inaccessible areas.

2. Evaluation of plausibility of proposed values of shortening, estimated with the use of kinematical restoration methods. The results were compared to two different mechanical models (one with strong mechanical anisotropy between the formations and second, additionally utilising the bedding parallel inter-layer slip) in the investigated area located in the Simply Folded Zone.
3. Fracture mapping, utilising remote sensing methods and outcrop studies, resulting in a deformation model, explaining the evolution of the investigated presently folded, Jurassic to Pliocene sedimentary succession.

### Applied methods

During the study, we applied various methods, both traditional as well as new ones, which are still being improved. The results of the used methods were also correlated with existing data to evaluate the reliability of the used techniques. Following methods for quantitative analysis of the study area were used:

- *Outcrop-based analysis of the fracture systems* (including joints and faults), resulting in definition of five fracture assemblages and with that connected deformations and their relative age, based on cross-cutting and abutting relations between them.
- *Remote sensing measurements of sedimentary bedding dip* using the newly tested and simultaneously developed WinGeol software, with a two-fold goal: To practically apply this method by constructing a balanced cross-section based on these measurements and as well to test and statistically evaluate the results, based on the correlation with outcrop-based measurements.
- *Remote sensing mapping of formation boundaries*, using the ERDAS Imagine, ENVI and WinGeol software, to verify the surface outcrops of formations mapped in the geological map by Sissakian et al., 1997.
- *Dynamic unfolding using Finite Elements Models (FEM)* of the folded sedimentary succession, based on a 55.5 km long, balanced geological cross-section through the studied area. The two developed models were compared with purely kinematic shortening results.
- *Construction of geological cross-sections* with the use of specialized LithoTect software utilizing the classical Dip Domain method (Tearpock and Bischke, 2003). The constructed line- and area-balanced cross-sections were used to estimate the shortening changes through the complete study area, showing significantly rising deformation rates from the southwest to the northeast of the investigated area.

- *Optically Stimulated Luminescence (OSL)* dating was applied to date the river terrace sediments. The determined ages of the river terraces (located on the anticline limbs) were used in combination with simultaneously measured orientations and investigation results of the passively tilted sedimentary layers. The goal was to calculate the sub-recent folding rates during the on-going sedimentation.



## Synthesis

### Published results:

In appendices 1 to 3, the scientific papers, resulting from the investigation of the study area using different approaches are presented.

Appendix 1 concerns the first phase of the project, where scarce structural data from the study area were available and thus concentrates on field-based data acquisition and suitable methods to improve the results of previous field mapping using remote sensing methods. The study also correlates the results with real data from the field to estimate the error of such methods and uses acquired remote sensing measurements based on an ASTER digital elevation model for construction of a simple, 55 km long line- and area-balanced cross-section.

Appendix 2 deals with the use of the finite element models (FEM) for restoration of line- and area-balanced cross-sections. Final shortening is calculated from the resulting stretching value, which is indirectly proportional to it. It correlates also shortening values from different balanced cross-sections in the study area. Two different finite element models were constructed. The first model allows no interlayer slip and utilises so called “welded layers”. This results in unrealistically high extension necessary for the restoration of the layers in the undeformed state. The second model, where thin incompetent layers are introduced on the boundaries between competent units allows a bedding-parallel slip and produces very realistic results. This shows how important this mechanism is during the deformation of the Zagros Orogeny.

Appendix 3 summarizes the results of the previous two scientific papers adding additional information resulting mainly from the field mapping of fracture systems developed during the different tectonic regimes which deformed the investigated formations. Three pervasive and two less developed fracture systems are defined, first one connected with the extensional regime, the later with the compressional regime predating the folding. The next comprises the main folding-related fractures, followed by E-W extensional deformation and finally N to NE directed thrusting of the sedimentary succession, connected with the recent compressional regime. The relative age of the main mapped fracture systems was determined, based on cross-cutting and abutting relations found in the formations with known age.

Unpublished results:

**Use of IRSL/OSL methods for the age determination of the fluvial sediments, tilted during the simple folding, Kurdistan Region of Iraq**

(Preliminary report)

D. Reif <sup>a</sup>, J., Lomax <sup>a,b</sup>, M. Fiebig <sup>b</sup>, B. Grasemann <sup>a</sup>

<sup>a)</sup> *Department of Geodynamics and Sedimentology, University of Vienna, Althanstrasse 14, 1090 Vienna, Austria*

<sup>b)</sup> *Institute of Applied Geology, , University of Natural Resources and Life Sciences, Peter Jordan-Strasse 70, 1190 Vienna, Austria*

## **1. Introduction**

This preliminary report summarizes the results of the field sampling and laboratory measurements of the luminescence age of the Quaternary and Tertiary sand lenses in fluvial sediments of the Greater Zab River and its tributaries, NW of the city of Erbil. The luminescence age measurements were provided in cooperation with the University of Natural Resources and Life Sciences, Vienna. With the use of optically stimulated luminescence (OSL) dating the last time exposition to the daylight and through this the last re-deposition of the sediment can be determined typically from 300 to 100,000 years BP. Ages can be obtained outside this range, but they should be regarded with caution. The accuracy obtainable under optimum circumstances is about 5% (Aitken, 1998).

The long folds are formed from Mesozoic carbonates (limestones, dolomites), giving way in the foothills to the sediments as young as Pleistocene. The Pleistocene and Pliocene sediments of the Bakhtiary Formation, consisting mainly of interlayering sandstone, claystone, siltstone and conglomerate can reveal the deformation rates in the convergent setting of this part of Zagros simply folded belt during their sedimentation. These Upper Tertiary growth strata are too old to be dated using this method, but the younger quaternary river terraces, consisting of conglomerate with lenses of sandstone and siltstone, can be dated using OSL (optically stimulated luminescence) methods. As far as known the last glaciation period in Kurdistan was during the Pleistocene. The rivers contain Pleistocene glacio-fluvial gravels with thickness approximately 30 m in terraces reaching up to 60 m above the present level of the riverbed. According to the remote sensing data there is minimum of three localities, where the formations are exposed and accessible: On the NW part of the Safeen Anticline, S of the Peris Anticline and SE of the Bradost Anticline (Fig. 4). The rates of recent movement in this part of Zagros are varying between 5-15 mm/yr with minimal change since the Cretaceous. The results together with field studies of the river terraces can lead to conclusions about the deformation rates during the simple folding of the Triassic to Tertiary Zagros sedimentary formations in the study area.

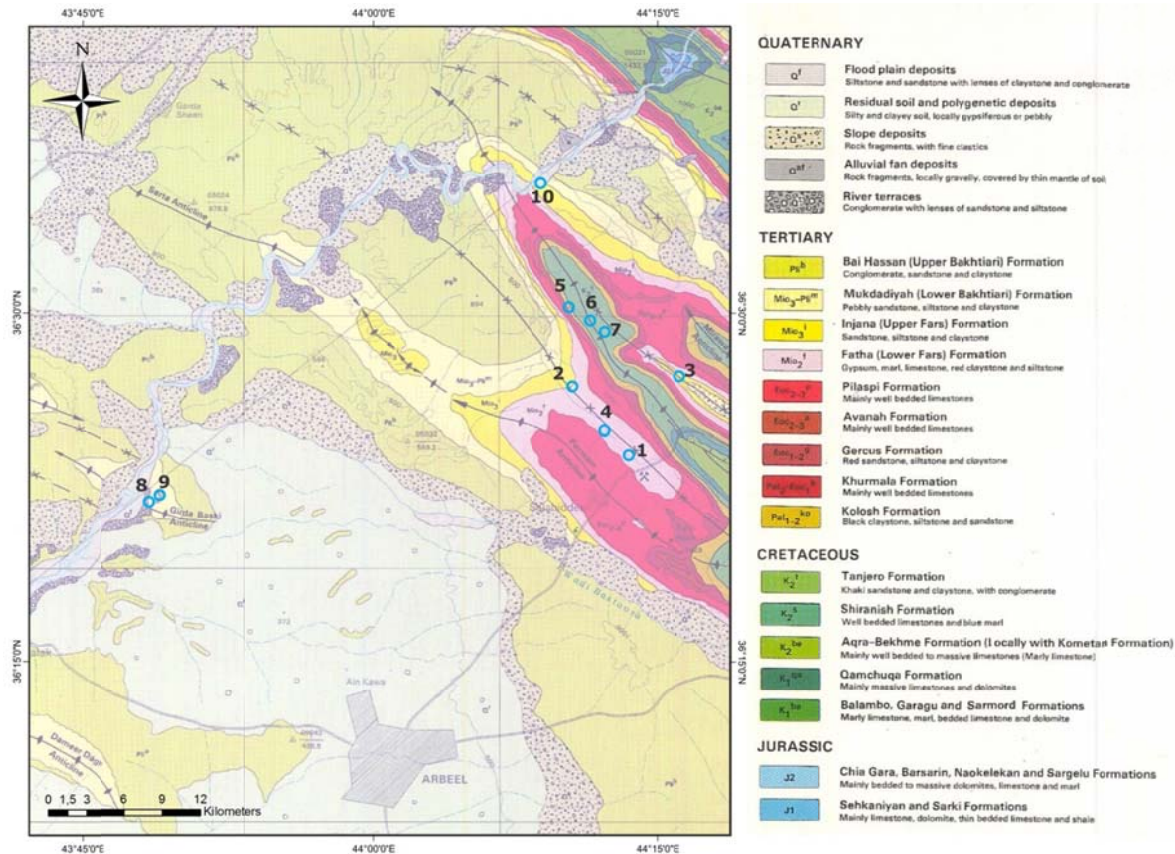


Fig. 4: Position of the analysed and sampled localities on a geological map (redrawn from Sissakian et al., 1997).

## 2. Field studies

Folding in the area started in the Pliocene (possibly Upper Pliocene). The Tigris River and its tributary Greater Zab River incised into the area. A deeper and faster rate of incision was probably enhanced by active uplift and higher precipitation during the climatic fluctuations of the Pleistocene. The softer parts of the lithologic cycles were progressively exposed from the core of anticlines towards the flanks and plunge areas. An intricate dendritic drainage pattern was developed which eroded the softer sequences laterally due to its inability to cut through the underlying harder lithologies. In the field we selected 10 locations mainly on river terraces or in road-cuts, where we considered the sediments to be of fluvial origin. The sampled locations were photographed and described and the dip direction and dip angle of the river terraces were measured or approximated (Tab. 1). Two samples per each outcrop were taken. One sample for the OSL dating using a steel cylinder that was forced in the sediment and covered to prevent daylight exposition of the sample and second sample of the surrounding sediment for the gamma spectrometry to measure the environmental dose rate. For all samples the depth of burial below the landform, latitude, longitude as well as elevation were recorded to calculate cosmic dose rate. Finally not all of the samples were suitable for measurements because of too large grain size of the surrounding sediment.

Date	Number	UTM X (m)	UTM Y (m)	Elevation (m)	Dip direction (°)	Dip (°)	Description	Sample
22042010	1	4028856	430345	751,5	320	4	N-Permam	DR1
22042010	4	4039230	428009	609	325	4	N-Safeen	DR2
22042010	5	4035851	433782	693	176	3	S-Mirawa	DR3
23042010	1	4032154	428006	687,6	181	3	S-Safeen	DR4
23042010	2	4040393	426141	554,04	225	2	S-Safeen	DR5
23042010	3	4039069	428111	598,19	30	2	N-Safeen	DR6
23042010	4	4038514	428852	606	53	3	N-Safeen	DR7
24042010	1	4027119	392427	311,17	338	1	N-Girda Baski	DR8
24042010	2	4027848	392638	302,91	292	1	N-Girda Baski	DR9
24042010	4	4027848	392638	407,7	353	3	N-Safeen	no sample
24042010	5	4053467	426816	391,67	357	2	N-Safeen	DR10

**Tab. 1: The localisation and measured orientation of all river terrace outcrops. No sample was taken on outcrop with date 24042010 no.4 because of extensive cementation and missing sand lenses in the river terrace conglomerate.**

### 3. Laboratory methods

The optical dating method relies on the assumption that the mineral grains were sufficiently exposed to sunlight, which is sure in the case of the studied fluvial sediments. All sediments and soils contain trace amounts of radioactive isotopes including uranium, thorium, rubidium and potassium. These slowly decay over time and the ionizing radiation they produce is absorbed by other constituents of the soil sediments such as quartz and feldspar. The resulting radiation damage within these minerals remains as structurally unstable electron traps within the mineral grains. Stimulating samples using blue, green or infrared light causes a luminescence signal to be emitted as the stored unstable electron energy is released, the intensity of which varies depending on the amount of radiation absorbed during burial. The radiation damage accumulates at a rate over time determined by the amount of radioactive elements in the sample. Exposure to sunlight resets the luminescence signal and so the time period since the soil was buried can be calculated. The age is calculated as follows:

$$\text{Luminescence age} = D_e \text{ (total absorbed radiation dose)} / D_0 \text{ (radiation dose rate)} \quad (1)$$

The radiation dose rate is calculated from measurements of the radioactive elements ( $^{232}\text{Th}$ ,  $^{238}\text{U}$ ,  $^{235}\text{U}$  and their decay products  $^{40}\text{K}$  and  $^{87}\text{Rb}$ ) within the sample and its surroundings and the radiation dose rate from cosmic rays, which can be calculated according to the geographical position and elevation of the sampled locality (Prescott und Hutton 1994). The dose rate is usually in the range 0.5 - 5 grays/1000 years. The total absorbed radiation dose is determined by exciting quartz or feldspar extracted



from the sample with light and measuring the light emitted as a result. The photons of the emitted light must have higher energies than the excitation photons in order to avoid measurement of ordinary photoluminescence. A sample in which the mineral grains have all been exposed to at least a few seconds of daylight can be said to be of zero age; when excited it will not emit any such photons. The older the sample is, the more light it emits.

Sample	Mineral	Method	D <sub>e</sub> (Gy)	n	D <sub>0</sub> (Gy/ka)	Depth (m)	Water (%)	Age (ka)
DR1	Feldspar	IRSL	? (only approximate result)	3		1.6	8 ± 5	Holocene
DR3	Feldspar	IRSL	267 ± 40	10	2.71 ± 0.21	9.1	8 ± 5	97 ± 16
DR8	Feldspar	post-IR-IRSL	99 ± 9	4	1.89 ± 0.16	4.5	8 ± 5	52 ± 6
DR8	Quartz	OSL	59 ± 5	15	1.30 ± 0.08	4.5	8 ± 5	45.4 ± 4.7
DR9	Feldspar	post-IR-IRSL	78 ± 5	4	1.81 ± 0.15	4.9	8 ± 5	47.6 ± 4.7
DR10	Feldspar	IRSL	? (extremely badly bleached)	16	2.39 ± 0.19	4.7	8 ± 5	Lower Holocene ?

**Tab. 2: Measured luminescence ages of selected samples, showing the used method. The samples DR1 and DR10 (results denoted with a question-mark) were too young to provide exact luminescence age values.**

#### Explanation of the abbreviations

IRSL (Feldspar): infra-red stimulated luminescence of the feldspar coarse grain fraction (100-200 µm). The D<sub>e</sub> was determined with the use of Single-Aliquot-Regenerative-Dose-Protocols on an aliquot part of the sample (Wallinga et al. 2000). The age, determined by this protocol is often underrated. The phenomenon responsible for this underrated is called “Fading”. The underrated can reach up to 30%.

Post-IR-IRSL (Feldspar): The D<sub>e</sub> is calculated according to the signal, received during “conventional” IR-Stimulation at 50°C (Buylaert et al. 2009). This second stimulation followed at 225°C, according to the hypothesis that the signal will be less influenced by the „fading“. With that is possible to remove or significantly decrease the effect of the underrated. Admittedly is this protocol relatively new and still not sufficiently tested. It is probably not applicable on very young or very badly bleached samples.

OSL (Quartz): Optically Stimulated Luminescence used on the quartz coarse grain fraction (100-200 µm). The D<sub>e</sub> was determined from a small aliquot part of the sample

with use of the SAR-Protocol (Murray und Wintle 2000). The dating of quartz is usually more exact than the feldspar dating. But in some environments are the quartz luminescence signals so weak, that the dating of feldspar fraction is the only applicable method.

$D_0$ : It is the Radiation dose rate based on the radionuclide concentrations measured with the use of the laboratory gamma spectrometry.

#### **4. Reliability of the luminescence age measurements**

The luminescence age values summarized in the Tab. 2 are to be taken as preliminary results.

Sample DR1 (Fig. 5) was only approximately measured, but shows already very young age, probably Holocene.

In the sample DR3 (Fig. 6) the feldspar fraction was measured using conventional IRSL-SAR-Protocol. The dating of the quartz fraction is problematic, most probably because of the age reaching the upper limit of the measurable range. The scatter of the single  $D_e$ -values ( $n=10$ ) with 39% standard deviation seems to be very high. This could be a sign of insufficient bleaching of the sample and could cause age overrating. If the “fading” is causing this problem was not yet tested. For a reliable result it is necessary to do another “fading-test” using the post-IR-IRSL protocol. Until then the luminescence age of the sample should be used with caution.

Sample DR8 (Fig. 7) was dated using the quartz and feldspar fraction (post-IR-IRSL). Both ages are matching in the range of their errors. But both ages are as relatively unreliable. The reason for this is that the quartz signal shows unwanted characteristics (too slow extinction, low signal intensity and partial contamination with feldspar). In the case of the post-IR-IRSL-ages only 4 sub-samples were measured and further measurements are necessary.

From sample DR9 (Fig. 8) were till now also only 4 sub-samples measured, which is theoretically not sufficient. But the scatter of the measurements was very low so this result can be taken as relatively reliable, nevertheless also here further measurements from the quartz fraction should be carried out as well.

Sample DR10 (Fig. 9) was measured using the conventional IRSL-Protocol. The results show very strong scatter, probably caused by insufficient bleaching of the sample. A reliable result is impossible to measure. It is possible, that the quartz fraction dating will provide further information on the age of the sample. A Upper Holocene age will be a probable result.

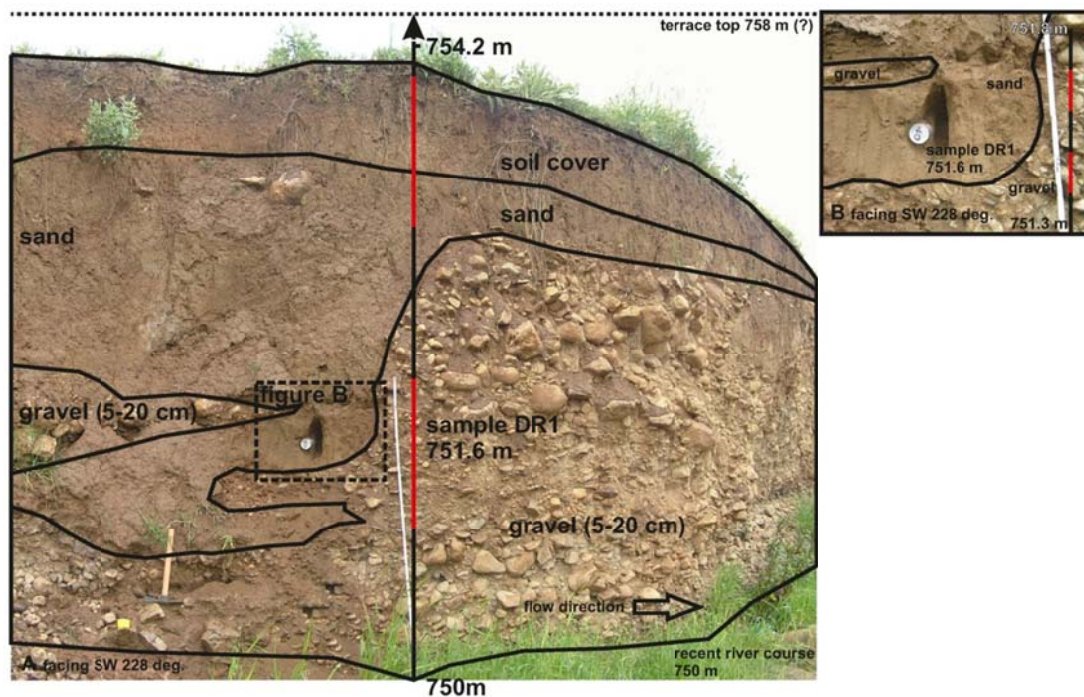


Fig. 5: Outcrop DR1, with only approximate result - Holocene age (IRSL feldspar dating).

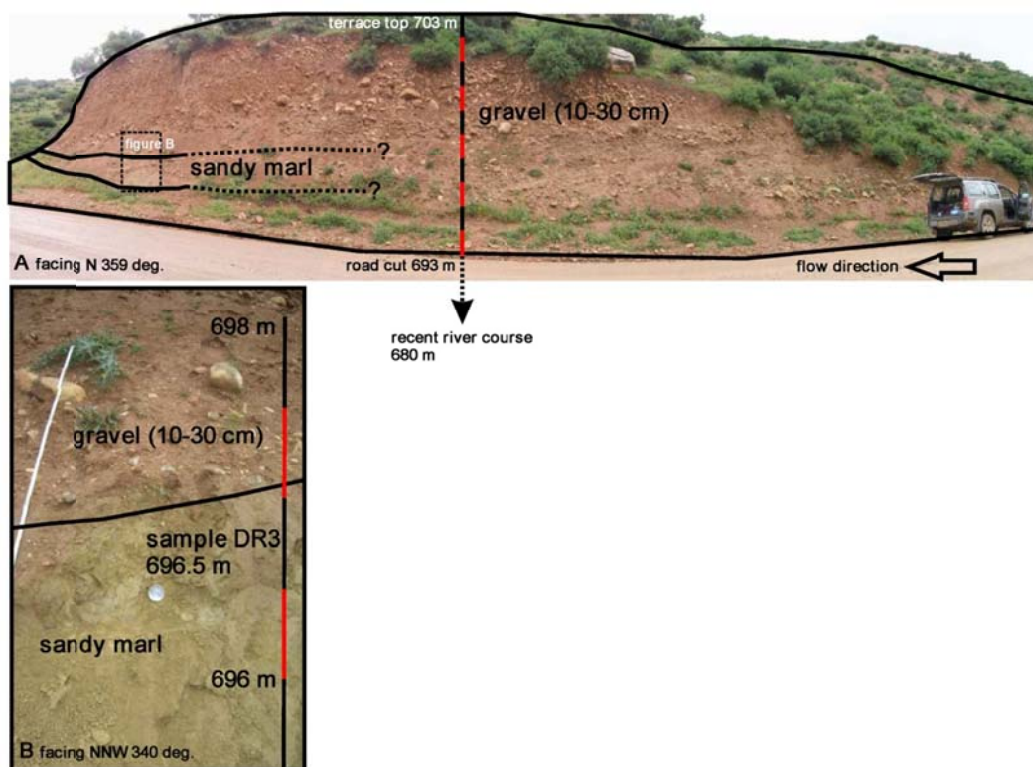


Fig. 6: Outcrop DR3, with resulting age  $97 \pm 16$  ka (thousand years), IRSL feldspar dating.



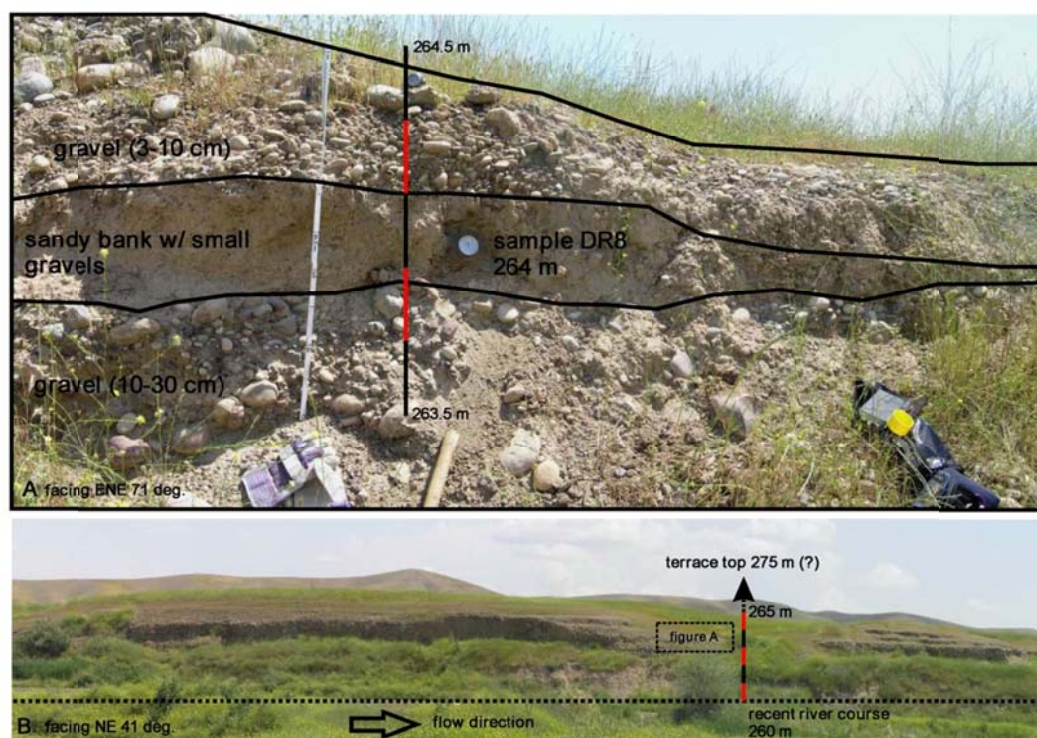


Fig. 7: Outcrop DR8, with resulting age  $52 \pm 6$  ka (post-IR-IRSL feldspar dating) and  $45.4 \pm 4.7$  ka (OSL quartz dating).

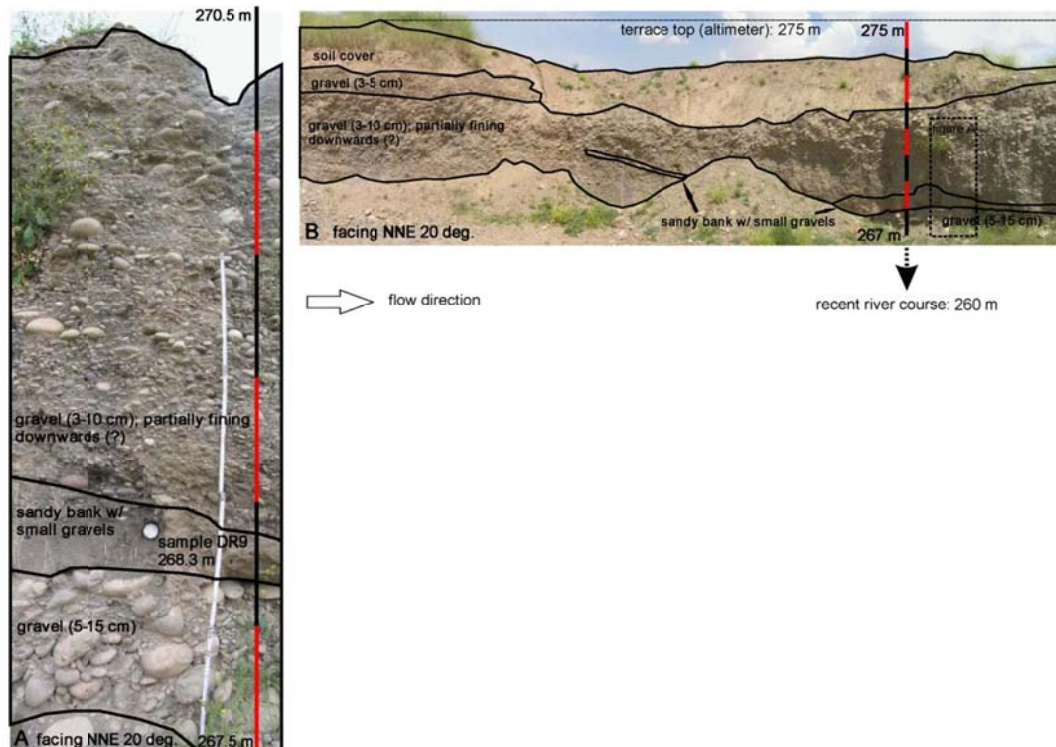


Fig. 8: Outcrop DR9, with resulting age  $47.6 \pm 4.7$  ka (post-IR-IRSL feldspar dating).



Fig. 9: (A) Outcrop of the river terrace located 100 m SE from the outcrop DR10. (B, C) Outcrop DR10, with badly bleached sample, the estimated age is Young Holocene,  $8 \pm 5$  ka (IRSL feldspar dating).

## 5. Preliminary results

We conclude that the results prove the application of the IRSL/ OSL quartz and feldspar dating in the sediments of the tributaries of Greater Zab River possible but difficult. The sampled river terraces show generally increasing dip on the higher, older terraces than on the lower and younger ones. This can be explained by rotation of the sedimentary bedding orientation during the folding. Because of the low number of suitable outcrops (badly sorted quartz or only carbonate sediments, no sand lenses or layers, extensive cementation of the sediment) in the study area, which made continuous sampling along more river terraces impossible, insufficient data for exact estimation of the folding rates were acquired. It is recommendable to repeat the sampling in the SW of the study area along the Great Zab River with more samples situated along a cross-section over the different river terraces to provide reliable results. Suitable targets for dating in the Foothill Zone are Girda Baski, Sarta and Dammer Dagh Anticlines and in the High Folded Zone the Mirawa Anticline. From the data it can be roughly approximated that the change in the dip angle of the river terraces situated on the limbs of the anticlines in the study area during the last 40 000 years is about 2-3 degrees. The number of river terraces identified during the pilot study on the tributaries of the Greater Zab River is three.

---

## References

- Aitken, M.J., 1998. An introduction to optical dating: The dating of Quaternary sediments by the use of photon-stimulated luminescence. Oxford, University Press, 267 pp.
- Alsharhan, A. S. and Nairn, A. E. M., 1997. Sedimentary basins and Petroleum Geology of the Middle East. Amsterdam, Elsevier.
- Aziz, M., 2003. Agrometeorology in Kurdistan of Iraq: a contemporary history: <http://www.agrometeorology.org/topics/history-of-agrometeorology/agrometeorology-in-kurdistan-of-iraq-a-contemporary-history> (accessed November 20, 2011).
- Banerjee, S., and S. Mitra, 2004. Remote surface mapping using orthophotos and geologic maps draped over digital elevation models: Application to the Sheep Mountain anticline, Wyoming. AAPG Bulletin, v. 88, 1227–1237, doi:10.1306/02170403091.
- Buylaert, J. P., Murray, A. S., Thomsen, K. J. and Jain, M., 2009. Testing the potential of an elevated temperature IRSL signal from K-feldspar. Radiation Measurements 44, 560-565.
- Demir, T., Westaway, R., Bridgland, D. R., Seyrek, A., 2007. Terrace staircases of the River Euphrates in southeast Turkey, northern Syria and western Iraq: evidence for regional surface uplift. Quaternary Science Reviews Volume 26, Issues 22-24 November 2007, 2844-2863, doi:10.1016/j.physletb.2003.10.071.
- Dunnington, H.V., 1958. Generation, migration, accumulation and dissipation of oil in Northern Iraq. In Habitat of Oil: a Symposium, Tulsa, OK. American Association of Petroleum Geologists, ed. G. L. Weeks, 1194-251.
- El Zarka, M. H., 1993. Ain Zalah field – Iraq Zagros Folded Zone, northern Iraq. In Structural Traps, vol. VIII, ed. N. H. Foster and E. A. Beaumont. American Association of Petroleum Geologists Atlas of Oil and Gas Fields, 56-57.
- Ghasemi, A. and Talbot, C.J., 2006. A new tectonic scenario for the Sanandaj–Sirjan Zone (Iran). Journal of Asian Earth Sciences 26, 683–693.
- Klett, T. R., Ahlbrandt, T. S., Schmoker, J. W. and Dolton, G. L., 1997, Ranking of the world's oil and gas provinces by known petroleum volumes. US Geological Survey Open file report, 97-463.
- Letouzey, J., Sherkati, S., Motiei, H., 2003. Salt tectonics and compressive structures in the Central Zagros fold and thrust belt (Iran). AAPG Annual Meeting, Salt Lake City, Utah, Official program, Vol. 12, Tulsa, OK: American Association of Petroleum Geologists, A103.
- Mobasher, K. and Babaie, A., H., 2007, Kinematic significance of fold- and fault-related fracture systems in the Zagros Mountains, southern Iran, Tectonophysics Volume 451, Issues 1-4, 28 April 2008, 156-169, doi:10.1016/j.tecto.2007.11.060.

Murray, A.S., Wintle, A.G. (2000). Luminescence dating of quartz using an improved single-aliquot regenerative-dose protocol. *Radiation Measurements*, 32, 57-73.

Nemčok, M., Schamel, S. and Gayer, R., 2005. Thrust-belts. Structural Architecture, Thermal Regimes, and Petroleum Systems. Cambridge University Press, Cambridge, 554 p.

Prescott, J.R., Hutton, J.T., 1994. Cosmic ray contributions to dose rates for luminescence and ESR dating: large depth and long-term time variations. *Radiation Measurements* 23, 497-500.

Roeder, D., 2010. Fold-thrust belts at peak oil, In: Geoffey, G. P., Craig, J., Needham, T. & Scott, R., 2010, Hydrocarbons in contractional belts. Geological Society, London, Special Publications, 348, 7-31.

Sinclair, H.D. (1997) Tectonostratigraphic model for under-filled peripheral Foreland Basins: an Alpine perspective. *Geol.Soc. Am. Bull.*, 109, 324-346.

Tearpock, D. J. and Bischke, R. E., 2003. Applied subsurface geological mapping. New Jersey, Prentice Hall, 822 p.

Vrielynck, B., Odin, G.S., Dercourt, J., 1997. Miocene palaeogeography of the Tethys Ocean: potential global correlations in the mediterranean. In: Montanari, A., Odin, G.S., Coccioni, R. (Eds.), *Miocene Stratigraphy: An Integrated Approach*. Elsevier, Amsterdam, 157–165.

Wallinga, J., Murray, A.S., Wintle, A.G., 2000. The single-aliquot regenerative-dose (SAR) protocol applied to coarse-grain feldspar. *Radiation Measurements* 32, 529-533.



## Contribution to the published studies

### Study I (App. 1)

#### **Quantitative structural analysis using remote sensing data Kurdistan, Northeast Iraq.**

**Reif, D., Grasemann, B. & Faber, R. H.**

*Published in AAPG Journal, 2011*

Faber, R. H.	20%	Software concept and development, data preparation
Grasemann, B.	20%	Concept, discussion, manuscript preparation
Reif, D.	60%	Concept, software testing, data analysis and results interpretation, discussion, manuscript preparation

### Study II (App. 2)

#### **Mechanical versus kinematic shortening reconstructions of the Zagros High Folded Zone (Kurdistan Region of Iraq), Northeast Iraq.**

**Reif, D., Frehner, M., & Grasemann, B.**

*Submitted to Tectonics Journal*

Frehner, M.	40%	Concept, model development, modeling, discussion, manuscript preparation
Grasemann, B.	10%	Concept, manuscript preparation
Reif, D.	50%	Concept, data preparation, field geology interpretation and construction of balanced cross-sections, discussion, manuscript preparation

### Study III (App. 3)

#### **Fracture patterns in the Zagros fold-and-thrust belt, Kurdistan Region of Iraq.**

**Reif, D., Decker, K., Grasemann, B. and Peresson, H.**

*Submitted to the special issue of Tectonophysics: "Into the deformation history of the folded rocks"*

Decker, K.	25%	Concept, results evaluation, manuscript preparation
Grasemann, B.	10%	Concept, manuscript preparation
Peresson, H.	5%	Manuscript preparation
Reif, D.	60%	Concept, field mapping, data analysis and results interpretation, discussion, manuscript preparation,



## Appendices (Manuscripts)

### Appendix 1

---

***Reif, D., Grasemann, B. & Faber, R. H. (2011) Quantitative structural analysis using remote sensing data Kurdistan, Northeast Iraq. AAPG Journal, 2011***

# Quantitative structural analysis using remote sensing data: Kurdistan, northeast Iraq

**Daniel Reif, Bernhard Grasemann, and  
Robert H. Faber**

## ABSTRACT

The use of remote sensing data increases the efficiency of field mapping, especially in areas with difficult access or where geologic fieldwork is expensive or hazardous. This study presents a newly developed software tool for interactively mapping and measuring the spatial orientation (i.e., dip angle and dip direction) of finite planar geologic structure from digital elevation models (DEMs). The orientations of planar data (e.g., sedimentary bedding or fault planes) are derived by approximating a virtual plane to the intersection of the planar feature with the DEM topography. To increase the informative value of the DEM, satellite images can be draped onto the topographic data set. The software tool was tested in the Zagros fold and thrust belt, northeast of Erbil (Kurdistan, northeast Iraq), where the stratigraphy has been deformed into sub-cylindrical fold trains. Computed orientations have been compared with actual dip angles and directions measured in the field. Under favorable conditions (moderately dipping planes, strong competence contrast between stratigraphic boundaries, intersection with a rugged topography, low vegetation), statistical comparison of computed data with the field measurements demonstrates that the spatial data set can be reproduced from the DEM within an average error of approximately 10°. The strength of the method is demonstrated by integrating field data with computed values from inaccessible areas, resulting in a reasonably well-constrained balanced geologic cross section.

## AUTHORS

**DANIEL REIF** ~ *Department of Geodynamics and Sedimentology, University of Vienna, Althanstrasse 14, 1090 Vienna, Austria; daniel.reif@univie.ac.at*

Daniel Reif received his M.S. degree from the University of Vienna in 2008, studying neotectonics and hydrogeology, focusing his work on the Danube River Basin on the Slovakia-Austria border. Recently, he has been working on his Ph.D., dealing with tectonic geomorphology of the Zagros fold and thrust belt, northeast of Erbil (Iraq). The study focuses on a 3-D structural model and on the growth history of an antiform-synform fold-train integrating remote sensing techniques and structural field data.

**BERNHARD GASEMANN** ~ *Department of Geodynamics and Sedimentology, University of Vienna, Althanstrasse 14, 1090 Vienna, Austria; bernhard.grasemann@univie.ac.at*

Bernhard Grasemann received his Ph.D. in geology from the University of Vienna. He studied in several international projects the geodynamic evolution and the active tectonics of the Himalayas. Since 2007, he has been a professor in geodynamics and structural geology at the University of Vienna. His scientific interests cover the evolution of mountain belts, metamorphic core complex formation, and the quantification of structural processes at various scales.

**ROBERT H. FABER** ~ *TerraMath, SPARKS Commercial B No. 23, Jl. Raya Kelapa Dua, Gading Serpong, 15310 Serpong-Tangerang, Banten, Indonesia; robert.faber@terramath.com*

Robert Faber received his magister degree in geology (2000) and doctorate in geology (2002) both from Vienna University, Austria. In 2003, he founded the company TerraMath. Current projects include three-dimensional modeling and interpolation, geothermal simulations, and remote sensing (all in combination with software development). His interests comprise the numerical simulation of geologic processes, remote sensing in combination with structural geology, software development, and applied mathematics.

Copyright ©2011. The American Association of Petroleum Geologists. All rights reserved.

Manuscript received June 30, 2010; provisional acceptance July 28, 2010; revised manuscript received September 13, 2010; final acceptance November 15, 2010.

DOI:10.1306/11151010112

## ACKNOWLEDGEMENTS

We thank OMV Austria, Exploration and Production Company, for support and ideas, especially Gerhard Milan and Duncan Lockhart as well as Dana Mawlood and Azad Ibrahim for organization, logistics, and security. Bernhard Bretis and Nikolaus Bartl are thanked for their cooperation during fieldwork in Kurdistan. Furthermore, we thank M. Snidero and his colleagues from the University of Barcelona for discussions about remote sensing and H. K. A. Khamal, from the Sulaimaniya University in Iraq, for supplying us with the available local geologic publications. We thank the AAPG reviewers Garry L. Prost and Sandro Serra for their helpful reviews on this manuscript. The AAPG Editor thanks the following reviewers for their work on this paper: Gary L. Prost and Sandro Serra.

## INTRODUCTION

Data derived by remote sensing techniques can significantly increase the efficiency of field mapping, especially in areas with difficult access, and represent a low-cost complement to geologic fieldwork (Rencz and Ryerson, 1999). For investigating large-scale geologic structures that control landforms, geologists traditionally used stereoscopic aerial photographs to collect qualitative three-dimensional (3-D) information. Quantitative measurements, especially the spatial orientation (dip direction and dip angle) of features such as bedding or fault planes, can be derived from stereoscopic aerial photographs by measuring the relative parallax (i.e., the difference of the location of a point viewed from two different locations) of a 3-D structure (Colwell, 1955; Tator, 1960; Kraus, 2007). Spatial orientations can be determined from best fit planes to (at least) three or more intersection points between a planar feature and the topography. Computational methods can increase the efficiency of this time-consuming method by digitizing the edges of such a feature in stereoscopic pairs of aerial photographs (Bilotti et al., 2000).

With the increasing quality and resolution of digital elevation models (DEMs) and with the enormous advantage of the almost global coverage and free availability of such data, mapping of 3-D information from true-to-scale 3-D images provides an efficient and accurate alternative to stereoscopic mapping using aerial photographs and satellite images (Banerjee and Mitra, 2004; Snidero et al., 2009). Recently, it has been demonstrated that the integration of regional to outcrop digital data can be used to visualize 3-D multiscale structural geologic models (Bernardin et al., 2006; Alfarhan et al., 2008; Jones et al., 2009).

Following these ideas, we present here a practical application of a newly developed add-on tool (PlaneTrace) for the software WinGeol. This allows interactive mapping, visualization, and calculation of the spatial orientations of planar surfaces from DEMs. The strength of this tool is that the geologic feature is traced by a virtual transparent plane, which allows visual approximation of the planar structure. The accuracy of the PlaneTrace tool has been tested in the Zagros fold and thrust belt (Kurdistan, northeast Iraq) by comparing computed bedding orientation with field data.

## REGIONAL GEOLOGY OF THE STUDY AREA

The Zagros Mountains extend for 1800 km between the central Iran plateau in the north, the Taurus in Turkey to the northwest,



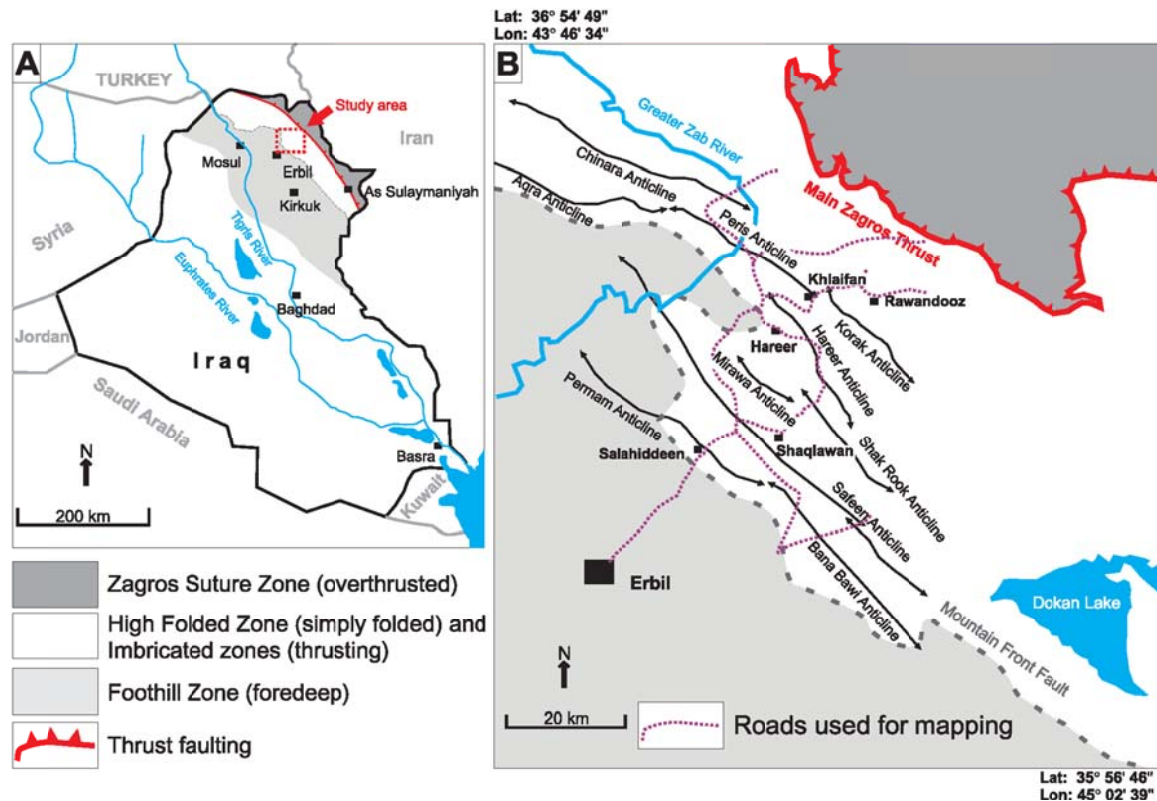


**Figure 1.** (A) Map of Iraq and the location of the study area northeast of the city of Erbil. (B) Map of the study area with the major anticlinal fold axes (modified from Buday and Jassim, 1984). The Mountain Front fault line separates the foredeep from the high folded zone. The main Zagros fault is the proposed Neotethys Ocean suture zone between the Arabian plate and Eurasia.

the Oman fault in the southeast, and the Persian Gulf foreland to the southwest (Stocklin, 1968; Haynes and McQuillan, 1974; Talbot and Alavi 1996), forming a major segment of the Alpine-Himalayan orogen. The orogen started to form in the Late Cretaceous, following the collision between the Arabian and Eurasian plates as a result of the closure of the Neotethys oceanic basin (Berberian and King 1981; Snyder and Barazangi 1986; Berberian 1995; Talbot and Alavi 1996). The shortening rate between the Arabian and Eurasian plates, which is still on the order of 2 to 2.5 cm/a, is partitioned into south-southwest-directed folding and thrusting of the Tethyan sediments and northwest-southeast to north-south-trending dextral strike-slip faulting (Jackson and McKenzie, 1984; Berberian, 1995; Jackson et al., 1995; McQuarrie et al., 2003). The Zagros fold and thrust belt, which hosts more than

5% of the world's hydrocarbon reserves (mostly in anticlinal traps), is divided into four northwest-southeast-striking tectonic units in Iraq: the Zagros suture, the imbricated zones, the high folded zone, and the foothill zone (figure 6-1, p. 72, in Jassim and Goff, 2006). The last three zones are broadly equivalent to the High Zagros overthrust zone, the Zagros simply folded zone, and the Zagros foredeep, respectively, as defined in Iran (Stocklin, 1968; Haynes and McQuillan, 1974; Berberian, 1995). The boundary between the high folded zone and the foothill zone is defined by the Mountain Front fault parallel to the general trend of the Zagros belt. The boundary between these zones also coincides with a deep-seated fault along the southwest limb of the Aqra anticline, with approximately 3000 m (9843 ft) displacement (Jassim and Goff, 2006). The Mountain Front fault likely represents a forced

fold forming above a reactivated basement fault (Motiei, 1995; Berberian, 1995). According to Buday and Jassim (in Jassim and Goff, 2006), the high folded zone has an elevated basement compared with the foothill zone, with approximately 5-km depth difference, estimated from the thickness of the sedimentary megasequences.

The area used to test the PlaneTrace-WinGeol software lies in the high folded zone and in the imbricated zones of the Zagros Mountains, north-east of Erbil (Figure 1). Deposition of the approximately 9- to 10-km (5.6- to 6.2-mi)-thick sedimentary sequence, which rests on a Precambrian polymetamorphic basement (Jassim and Goff, 2006), started in the Late Permian to Late Triassic, reflecting continental rifting along northwest-southeast-striking normal faults and the opening of the Neotethyan Ocean (Alavi, 2004, and references cited therein). During the Cretaceous, northeast-directed subduction of Neotethys started, followed by southwest-directed obduction of ophiolites and the elevation of the inner Zagros orogen (Hooper et al., 1995). As a result of ongoing subduction, Neotethys closed in the Miocene. In the Pliocene to Pleistocene, continent-continent collision between the Arabian and Eurasian plates resulted in the main phase of Zagros orogenic compression, with the development of the fold and thrust belt (Allen et al., 2002; Homke et al., 2004; Ziegler, 2001). Locally, Permian–Triassic normal faults were reactivated in the basin, leading to inversion of the overlying sedimentary cover in small basins and the formation of ejective anticlines (i.e., compressive reactivation of older faults bounding large elongated tilt blocks (Numan et al., 1998).

Ongoing deformation in the fold and thrust belt in northeast Iraq is dominated by open to gentle folding, with a characteristic wavelength between 5 and 10 km (3.1 and 6.2 mi) (Figure 1B), considerably less than the average values of 15 to 25 km (9.3–15.5 mi) in the southeastern parts of the Zagros fold and thrust belt (Mouthereau et al., 2007). The major cause for this significantly shorter wavelength is the absence of major faulting and also the absence of thick salt horizons (e.g., the Neo-Proterozoic Hormuz salt overlying the crystalline basement in the southeastern part of the Zagros),

Period	Tectonic history	Epoch	Formation/ Mech. behavior
Neogene	Compression and continental collision	Holocene	Flood plain deposits /Residual soil and polygenetic deposits
		Pleistocene	Slope and alluvial fan deposits
		Pliocene	River terraces
			Bai Hassan (Upper Bakhtiari) Formation
		Miocene	Mukdadiyah (Lower Bakhtiari) Formation
			Injana (Upper Fars) Formation
Paleogene		Oligocene	Late
			Early
		Eocene	Late
			Early
		Paleocene	Late
			Early
Cretaceous	Foreland basin formation and closure of the Neotethys	Late	Tanjero Formation
			Shiranish Formation
			Kometan Fm.
			Agra-Bekhme Formation
			Qamchuqa Formation
	Opening of the Southern Neotethys	Early	Balambo, Garagu and Sarmord Formations
Jurassic	Subsidence and rifting	Late	Chia Gara, Barsarin, Sargelu and Naokelekan Formations
		Middle	
		Early	Sehkaniyan and Sarki Formation **
Triassic	Rifting	Late	Baluti and Kurra Chine Formation

**Figure 2.** Stratigraphy of the studied area. Formations marked with an asterisk (\*) are incompetent, and those marked with double asterisks (\*\*) are possible local detachment horizons. The stratigraphic table is significantly modified from Buday and Jassim (1984).



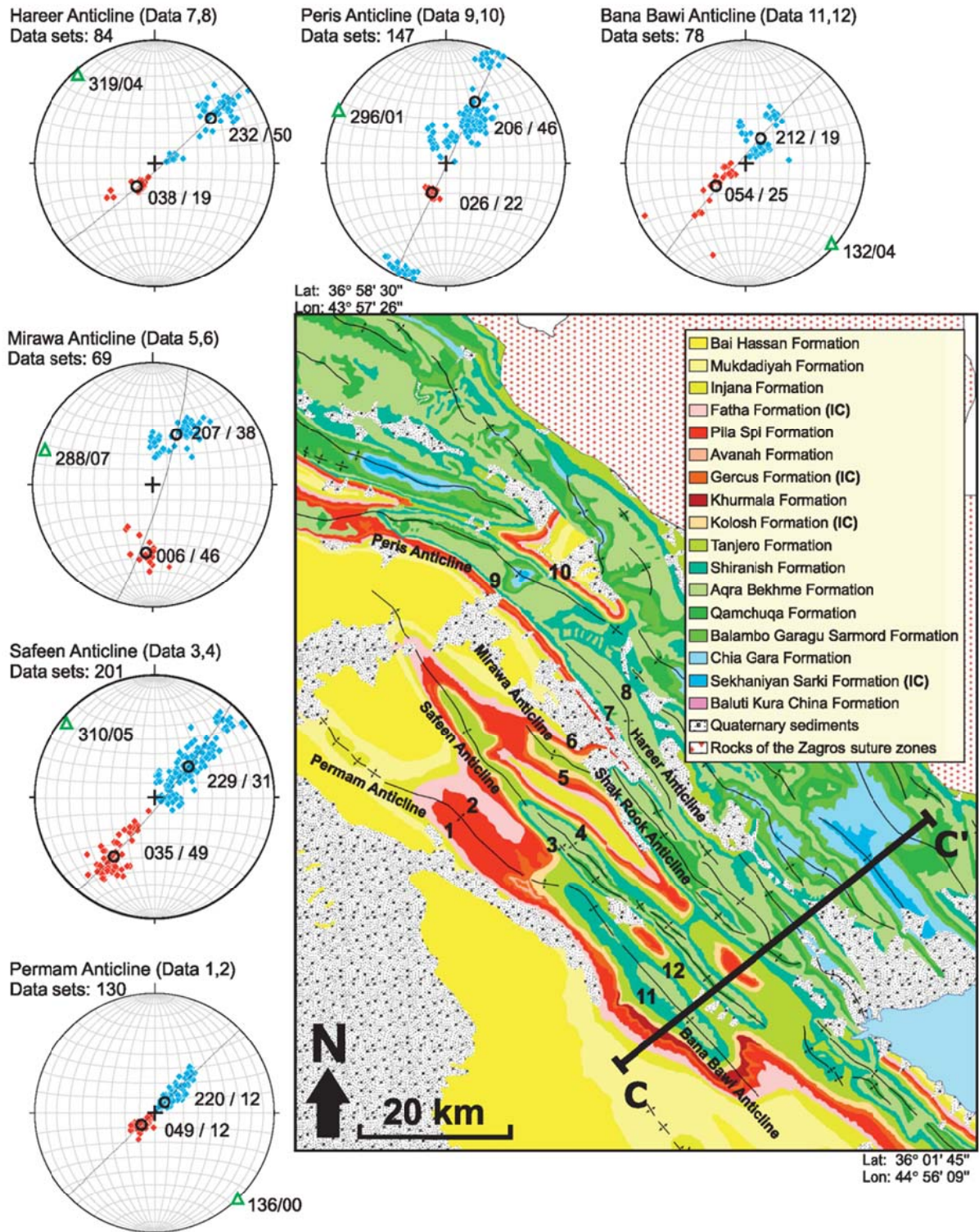
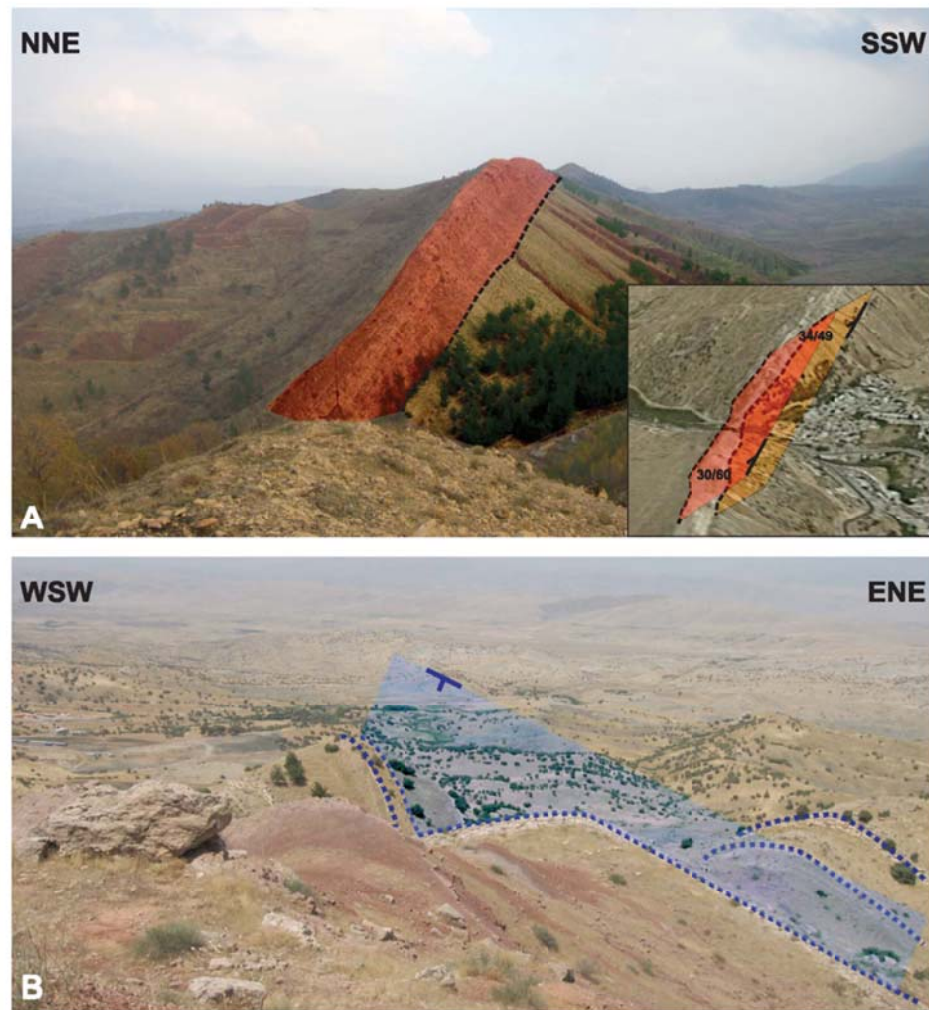


**Figure 3.** Geologic map significantly modified from Buday and Jassim (1984). The numbers indicate the location of structural field measurements of forelimbs and back limbs of anticlines. The data are presented in stereographic projections (equal area, lower hemisphere). Blue dots indicate measurements from forelimbs; red dots are measurements from back limbs. Green triangles represent the calculated  $\pi$  pole corresponding to the best fit cylindrical fold axis. Great circles indicate the orientation of the calculated mean  $\pi$  circle. In the legend, the incompetent formations are marked with (IC). The cross section CC', supported by limited field data and constructed using the software tool PlaneTrace, is shown in Figure 7.



**Figure 4.** (A) Lithologic boundary (black dashed line) between Pila Spi limestone (shaded red) and underlying Gercus red sandstone, siltstone, claystone (shaded orange). Because of a significant different resistance to erosion, the more competent limestone forms sharp ridges with steeply sloping sides along the eroded flanks of the anticlines. The inset shows the satellite image of the same location draped on the digital elevation model (DEM). The red and orange planes show the sedimentary bedding orientation (black values) of the Pila Spi limestone (030/60) resp. Gercus red sandstone, siltstone, and claystone (034/49). Black dashed lines visualize the intersection of the projected planes with the DEM. (B) Triangular shaped hogback, consisting of Pila Spi Formation, which perfectly outlines the dip of the strata. The blue dashed lines highlight the outcropping sedimentary beddings, and the blue inclined plane indicates their orientation.



which acted as ductile detachments during deformation (Bahroudi and Koyi, 2003; Sherkati et al., 2005; Mouthereau et al., 2007).

The fold trains in the investigated area comprise Cretaceous to Cenozoic sediments (Figure 2) consisting mainly of limestones, dolomites, sandstones, siltstones, claystones, and conglomerates. Sepehr et al. (2006) noted that in the Iranian part of the Zagros fold and thrust belt, the mechanical anisotropy of the formations consisting of a succession of relatively competent (massive dolomite and limestone) and incompetent (claystone, siltstone, and shale) sediments essentially controls the style of the folding (Figure 3). In addition, the folding is influenced by a few low-shear strength layers that may act as local detachment horizons: The Upper Tertiary Fatha (i.e., lower Fars) Formation contains

thin layers of claystone, gypsum, and anhydrite. Other local detachments are found in the Lower Jurassic sediments, particularly in the Sehkanian and Sarki formations (De Vera et al., 2009), consisting mainly of limestone and dolomite, but also containing thin-bedded shales (Figure 2).

## STRUCTURAL FIELD MEASUREMENTS

More than 500 bedding orientations were recorded in the Zagros high folded zone during field studies (Figure 3), mostly from road cuts. Although security in this part of the Zagros is much better than elsewhere in Iraq, off-road access was severely restricted because of serious contamination of the



area with land mines and unexploded ordnance, a problem dating back to the end of World War II. Thus, only two short cross sections, along main roads oriented perpendicular to the trend of the fold axes, could be measured, as a result of which large parts of the fold trains remained unexamined. The length of these cross sections limited their use for any conclusions, and thus, they are not published in this work.

Fieldwork focused on detailed structural measurements of lithologic boundaries between formations that have strong competence contrasts (Figure 4A). Because of faster erosion of softer rocks, the more competent lithologies form sharp ridges, with steeply sloping sides along the eroded flanks of the anticlines. These hogbacks, as much as several hundred meters high, form triangular-shaped flanks that perfectly outline the dip of the strata and can be easily identified in the DEM. Hogbacks were, therefore, the major target for structural field measurements (Figure 4B).

Dip directions and angles of the limbs of six anticlines were measured in detail (Figure 3). Except for the symmetric and upright Permian and Bana Bawi anticlines, the measured folds are clearly asymmetric, with steep southwest-dipping forelimbs and shallower northeast-dipping back limbs (Safeen, Hareer, Peris, and Mirawa anticlines). Although the geologic map (Buday and Jassim, 1984) indicates a thrust cutting the core of the Safeen anticline, this could not be identified in the field and is probably of minor importance. Another possible thrust fault was mapped between the Shak Rook and the Hareer anticline, but the offset is unknown because the scarp is covered by Quaternary slope deposits.

## DESCRIPTION AND USE OF THE PLANETRACE TOOL

PlaneTrace, an add-on tool for the remote sensing software package WinGeol, was developed for the analysis and visualization of intersections of planar structures of any spatial orientation with irregular and rugged surfaces (e.g., the topography). Such intersections can be used to calculate the spatial

orientation of the feature, constrained by the dip direction and dip angle, if the topography is rugged and the feature cuts across a ridge or a valley forming a triangular or V-shaped intersection (the V-rule in textbooks) or if it crops out as a result of selective erosion of less resistant surrounding lithologies. PlaneTrace is designed to display the intersections between a rugged topographic surface (e.g., the DEM) and a virtual transparent plane in two-dimensional ([2-D] cross section view) or 3-D (block diagram view). The virtual planes have the following parameters: geographic coordinates and elevation of the center, the dimensions of the rectangle defining the plane, the dip angle and direction, and a Boolean variable representing the polarity of the plane (upright or overturned). The planes can be translated and rotated in any direction until it fits the spatial orientation of the geologic planar feature (i.e., fault, sedimentary bedding), recording the geographic position, the dip direction, and the dip angle.

To increase the geologic information of the DEM, any bitmaplike referenced geologic map or rectified aerial or satellite image can be draped over the topography. The geographic location and the angles specifying the spatial orientation of the surfaces can be exported into most common database formats or into an ASCII file, and the intersection lines of the surfaces with the DEM can be exported into AutoCAD dxf files, ArcGis shape files or into an ASCII file.

An important feature of PlaneTrace is that any change in the position and orientation of the measured plane instantly updates the shape and position of the polyline representing the intersection of the measured surface with the DEM. As a result, the lateral continuation of the planar feature or the deviation of this feature from an ideal plane geometry can be directly compared with independent data such as a geologic map or field photographs. If the feature is not truly planar (e.g., the limbs of a noncylindrical fold), the whole structure can be subdivided into several smaller essentially planar elements, approximating the 3-D surface. Thus, the size of individual planes can be varied depending on the size of the structural model.

**Figure 5.** Flowchart and screen-shots of the individual working steps in PlaneTrace demonstrated with data from the investigated area northeast of Erbil: (A) assemblage of remote sensing data and available maps; (B) mapping and calculation of the dip directions ( $\theta$ ) and dip angles ( $\delta$ ) of geologic planar structures (given example is from the northeast limb of the Safeen anticline); (C) further processing of measurements with WinGeol (e.g., interpolation of subsurface structures in a three-dimensional model between the Safeen and Peris anticlines based on surface dip measurements); (D) balanced southwest-northeast cross section over the Permian and Safeen anticlines based on projection of the calculated dip values into a two-dimensional section. DEM = digital elevation model.

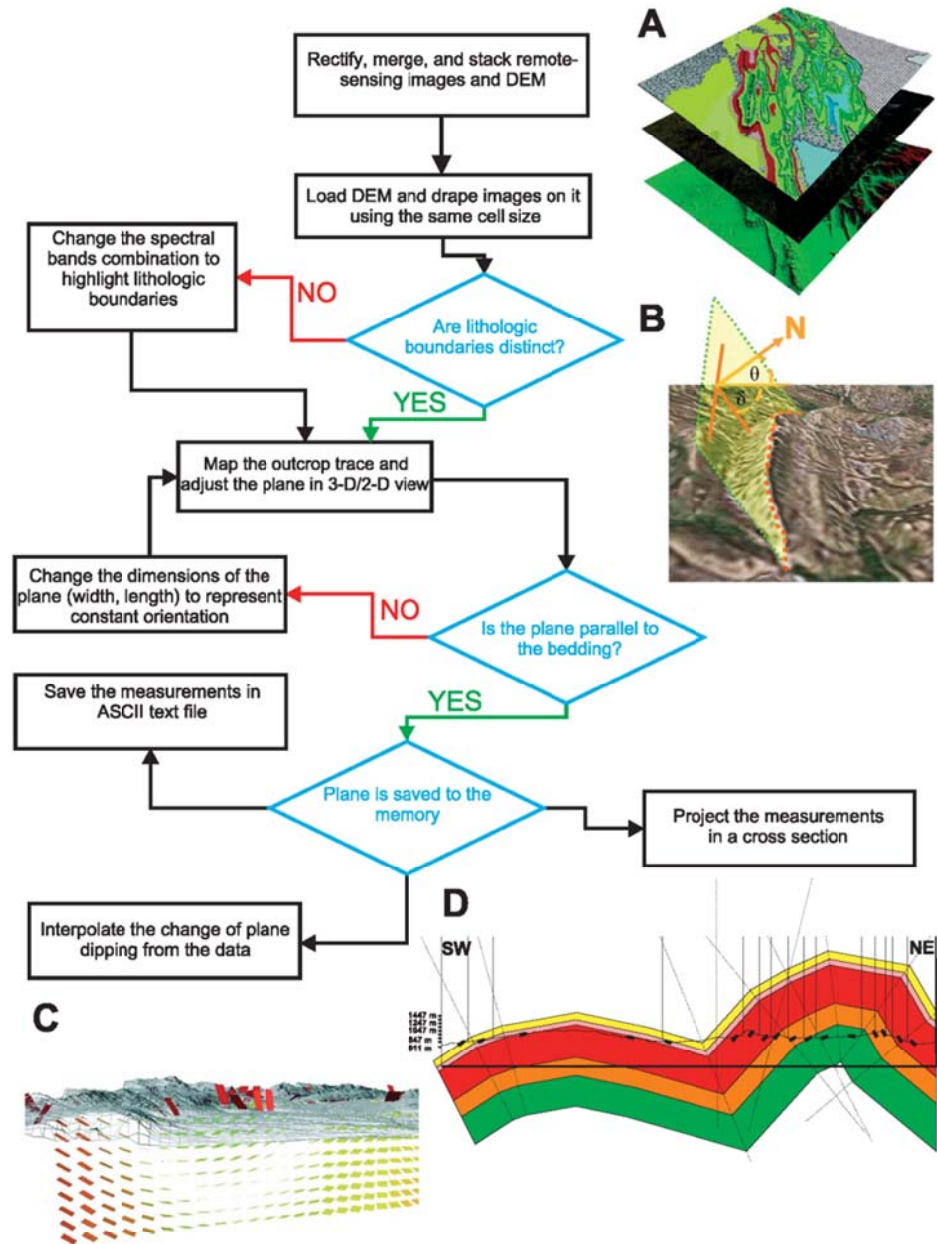


Figure 5 shows the extended workflow of the quantitative spatial analysis of geologic planar structures (in this case, sedimentary bedding) depicted from DEM data. The first step comprises georeferencing, rectifying, merging, and band stacking of imagery that will be draped on the DEM (Figure 5A). Although the necessary functions are available in WinGeol, these procedures can be also accomplished by other software packages and imported. The second step includes resampling of the reso-

lution of other bitmap data (e.g., the geologic map, satellite image) to match the resolution of the DEM. This step should also be used to test the quality and the contrast of the geologic planar features. It is also useful to crop the images to the dimensions of the study area to reduce processing time. In the third step, the prepared data are loaded into the WinGeol package. WinGeol works as a simple geographic information system application that allows the draping of additional bitmap data onto the DEM. Using



**Table 1.** Detailed Description of the 14 Advanced Spaceborne Thermal Emission and Reflection Radiometer Instrument Bands with Their Wavelengths and Resolutions

Instrument	VNIR*	SWIR*	TIR*
Bands	1–3	4–9	10–14
Resolution	15 m	30 m	90 m
Cross-track pointing	±318 km (±24°)	±116 km (±8.55°)	±116 km (±8.55°)
Swath width	60 km	60 km	60 km
Quantization (bits)	8	8	12

\*VNIR = visible near infrared; SWIR = short-wave infrared; TIR = thermal infrared.

the PlaneTrace tool in either a 2- or a 3-D view, sedimentary bedding or fault planes are identified and overlain by transparent virtual planes. The virtual planes are then interactively adjusted to the orientations that best represent the traces of the intersection of the geologic features with the DEM. Even without exposed rocks, the dip direction and dip angle can be measured approximately if it can be reasonably assumed that the topography reflects the distribution of the underlying sedimentary bedding. In the next step, the size of the virtual plane is adjusted to represent a section of the geologic structure, which can be approximated by a plane (Figure 5B). Finally, the parameters of the best fit virtual plane can be saved for further processing in three dimensions (e.g., interpolation of non-planar surfaces; Figure 5C) or the dip angles can be projected into a 2-D profile to construct balanced cross sections (Figure 5D). As the data are organized in separate layers (i.e., geologic map, false color satellite image, dip marks, faults, seismic cross sections), the ones that should be projected onto the cross section can be chosen.

### STRUCTURAL MODELING OF THE ZAGROS FOLD AND THRUST BELT, NORTHEAST ERBIL

To test the PlaneTrace module, we calculated dip directions and angles at more than 100 lithologic boundaries in the fold trains northeast of Erbil. The aim of this was twofold. First, we compared the calculated spatial orientations with measurements of the same lithologic boundaries in the

field to test the accuracy of the technique. Second, the data were used to construct a structural model, including a simple balanced cross section, of an area not investigated in detail in the field because of security concerns; this was to demonstrate the applicability of the method.

All data (advanced spaceborne thermal emission and reflection radiometer [ASTER] and SPOT [satellite pour l'observation de la terre] satellite imagery, geologic map) were loaded into WinGeol

**Table 2.** Correlated Dip Directions and Dip Angles of Field Measurements and Their Digital Elevation Model-Derived Equivalents\*

Location	3a	3b	3c	3d	4a	4b	4c
Derived dip direction	224	223	226	226	245	41	36.97
Measured dip direction	224	218	224	224	225	36	34
Derived dip angle	65	70	40	40	47	65	60
Measured dip angle	46	78	40	40	45	64	59

Location	4d	4e	4f	5a	5b	5c
Derived dip direction	34	37	42.12	203	225	233
Measured dip direction	35	36	30	180	207	225
Derived dip angle	49	30	14	28	24	40
Measured dip angle	50	40	24	29	25	44

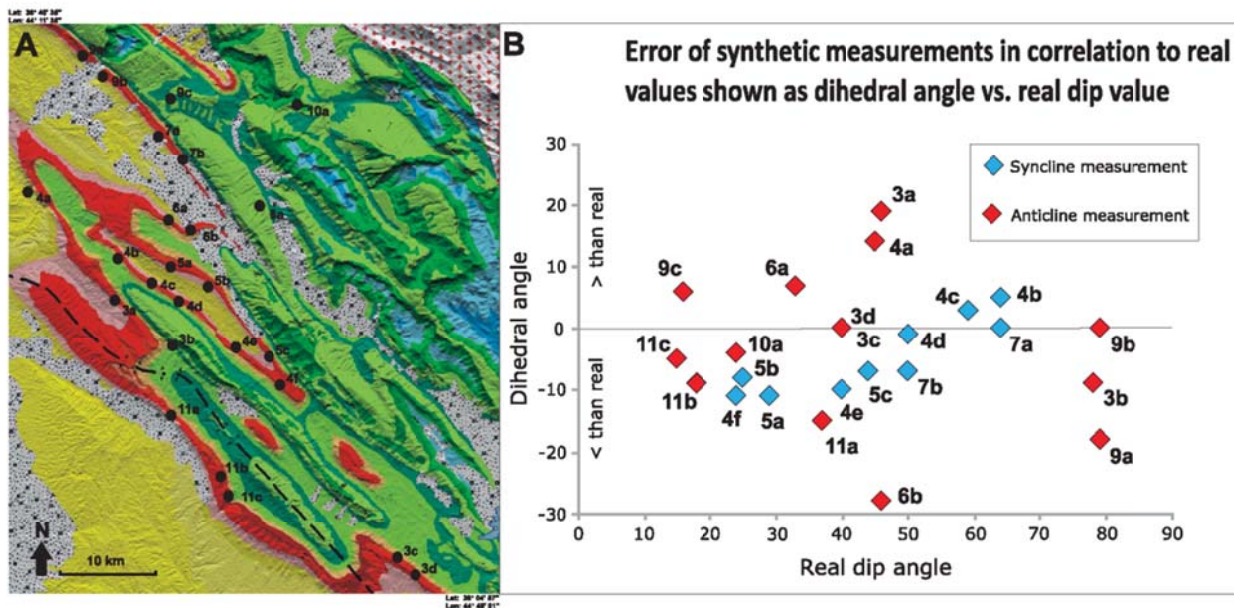
  

Location	6a	6b	7a	7b	8a	9a
Derived dip direction	34	318.5	232	232	78	221
Measured dip direction	31	360	232	224	74	203
Derived dip angle	40	35	64	47	40	77
Measured dip angle	33	46	64	50	40	79

Location	9b	9c	10a	11a	11b	11c
Derived dip direction	221	28	170	230.1	250	250
Measured dip direction	207	30	170	213	225	240
Derived dip angle	79	22	20	25	11	11
Measured dip angle	79	16	24	37	18	15

\*The location name consists of the area number (1–12) according to Figure 3 and the letter representing the individual measurement location starting from the northwest to the southeast (see Figure 6).



**Figure 6.** (A) ASTER (advanced spaceborne thermal emission and reflection radiometer) digital elevation model with the different stratigraphic formations of the investigated area showing the location of the 25 test sites, where field measurements and calculated orientations have been compared. (B) Scatter plot comparing the field measurements and measurements acquired using PlaneTrace from 25 locations in the study area. The y axis shows the dihedral angle (given via the dot product of the normals of these planes) between the measured planar structure and calculated plane; the x axis shows the real dip angle of the measured planar structure. The red and blue points symbolize measurements from anticlines and synclines, respectively.

and combined with the DEM to calculate the spatial directions of lithologic boundaries using PlaneTrace. Several spectral band combinations of different sensors (V1, V2, and the infrared V3n and V3b) provided by the ASTER satellite (Table 1)

**Table 3.** Evaluation of Correlation between Field Measurements and Digital Elevation Model-Derived Values at 25 Localities that Shows the Time and Accuracy Variation of the Method\*

Value	Dimensions	Dip Direction	Dip Angle
Average error	Decimal degrees	9.70	4.56
Standard deviation	–	10.26	4.89
Amount of exact measurements	n of 25	3	5
Average time	Minutes	7.66	–
Maximal difference	Decimal degrees	41.48	19

\*The average time required is stated for one complete process (i.e., one dip direction and dip angle measurement).

were used to enhance the contrast of the stratigraphic formations, focusing on boundaries between competent and incompetent lithologies. The excellent outcrops and the low vegetation cover facilitated an accurate visualization of the virtual plane onto the lithologic boundaries.

The structural field measurements (measured with a geologic field compass and based on at least 10 independent measurements at that site) have been compared with spatial orientations derived by the PlaneTrace tool (Table 2) at 25 locations (Figure 6). Comparison of these values reveals that the dip directions measured in the field were reproduced by PlaneTrace measurements within an error of  $\pm 9^\circ$ , and the dip angles derived from the remote sensing data deviate from the field measurements within an error of  $\pm 5^\circ$  (Table 3).

The presented method has been used to derive approximately 100 measurements from remote sensing data, sufficient to construct a simple balanced cross section through the area. Because the profile was not investigated during fieldwork,



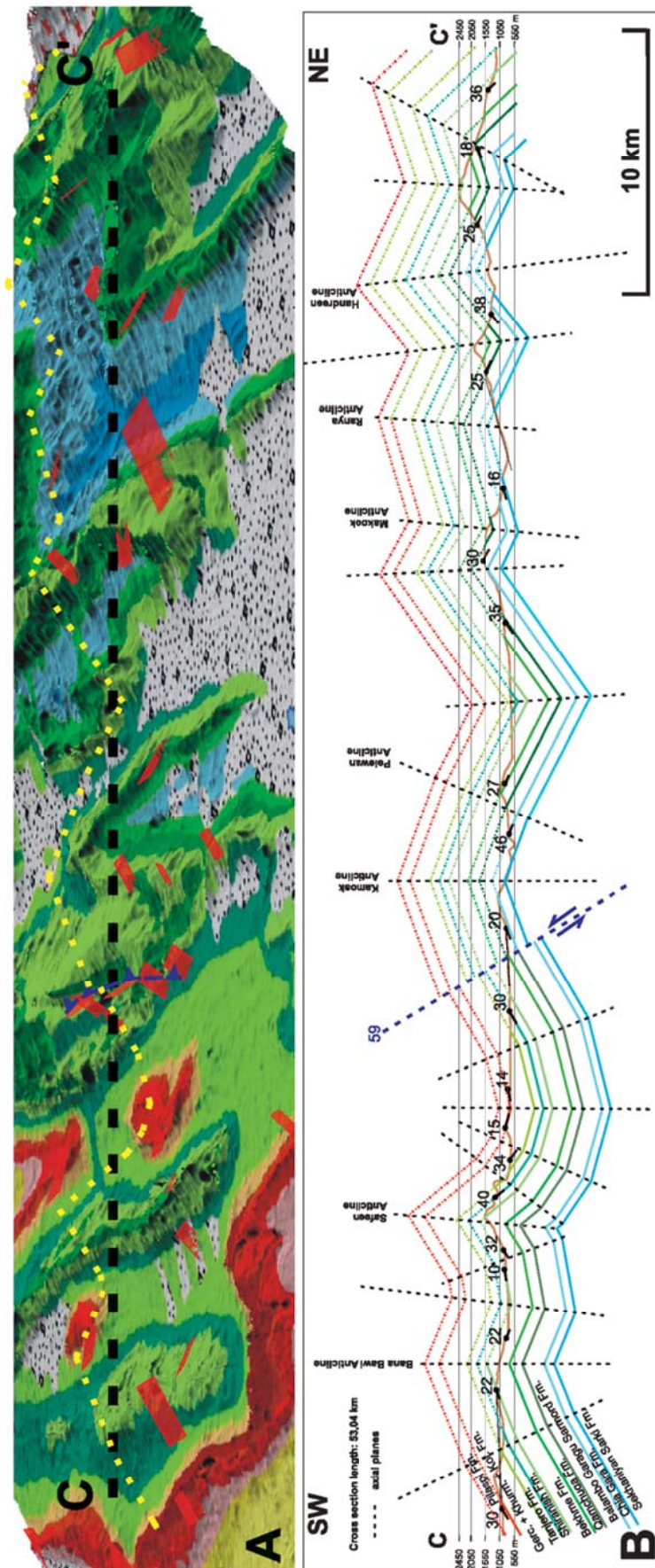


**Figure 7.** (A) ASTER (advanced spaceborne thermal emission and reflection radiometer) digital elevation model (DEM) with the different stratigraphic formations of the investigated area showing the location of the cross section CC' and the dip direction and dip angle measurements calculated with PlaneTrace (the measurements used for the construction of the cross section CC' are shown as red inclined planes cutting the DEM). The fault measured using PlaneTrace and the projection of the balanced cross section (dotted line) are shown in blue and yellow, respectively. (B) Cross section CC' constructed only from the calculated dip angles with PlaneTrace using the constant dip domain method (Tearpock and Bischke, 2003).

all the available orientation data are derived from the DEM, enhanced by draped satellite images and the geologic map (Buday and Jassim, 1984). An inclined view of the cross section (Figure 7A) shows the measurement locations (indicated as red planes) that have been projected onto the cross section (Figure 7B). The greatest projection distance of the measurements from the cross section was set in the program interface to 5000 m (16,404 ft). The correction of apparent dip angles for measurements with a dip direction oblique to the cross section is automatically performed by PlaneTrace. With the additional information of the georeferenced geologic map, the constant dip domain method was used to construct a simple balanced cross section (Tearpock and Bischke, 2003). This identifies sectors of similar dip angles across a folded region and separates these sectors with axial planes bisecting the dip angle between neighboring domains. By including the mapped lithologic boundaries, a simple line- and area-balanced cross section has been constructed. As previously noted, the investigated area is dominated by open upright folding, within which no major faults have been identified. No evidence in the remote sensing data was seen for the thrust fault marked on the geologic map by Buday and Jassim (1984). However, although it was not required to draw a balanced cross section, it has been included as a low-angle structure with an inferred minor displacement.

## DISCUSSION

Traditionally, mapping techniques have used structure contours to construct intersections of geologic structures with the topography on maps. However, even if the geologic structure is approximated by a plane and the structure contours are therefore equally spaced parallel lines, this technique is time consuming and inaccurate because the errors are cumulative.

The 30-m (98-ft) resolution of the worldwide available ASTER data sets used was sufficient for estimating the dip direction and dip angle of the larger scale structures. At localities where only structures less than 30 m (98 ft) in size or very indistinct

structures were present, it was necessary to use SPOT images to revise the estimations. Without these, estimating the surface orientation was not possible. The use of more data with higher resolution, such as SPOT (resolution 1.0–2.5 m [3.3–8.2 ft]) or Quickbird (high-resolution commercial earth observation satellite launched in 2001 with the resolution as much as 0.6 m [2 ft]), would make the method even more useful in the major part of the area of interest. Compared with other studies (Snidero et al., 2009), PlaneTrace gave good results, despite using mostly lower resolution data than usual for this type of work. Use of higher resolution DEM and satellite imagery like SPOT-HRG (high-resolution geometric instruments with the resolution as much as 2.5 m [8.2 ft]) can even improve the results. However, the accuracy of the method is not only dependent on the resolution of satellite images or aerial photography, but can be also strongly influenced and limited by other factors, such as geomorphology, vegetation cover, and the complexity of the tectonic deformation history. In case of dense vegetation, the method will still work as long as significant variations in elevation can be observed. Lithologic units might be covered, but in some (rare) cases, even amplified by supporting the growth of different plant types or variable support of plant growth. Soil-covered and/or deeply weathered zones especially in flat areas are of course where we expect the biggest difficulties with this method. A careful image processing might help increase the contrast of hidden geologic units, and to help interpretation, it would be useful to start from areas with less unfavorable conditions and to work toward the problematic zones. The accuracy of the method depends of course on the exposed elevation differences.

The measurements were showing that PlaneTrace is more accurate in the synclines than in the anticlines. This discrepancy was caused by a higher number of poor-quality outcrops in the anticlines (three very insignificant outcrops with an angle difference higher than 10°) than in the synclines and not by the measuring algorithm. In case of the same number of the outcrops with the same quality in the anticlines as well as in the synclines, there will be no difference in the accuracy.



Most measurements were derived from eroded limestone layers, closely followed by measurements derived from V-shaped river gorges. A few measurements were made on flatirons, using only the topography, without any visible outcrop on the satellite image. Despite the uncertainty of the latter measurements, they conformed to the overall structural pattern of the area.

For assessing the accuracy of PlaneTrace measurements, the dihedral angle between the calculated and the field orientations (dot product of the normals of these planes; Gellert et al., 1989) was determined (Figure 6). Negative values indicate that the orientation estimated from the DEM was steeper than the field measurement. The best accuracy was obtained from data measured on flatirons (average dihedral angle,  $\sim 7^\circ$ ), followed by V-shaped river gorges and eroded layers (average dihedral angle,  $\sim 10^\circ$ ).

At five outcrops, the maximum dihedral angle for the multiple field measurements was calculated; this gave a mean of  $14^\circ$ . Thus, field measurements also show a significant variance at a single outcrop. This variance is automatically taken into account by PlaneTrace because it effectively smoothes the orientation data over a large area. A comparison of dip angles for the 25 localities where results from both the field and PlaneTrace are available (Figure 6B) gave a correlation coefficient ( $R$ ) of 0.90. For dip directions, such a correlation would be meaningless because azimuth directions are arbitrary values; that is,  $176^\circ$  is not a higher azimuth value than  $045^\circ$ , so they cannot be plotted as values on a graph.

Before starting the work, exact rectification of all maps and other data draped on the DEM is essential for the accuracy of the measurements (in our study area, all geologic maps were shifted slightly to the southwest, which must be corrected during the rectification process).

The simple folding of the study area made estimation of the dip direction more accurate because generally, only two main orientations of the planes were possible (northeast or southwest dipping). In contrast, the dip angle varies considerably and the southwest-directed thrusting in the imbricated zones made determining accurate dip angles

more time consuming. For reliable results, the locality being measured must be viewed from several directions in 3-D.

In the north of the study area, dip angles become steeper, as a result of greater shortening, and the valleys are narrower. This reduces the quantity and dimensions of the outcrops with suitable planar surfaces. At dip angles greater than  $75^\circ$  are the outcrop surfaces in our study area commonly smaller, and thus, the accuracy of the method decreases greatly because of poor fitting of the very short strike line projected onto the DEM. These small outcrops are mostly situated in deeply incised valleys with a lot of shadows on the satellite imagery, complicating the correct identification of the lithologies. Estimating the best fitting of the projected plane becomes much more difficult even with use of different view angles in 3-D. Higher resolution DEM than the used ASTER data would highly increase the accuracy in such areas.

The time required to make one measurement varies according to the image quality, the topographic relief (e.g., the difference in erosional resistance between formations, river gorge depth) and well-defined formation boundaries (e.g., color differences) as well as the size of measured structures. The last is determined by the resolution of the remote sensing data. Changes in bedding orientations on small areas relative to the resolution of the DEM were ignored because they could not be properly imaged. Considering the general structure of the area can help reduce the measuring time during revision of the results, by helping identify and concentrate on unusual results. Such measurements, which do not fit the regional trend, can be the result of geologic processes like faulting or mass movements, but they can also represent geologically meaningless artifacts like quarry walls or road cuttings. For this study, from 3 to 25 min was required to make and revise one measurement (average time from 25 measurements is in Table 3).

The limitations of the method are mostly related to the quality of the available data (i.e., DEM, satellite images). A serious decrease of accuracy will occur if small outcrops, relative to the resolution of satellite images and DEM, are used. The presented method will be difficult to use in areas that

have a dense vegetation cover or that are strongly influenced by artificial constructions covering the lithologic boundaries and or causing significant changes in elevation, although the method will still work for measuring dip slopes as long as observable changes in elevation exist. Identification of overturned layers can be difficult if the stratigraphy is not well known. If the lithologic boundaries are not distinguishable on satellite images, likely where monotonous lithologies with little erosional contrast between formations are present, a geologic map can be draped over the DEM. In such cases, the accuracy is dependent on the quality of the DEM, on the quality of the geologic map, and on the draping accuracy.

In the study area, the syntectonic to posttectonic unconsolidated sedimentary fill in the valleys has buried the outcrop, making it impossible to estimate the orientation of the folded rocks in such areas. As a result, data from the fold limbs have to be projected into these blind areas, and because these generally overlie synclines, these have a sharper, more chevron-style profile compared with the anticlinal hinges. For the smoothing of such areas, we can use a suitable type of extrapolation or spline/curve. To the northeast, the narrowing of the synforms reduces both the size of the outcrops and their abundance. This typically causes a marked reduction in the number of domains with different dip angles on the fold limbs (sometimes down to only one domain), which also results in a too simple fold profile on the balanced cross section. We also assumed that the topography reflects the course of sedimentary bedding at deeper levels under the Earth's surface (i.e., dip slopes mapping). In our study area, simple folding, without any major decoupling at depth, was assumed because the salt horizons found in the Iranian part of the Zagros are missing.

## CONCLUSIONS

A comparison of the costs incurred during fieldwork with that required for the software and the DEM satellite data necessary for computer-aided

measurements indicates that this is a cost-effective method for gathering geologic orientation data. Furthermore, such work can identify important areas that can be targeted more efficiently during subsequent fieldwork, reducing fieldwork time and, hence, costs. It can also provide data in areas that turn out to be important after fieldwork has been completed or which were not accessible at that time. A low vegetation cover; a simple tectonic history, with only one main convergence direction; and well-exposed outcrops all facilitate the successful use of this method in this area.

The ASTER remote sensing data were used to derive approximately 100 measurements from the study area, increasing the coverage with structural measurements. The time required for each measurement was, on average, approximately 7 min. The mean error of the 25 correlated measurements is approximately 10° for the dip direction and 5° for the dip angle; the maximum error was 40 and 19°, respectively. A comparison of measured data from the field with interpolated spatial orientations from remote sensing data suggest that the calculated dip angles and dip direction values can be reproduced within the measurements error of a geologic field compass and the general roughness of most geologic planar surfaces. These data facilitated the construction of a balanced cross section in the previously unexplored eastern part of our study area.

Estimation of the bedding orientation is possible even where no rocks are exposed, if the topography can be assumed to have the same orientation as the underlying rocks (i.e., dip slopes mapping). The accuracy of the method depends mostly on the DEM resolution, on the size of the outcrops, and on accurate referencing and resolution of the maps and satellite images used.

## REFERENCES CITED

- Alavi, M., 2004, Regional stratigraphy of the Zagros fold-thrust belt of Iran and its proforeland evolution: *American Journal of Science*, v. 304, p. 1–20, doi:10.2475/ajs.304.1.1.
- Alfarhan, M., L. White, D. Tuck, and C. Aiken, 2008, Laser rangefinders and ArcGIS combined with three-dimensional



- photorealistic modeling for mapping outcrops in the Slick Hills, Oklahoma: *Geosphere*, v. 4, p. 576–587, doi:10.1130/GES00130.1.
- Allen, M. B., S. Jones, A. Ismail-Zadeh, M. D. Simmons, and L. Anderson, 2002, Onset of subduction as the cause of rapid Pliocene–Quaternary subsidence in the South Caspian Basin: *Geology*, v. 30, p. 775–778, doi:10.1130/0091-7613(2002)030<0775:OOSATC>2.0.CO;2.
- Autodesk AutoCAD dxf file technical description: <http://usa.autodesk.com/adsk/servlet/ps/dl/item?siteID=123112&id=2882295&linkID=9240617> (accessed July 10, 2010).
- Bahroudi, A., and H. Koyi, 2003, Effect of spatial distribution of Hormuz salt on deformation style in the Zagros fold and thrust belt: An analog modeling approach: *Journal of the Geological Society*, v. 160, p. 719–733, doi:10.1144/0016-764902-135.
- Banerjee, S., and S. Mitra, 2004, Remote surface mapping using orthophotos and geologic maps draped over digital elevation models: Application to the Sheep Mountain anticline, Wyoming: *AAPG Bulletin*, v. 88, p. 1227–1237, doi:10.1306/02170403091.
- Berberian, M., 1995, Master “blind” thrust faults hidden under the Zagros folds: Active tectonics and surface morphotectonics: *Tectonophysics*, v. 241, p. 193–224, doi:10.1016/0040-1951(94)00185-C.
- Berberian, M., and G. C. P. King, 1981, Toward a paleogeography and tectonic evolution of Iran: *Canadian Journal of Earth Sciences*, v. 18, p. 210–265.
- Bernardin, T., E. Cowgill, R. Gold, B. Hamann, O. Kreylos, and A. Schmitt, 2006, Interactive mapping on 3-D terrain models: *Geochemistry, Geophysics, Geosystems*, v. 7, p. Q10013, doi:10.1029/2006GC001335.
- Bilotti, F., J. H. Shaw, and P. A. Brennan, 2000, Quantitative structural analysis with stereoscopic remote sensing imagery: *AAPG Bulletin*, v. 84, p. 727–740.
- Buday, T., and S. Z. Jassim, 1984, Geologic map of Iraq: Baghdad Geological Survey of Iraq, Tectonic Map of Iraq, 1:1,000,000 scale series, sheet no. 2.
- Colwell, R. N., 1955, Some uses of three-dimensional models for illustrating photogrammetric principles: *Photogrammetric Engineering*, v. 21, p. 491–510.
- De Vera, J., J. Gines, M. Oehlers, K. McClay, and J. Doski, 2009, Structure of the Zagros fold and thrust belt in the Kurdistan Region, northern Iraq: *Trabajos de Geologia*, v. 29, p. 239–243, <http://fdrg.rhul.ac.uk/pubs/pubs.html>.
- ESRI ArcGIS shape file technical description: <http://www.esri.com/library/whitepapers/pdfs/shapefile.pdf> (accessed July 10, 2010).
- Gellert, W., S. Gottwald, M. Hellwich, H. Kästner, and H. Künstner, eds., 1989, *VNR concise encyclopedia of mathematics*, 2d ed.: New York, Van Nostrand Reinhold, 776 p.
- Haynes, S. J., and H. McQuillan, 1974, Evolution of the Zagros suture zone, southern Iran: *Geological Society of America Bulletin*, v. 85, p. 739–744, doi:10.1130/0016-7606(1974)85<739:EOTZSZ>2.0.CO;2.
- Homke, S., J. Vergès, M. Garcés, H. Emami, and R. Karpuz, 2004, Magnetostratigraphy of Miocene–Pliocene Zagros foreland deposits in the front of the Push-e Kush Arc (Lurestan Province, Iran): *Earth and Planetary Science Letters*, v. 225, p. 397–410, doi:10.1016/j.epsl.2004.07.002.
- Hooper, R. J., I. R. Baron, S. Agah, and R. D. Hatcher, 1995, The Cenomanian to recent development of the southern Tethyan margin in Iran, in M. I. Al-Husseini, ed., *Middle East petroleum geosciences: Bahrain, Gulf Petrolink*, v. 2, p. 505–516.
- Jackson, J. A., and D. P. McKenzie, 1984, Active tectonics of the Alpine-Himalayan belt between western Turkey and Pakistan: *Geophysical Journal of the Royal Astronomical Society*, v. 77, p. 185–264.
- Jackson, J., J. Haines, and W. Holt, 1995, The accommodation of Arabia Eurasia plate convergence in Iran: *Journal of Geophysical Research*, v. 100, p. 15205–15219, doi:10.1029/95JB01294.
- Jassim, S. Z., and J. C. Goff, 2006, *Geology of Iraq: First edition*: Brno, Czech Republic, Dolin, 352 p.
- Jones, R. R., K. J. W. McCaffrey, P. Clegg, R. W. Wilson, N. S. Holliman, R. E. Holdsworth, J. Imber, and S. Waggott, 2009, Integration of regional to outcrop digital data: 3-D visualization of multiscale geological models: *Computers and Geosciences*, v. 35, p. 4–18, doi:10.1016/j.cageo.2007.09.007.
- Kraus, K., 2007, *Photogrammetry: Geometry from images and laser scans*: Berlin, Germany, Walter de Gruyter, 459 p.
- McQuarrie, N., J. M. Stock, C. Verdel, and B. P. Wernicke, 2003, Cenozoic evolution of Neotethys and implications for the causes of plate motions: *Geophysical Research Letters*, v. 30, p. 2036, doi:10.1029/2003GL017992.
- Motiei, H., 1995, Petroleum geology of Zagros, in A. Hushmandzadeh, ed., *Treatise on the geology of Iran*: Geological Survey of Iran, p. 589.
- Mouthereau, F., J. Tensi, N. Bellahsen, O. Lacombe, T. De Boissgrolier, and S. Kargar, 2007, Tertiary sequence of deformation in a thin-skinned/thick-skinned collision belt: The Zagros folded belt (Fars, Iran): *Tectonics*, v. 26, p. 28.
- Numan, N. M. S., R. A. Hammoudi, and J. Chorowicz, 1998, Synsedimentary tectonics in the Eocene Pila Spi limestone formation in Iraq and its geodynamic implications: *Journal of African Earth Sciences*, v. 27, p. 141–148, doi:10.1016/S0899-5362(98)00052-9.
- Rencz, A. N., and R. A. Ryerson, 1999, Remote sensing for the earth sciences: *Manual of remote sensing*: Danvers, Massachusetts, John Wiley & Sons, v. 3, 728 p.
- Sepehr, M., J. Cosgrove, and M. Moieni, 2006, The impact of cover rock rheology on the style of folding in the Zagros fold-thrust belt: *Tectonophysics*, v. 427, p. 265–281, doi:10.1016/j.tecto.2006.05.021.
- Sherkati, S., M. Molinaro, D. Frizon de Lamotte, and J. Letouzey, 2005, Detachment folding in the central and eastern Zagros fold-belt (Iran): Salt mobility, multiple detachments and late basement control: *Journal of Structural Geology*, v. 27, p. 1680–1696, doi:10.1016/j.jsg.2005.05.010.
- Snidero, M., A. Amilibia, O. Gratacos, and J. A. Muñoz, 2009, 3-D Reconstruction of geological structures based on remote sensing data: Example from Anaran anticline



- (Lurestan province, Zagros fold and thrust belt, Iran) (abs.), Geophysical Research Abstracts, v. 11, p. EGU2009-11180.
- Snyder, D. B., and M. Barazangi, 1986, Deep crustal structure and flexure of the Arabian plate beneath the Zagros collisional mountain belt as inferred from gravity observations: *Tectonics*, v. 5, p. 361–373, doi:[10.1029/TC005i003p00361](https://doi.org/10.1029/TC005i003p00361).
- Stöcklin, J., 1968, Structural history and tectonics of Iran: A review: *AAPG Bulletin*, v. 52, p. 1229–1258.
- Talbot, C. J., and M. Alavi, 1996, The past of a future syn-taxis across the Zagros: Geological Society (London) Special Publication 100, p. 89–109.
- Tator, B. A., 1960, Photo interpretation in geology, in R. N. Colwell, ed., *Manual of photographic interpretation*: Washington, DC, American Society of Photogrammetry, p. 169–342.
- Tearpock, D. J., and R. E. Bischke, 2003, *Applied subsurface geological mapping*: New Jersey, Prentice Hall, 822 p.
- Ziegler, M. A., 2001, Late Permian to Holocene paleofacies evolution of the Arabian plate and its hydrocarbon occurrences: *GeoArabia*, v. 6, p. 445–504.

## Appendix 2

---

***Reif, D., Frehner, M., & Grasemann, B. (under review) Mechanical versus kinematic shortening reconstructions of the Zagros High Folded Zone (Kurdistan Region of Iraq), Northeast Iraq. Tectonics***

---

## Mechanical versus kinematic shortening reconstructions of the Zagros High Folded Zone (Kurdistan Region of Iraq)

D. Reif <sup>a</sup>, M. Frehner <sup>a,b</sup>, B. Grasemann <sup>a</sup>,

<sup>a)</sup> *Department of Geodynamics and Sedimentology, University of Vienna, Althanstrasse 14, 1090 Vienna, Austria*

<sup>b)</sup> *Now at: Geological Institute, ETH Zurich, Sonneggstrasse 5, 8092 Zurich, Switzerland*

### Abstract

This paper compares kinematical and mechanical techniques for the palinspastic reconstruction of a folded belt in collision orogens. The studied area and the reconstructed NE-SW-trending, 50 km long cross-section is located in the High Folded Zone of the Zagros fold-and-thrust belt in the Kurdistan Region of Iraq. The present-day geometry of the cross-section has been constructed from field as well as remote sensing data. In a first step the structures and the stratigraphy are simplified focusing on the identification of the main geometric and rheological parameters controlling the deformation. In a second step, the folding process is numerically “unfolded” resulting in the ideal case in sub-parallel, subhorizontal pre-folding layering. During this dynamic unfolding-simulation also the mechanical properties of the layers are taken into account. We estimated the shortening recorded in the folded cross-section using kinematic models based on a length- and area-balancing, which were constructed using the dip domain method. The results of the kinematic models were compared with two different mechanical models, which consider perfectly welded layer interfaces and the layer-parallel slip respectively. The kinematic shortening estimates range from 4.5% in the SW to 17% in the NE, with a mean value of 11.8%. The shortening estimate of the dynamic unfolding-simulation allowing for interlayer slip agrees with these values, while welded interfaces between the units result in unrealistically high shortening values. We therefore suggest that interlayer slip on local detachment horizons is an important deformation mechanism that controlled the folding processes in the Zagros High Folded Zone.

### 1. Introduction

The estimation of parameters that influence the shortening value calculated from a two-dimensional geological cross-section, such as material properties of a layered stratigraphy is fundamental for understanding the evolution of fold-and-thrust belts in collision orogens. In this work we perform dynamical unfolding-simulations using a mechanical finite element model and correlate the results with parameters derived from geometrical restoration (constant length and area balancing) of the same cross-section.

There is a large number of numerical studies investigating the evolution of geological folds, but most of them consider a forward directed time evolution. Only very few consider the time-reverse approach (Schmalholz, 2008; Lechmann et al., 2010), where the folded

geological layers are taken as initial conditions for the numerical simulation and the folding process is reversed. The kinematic unfolding (i.e., constant arc-length) of numerically calculated folds with a known amount of shortening has revealed that the kinematic method underestimates the amount of shortening necessary for a certain fold geometry (Ghassemi et al., 2010; Lechmann et al., 2010). This mismatch is due to the layer-parallel shortening (and layer thickening) prior to folding, which is not accounted for in kinematic constant-arc-length methods. Schmalholz (2008) presented a new method to estimate the shortening history of a folded layer, called dynamic unfolding. This method uses the present-day fold geometry as the initial condition of a mechanical numerical model. This geometry is then unfolded and flattened by applying extensional boundary conditions. In other words, dynamic unfolding can be regarded as a reverse-time simulation. It has been shown that this method successfully unfolds two-dimensional theoretically calculated folds in the case of a linear viscous (Newtonian) or power-law viscous rheology (Lechmann et al., 2010), as well as three-dimensional folds in the case of linear viscous rheology (Schmalholz, 2008). Despite these successful theoretical studies, dynamic unfolding has to our knowledge only been applied once to a natural fold in Lechmann et al. (2010).

In this study, the concept of mechanical restoration is applied to a two-dimensional 50 km long NE-SW-directed cross-section through the Zagros High Folded Zone in the Kurdistan Region of Iraq, NE from the city of Erbil (Figure 1 and 2). This area is dominated by harmonic folding of mainly Mesozoic to Paleogene and Neogene rocks, which form open anticline and syncline fold trains without any evidence of significant faulting, which has been confirmed by various seismic cross sections (personal communication, Herwig Peresson, OMV, 2010). To the NE of the study area the synclines become closed and thrusting dominated the shortening process. In comparison to the Iranian part of the Zagros fold-and-thrust belt, the study area is missing a thick salt horizon that serves as one major detachment surface. The Hormuz Salt, which is forming the main detachment in the SE part of the Iranian Zagros, is thinning towards the NW (e.g. Mouthereau et al., 2007).

The aim of this paper is to use the High Folded Zone in the NW Zagros as an ideal example for testing various kinematic and mechanic reconstruction techniques and to derive important parameters which controlled the shortening and folding.

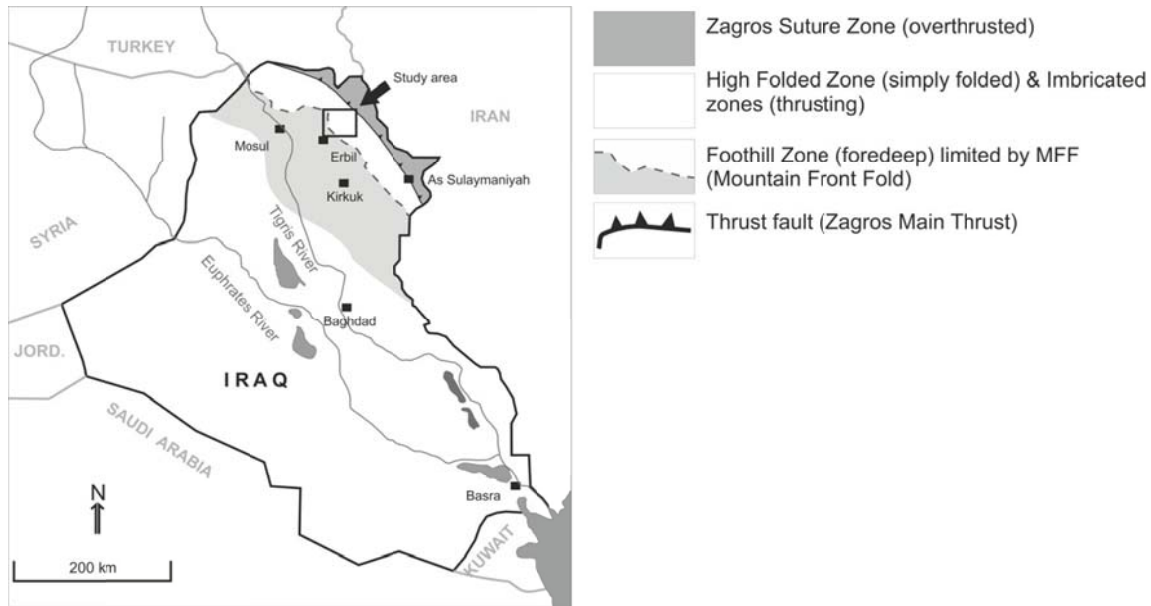


**Figure 1: Position of the studied area in the High Folded Zone of the Zagros fold-and-thrust belt. The thick dotted line denotes the MFF (Mountain Front Fault).**

The Zagros Mountains extend for about 1800 km in NW-SE direction and are bordered by the Central Iranian Plateau in the NE, the Taurus Mountain range in Turkey in the NW, the Oman Fault in the SE, and the Persian Gulf foreland in the SW (Talbot and Alavi, 1996), forming a major segment of the Alpine-Himalayan Orogeny (Figure 3). The orogeny started to form in the Upper Cretaceous, following the collision between the Arabian and Eurasian plates as a result of the closure of the Neotethys oceanic basin (Berberian, 1995; Talbot and Alavi, 1996). The shortening between the Arabian and Eurasian plates, whose horizontal velocity still reaches 2-2.5 cm/a, is partitioned into S-SW directed folding and thrusting of the Tethyan sediments and NW-SE to N-S trending dextral strike-slip faulting (McQuarrie et al., 2004). Deposition of the ~8 km thick sedimentary sequence, which rests on a Precambrian polymetamorphic basement (Jassim and Goff, 2006), started in the Upper Permian to Upper Triassic, reflecting continental rifting along NW-SE striking normal faults and the opening of the Neotethyan Ocean (Alavi, 2004 and references therein). During the Cretaceous, NE-directed subduction of Neotethys started, followed by SW-directed obduction of ophiolites and the uplift of the inner Zagros Orogeny (Hooper et al., 1995). As a result of ongoing subduction the Neotethys closed in the Miocene. In the Pliocene to Pleistocene, continent-continent collision between the Arabian and Eurasian plates resulted in the main phase of the Zagros orogenic compression and the development of the fold-and-thrust belt (Homke et al., 2004). Locally, Permian to Triassic normal faults were reactivated in the basin, leading to inversion of the overlying sedimentary cover in small basins and the formation of ejective anticlines (i.e., compressive reactivation of older faults bounding large elongated tilt blocks (e.g., Numan et al., 1998)).



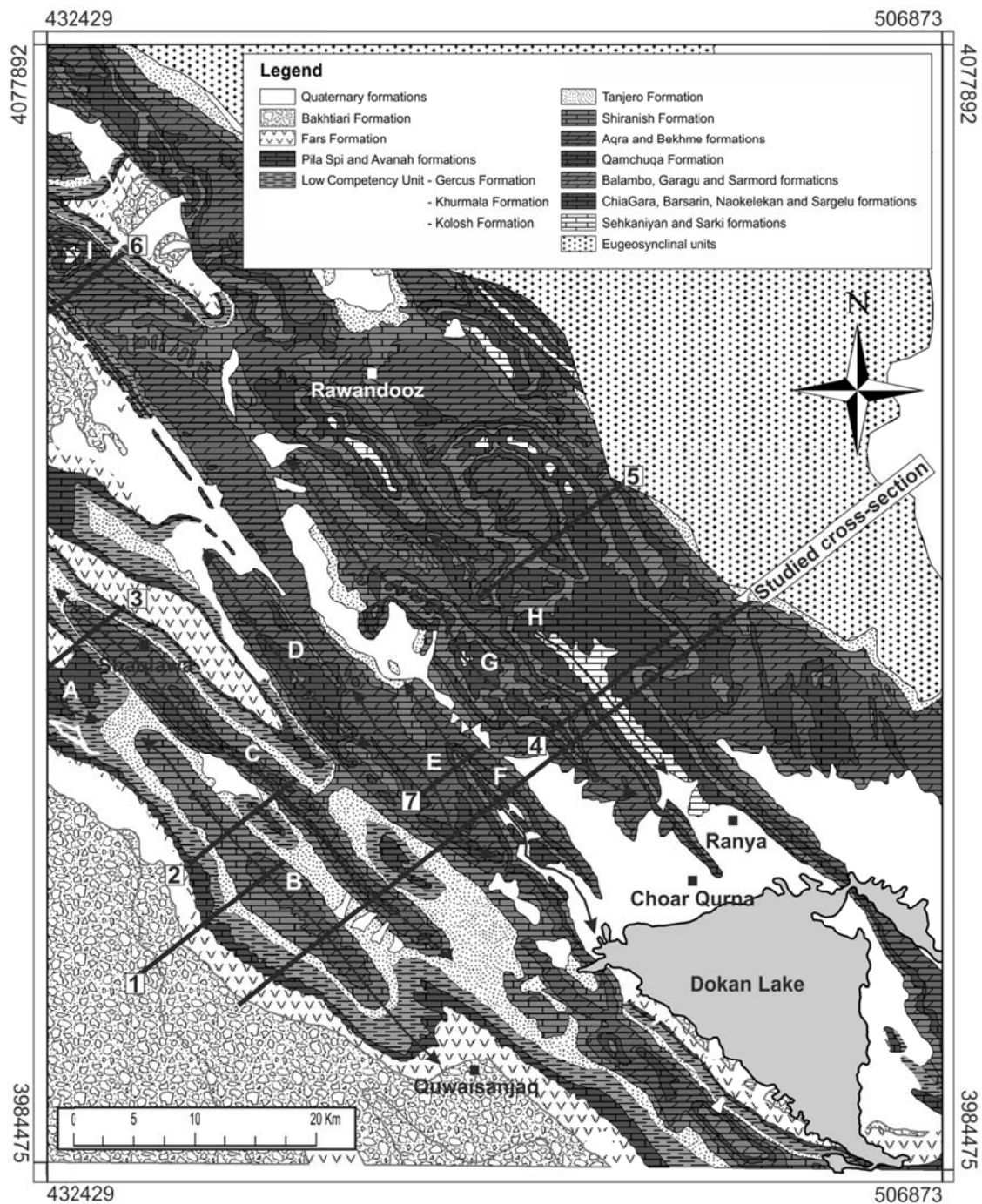


Figure 2: Geological map of the area (modified after (Sissakian et al., 1997) with the position of the studied, 50 km long cross-section and shortening values kinematically calculated from short balanced cross-sections. Between the Foothill Zone in the SW and the High Folded Zone there is a significant increase (~10%) of shortening over a short distance. The studied anticlines are indicated: A – Permam Anticline, B- Bana Bawi Anticline, C- Safeen Anticline, D- Shak Rook Anticline, E- Kamosk Anticline, F- Pelewan Anticline, G- Makook Anticline, H- Ranya Anticline and I- Peris Anticline. The shortening of the numbered cross-sections: 1- 4.5%, 2- 14%, 3- 14%, 4- 15.3%, 5- 16.9%, 6- 14.6% and 7- 13.5%. Coordinates are in WGS1984, Zone UTM 38N.

## 2. Geological setting

### 2.1 Tectonic setting

The Zagros fold-and-thrust belt hosts more than 5% of the world's hydrocarbon reserves, mostly in anticlinal traps. In the Kurdistan Region of Iraq it is divided into four NW-SE striking tectonic units (Figure 1, Jassim and Goff, 2006): the Zagros Suture, the Imbricated Zones, the High Folded Zone (equivalent to the Simply Folded Belt in the Iranian part of the Zagros, Berberian, 1995) and the Foothill Zone. The boundary between the High Folded Zone and the Foothill Zone is marked by a regional morphotectonic feature, the Mountain Front Fault, delineated by a clustering of seismic events, which causes a sudden change in the level of exposed sedimentary layers. The Mountain Front Fault (Figure 1) is trending parallel to the Zagros Belt and is interpreted as a result of the reactivation of Zagros basement structures (Berberian, 1995; Jassim and Goff, 2006; McQuarrie, 2004).

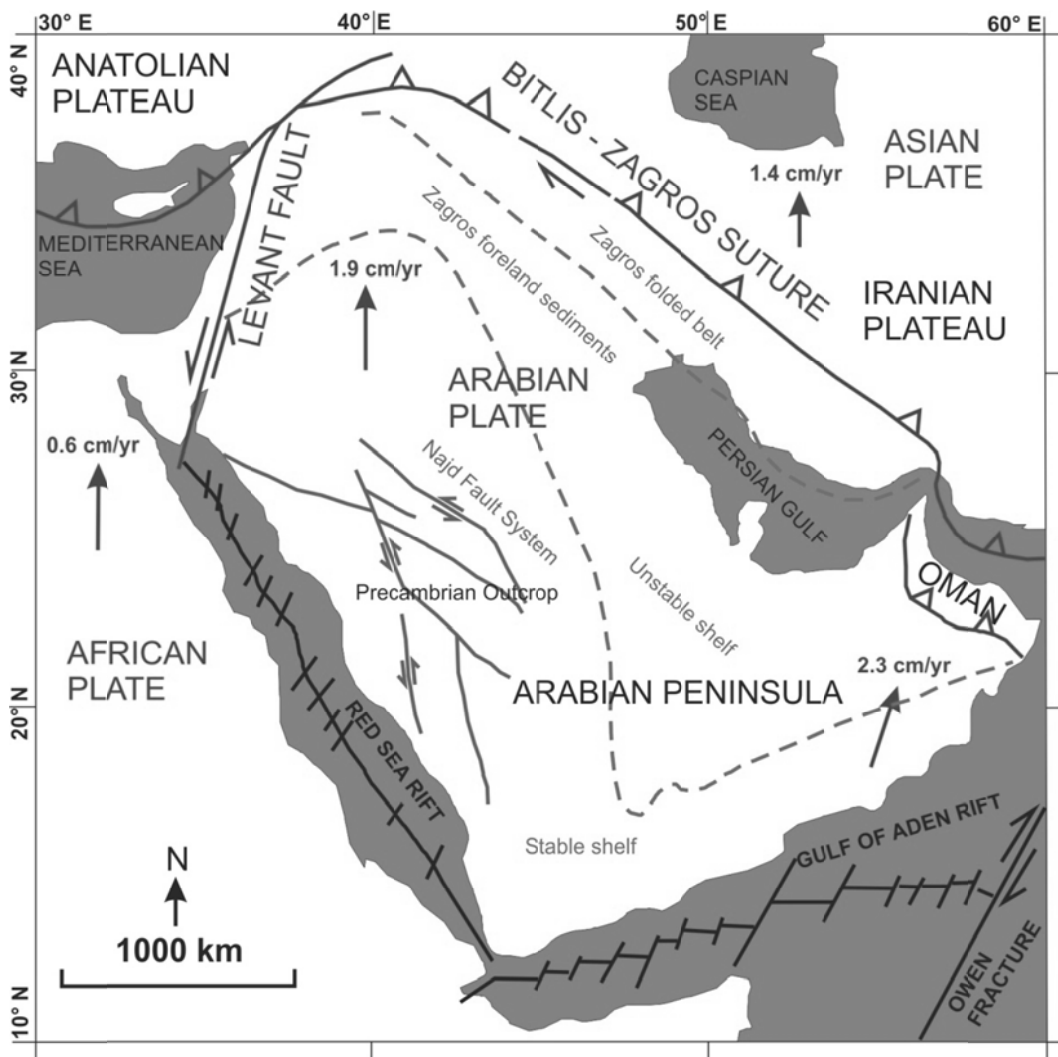


Figure 3: Tectonic setting of the Middle East. The convergence rates are based on recent GPS measurements (Hessami et al., 2006)

The fold-and-thrust belt in the Kurdistan Region of Iraq is dominated by open to gentle folding, with a characteristic wavelength of 5-10 km, therefore considerably lower than the average values of 15-25 km in the SE parts of the Zagros fold-and-thrust belt (Mouthereau et al., 2007), and amplitudes of less than 2.5 km. The two main reasons for this difference in fold-wavelength are the absence of major faults and the absence of thick salt horizons. For example, the Neo-Proterozoic Hormuz salt overlying the crystalline basement in the SE part of the Iranian Zagros, which acts as a ductile detachment during deformation (Mouthereau et al., 2007) is absent in the NW part of the Zagros, where our study area is located.

## 2.2 Lithostratigraphy

The fold trains in the investigated area comprise Cretaceous to Cenozoic sediments consisting mainly of limestone, dolomite, sandstone, siltstone, claystone and conglomerate. In the Iranian part of the Zagros fold-and-thrust Belt, Sepehr et al. (2006) noted that the mechanical anisotropy of the formations due to interlayering of relatively competent (massive dolomite and limestone) and incompetent (claystone, siltstone and shale) sediments strongly controls the style of folding. In context with the natural sediments we use "competence" to semi-quantitatively describe the degree of resistance of rocks to either erosion or deformation in terms of their relative mechanical strength. Additionally, the folding is influenced by a few low-shear-strength layers that may act as local detachment horizons. For example, the Miocene to Pliocene Lower Fars (also known as Fatha) Formation contains thin layers of claystone and evaporite (gypsum and anhydrite) and directly overlies the uppermost layer of the modelled cross-section. Another possible local detachment is found in the Lower Jurassic Sehkanian and Sarki Formations (De Vera et al., 2008), consisting mainly of limestone and dolomite, but also containing thin-bedded shale. The lowermost layer of the modelled cross-section directly overlies this possible local detachment horizon. However, these low-shear-strength layers are not capable of acting as large-scale detachment horizons, and are therefore not to be compared with the much thicker Hormuz salt in the Iranian part of the Zagros Mountains. In the following, the lithostratigraphic formations found in the cross-section are described in detail from the oldest to the youngest formation (Table 1, Figure 4):

Unit 1: Starting in the Middle Jurassic, the formations Sehkanian, Sargelu, Naokelekan/Sargelu, Barsarin and Chia Gara were grouped in one competent unit. The thicknesses of the different formations in the study area are: Sehkanian ~170 m, Sargelu ~150 m, Naokelekan/Sargelu ~150 m, Barsarin ~80 m, and Chia Gara ~230 m, resulting in a total thickness of 630 m. The Sargelu Formation is a thin-bedded, blackish, bituminous and dolomitic limestone and black shales with streaks of thin black chert. The Naokelekan Formation comprises three units: the lower unit consisting of laminated argillaceous bituminous limestone alternating with shale and fine-grained limestone; the middle unit consisting of thin-bedded dolomitic limestone; and the upper unit consisting of thin-bedded bituminous dolomite and limestone with black shale beds in the lower parts. The Barsarin

Formation consists of limestone and dolomitic limestone, which is locally rich in cherts. The Chia Gara Formation comprises thin-bedded limestone and calcareous shale.

Unit No.	Formations	Lithology	Age	Thickness [m]	Unit thickness [m]
8	Pila Spi	well bedded limestone	Eocene	120	300
	Avanah			180	
7	Gercus	black claystone, siltstone, limestone, red sandstone and claystone	Paleocene - Upper Eocene	80	585
	Khurmala			105	
	Kolosh			400	
6	Tanjero	khaki siltstone and claystone with conglomerate	Upper Cretaceous	300	300
5	Shiranish	well bedded limestone and blue marl	Upper Cretaceous	280	280
4	Kometan	well bedded to massive limestone (marly limestone)	Upper Cretaceous	20	200
	Aqra-Bekhme			180	
3	Qamchuqa	massive limestone, dolomite	Lower Cretaceous	660	660
2	Lower Balambo	marly limestone, marl, bedded limestone, dolomite	Lower Cretaceous	170	280
	Lower Sarmord			110	
1	Chia Gara	mainly bedded to massive dolomite, limestones and marl	Upper Jurassic	230	630
	Barsarin			80	
	Naokelekan/Sargelu			150	
	Sehkanian			170	
Profile thickness [m]					3235

**Table 1: Formations grouped in the modelled units with their average thickness and lithology (according to Sissakian et al., 1997), starting from the youngest to the oldest sediments. The less competent units are marked grey and the competent units white.**

Unit 2: This competent unit groups the formations of the Lower Cretaceous, namely the Lower Sarmord, and the Balambo Formations with an overall thickness of 280 m. The Lower Sarmord with a thickness which varies from 100 to 250 m comprises bluish and brown marls with beds of argillaceous limestone. The Balambo Formation consists of thin-bedded limestone with dark layers of green marl and dark blue shale. There is no evidence of Balambo Formation in the boreholes Shorish-1, NE of Erbil and Bana Bawi-1 on top of the Bana Bawi anticline (Herwig Peresson, OMV, 2010, personal communication).

Unit 3: This unit consists of the competent Lower Cretaceous Qamchuqa Formation with a thickness varying between 600 and 800 m. The formation comprises detrital and argillaceous limestones, which are partly dolomitized. The thickness of the Quamchuqa Formation in the studied cross-section is 660 m.

Unit 4: With thickness of 200 m the Upper Cretaceous Aqra-Bekhme Formation and locally the Kometan Formation (thin-bedded grey limestone with chert concretions) represent the competent Unit 4. Although the Kometan Formation reaches a thickness of up to 500 m (Jassim and Goff, 2006) it is only 20 m thick in the borehole Shorish-1 (Herwig Peresson, OMV, 2010, personal communication). The Aqra-Bekhme Formation comprises massive dolomitized limestone locally impregnated with bitumen.

Unit 5: The Upper Cretaceous Shiranish Formation defines Unit 5 with a thickness of ~280 m. It comprises thin-bedded marly limestone with high pyrite content (Lower Shiranish) and blue pelagic marls (Upper Shiranish). Towards NE this formation gradually passes into the Tanjero Formation (Jassim and Goff, 2006).

Unit 6: The overlying competent Upper Cretaceous Tanjero Formation has not been found in the boreholes Shorish-1 (Herwig Peresson, OMV, 2010, personal communication), but has been mapped in the investigated area (Sissakian et al., 1997). The thickness of the formation is very variable reaching locally 2000 m (Jassim and Goff, 2006). In the studied cross-section the Tanjero Formation is 300 m thick where the lower parts consists of claystones with conglomerate layers and the upper parts consists of siltstone beds.

Unit 7: Unit 7 comprises three different incompetent formations, Kolosh, Khurmala and Gercus, with significantly different mechanical behaviour. The oldest two formations, Kolosh and Khurmala, are of Paleocene age. The Kolosh Formation is about 400 m thick in the cross-section, but only about 300 m in the close by Kirkuk-117 borehole (Jassim and Goff, 2006). In the field the Kolosh Formation shows evidences of shear deformation between the underlying Cretaceous limestones and overlying competent Unit 8 (Avanah and Pila Spi limestones). This clastic formation comprises black claystone and shale with thin limestone beds occurring at the top of the formation. The calcareous beds of the Paleocene Khurmala Formation are inter-fingering or overlies the Kolosh Formation. The Mid-Upper Eocene Gercus Formation comprises molasse sediments deposited after the Mid Eocene surface uplift (Jassim and Goff, 2006) and contains red sandstone and claystone with some thin-bedded limestone.

Unit 8: This competent unit contains the Pila Spi Formation with a thickness of 120 m. This generally well bedded Mid-Upper Eocene limestone is sandwiched between the underlying Gercus and the overlying Lower Fars Formations, both of which are less resistant to weathering. Therefore, the Pila Spi Formation frequently develops topographic ridges throughout the Zagros Highly Folded Zone. In the investigated area the nummulitic Eocene Avanah Formation occurs in the basal part of the Pila Spi Formation (Jassim and Goff, 2006).

### 2.3 Structural style

Overall, the intensity of deformation increases northeastwards from the Persian Gulf foreland, where strata are undeformed and lie horizontally to the Zagros Highly Folded Zone, which is characterized by double plunging sub-cylindrical folds, gentle to open in the SW and close to locally SW-overtaken in the NE. The intensity of deformation continues to increase further to the NE, where thrust faulting is dominant in the Imbricated Zones. This deformation pattern suggests that the deformation front has migrated through time from the NE to its present position approximately in the centre of the Persian Gulf foreland (Alavi, 1994). The sedimentary column in the studied region has a total thickness of about 9-10 km and most of the younger sediments (Upper Triassic and younger) have been folded without evidences of major thrusting or large-scale detachment horizons in the High Folded Zone. However, the individual layers feature some competence differences relative to each other. On a local scale,



in the inner arc of the neutral surfaceshortening is accommodated by SW- and NE-directed blind thrusting with a strong displacement gradient and maximum offsets less than a few tens of meters. Occurrence of S- and Z-shaped higher-order folds have been only observed in less competent layers, where evidences for shear deformation like scc'-like geometries (Passchier and Trouw, 2005) and layer-parallel slickensides are locally preserved. They originate from shearing caused by the relative displacement between the competent thick, massive limestone layers that control the deformation.

A large number of thin, incompetent layers between the thick, competent Units, as in a case of the Upper Shiranish Formation (interlayering of blue marl and limestone), favours development of asymmetric higher-order folds, because they have a larger amplification rate and thus require less shortening in order to develop (Frehner and Schmalholz, 2006).

### **3. Balanced cross-sections**

#### **3.1 Derivation of dip domains**

More than 2000 measurements of bedding orientations and fracture systems were taken in the Zagros High Folded Zone during field studies, mostly from road-cuts. Although security in this part of the Zagros Mountains is much better than elsewhere in Iraq, off-road access was severely restricted due to contamination of the area with landmines and unexploded ordnance. Thus only a few short cross-sections, mostly along main roads oriented perpendicular to the trend of the fold axes, could be measured.

During the field work dip directions and angles of the limbs of six anticlines were measured in detail. Except for the symmetric and upright Permian Anticline, the measured folds are clearly asymmetric SW-vergent, with steeper SW-dipping forelimbs and shallower NE-dipping backlimbs (Figure 5). To complement structural measurements from the field campaign and to fill measurement gaps in inaccessible areas, remote sensing techniques were developed for extracting the sedimentary bedding orientation from the 15 m horizontal and 8 m vertical resolution ASTER (Advanced Spaceborne Thermal Emission and Reflection Radiometer) digital elevation model (Reif et al., 2011). Due to differences in erosion resistance, the more resistant lithologies form sharp ridges with steeply sloping sides along the eroded flanks of the anticlines (Burtscher et al., 2010). These hogbacks, up to several 100 m high, form triangular shaped flanks outlining the dip of the strata and can easily be identified in the digital elevation model.

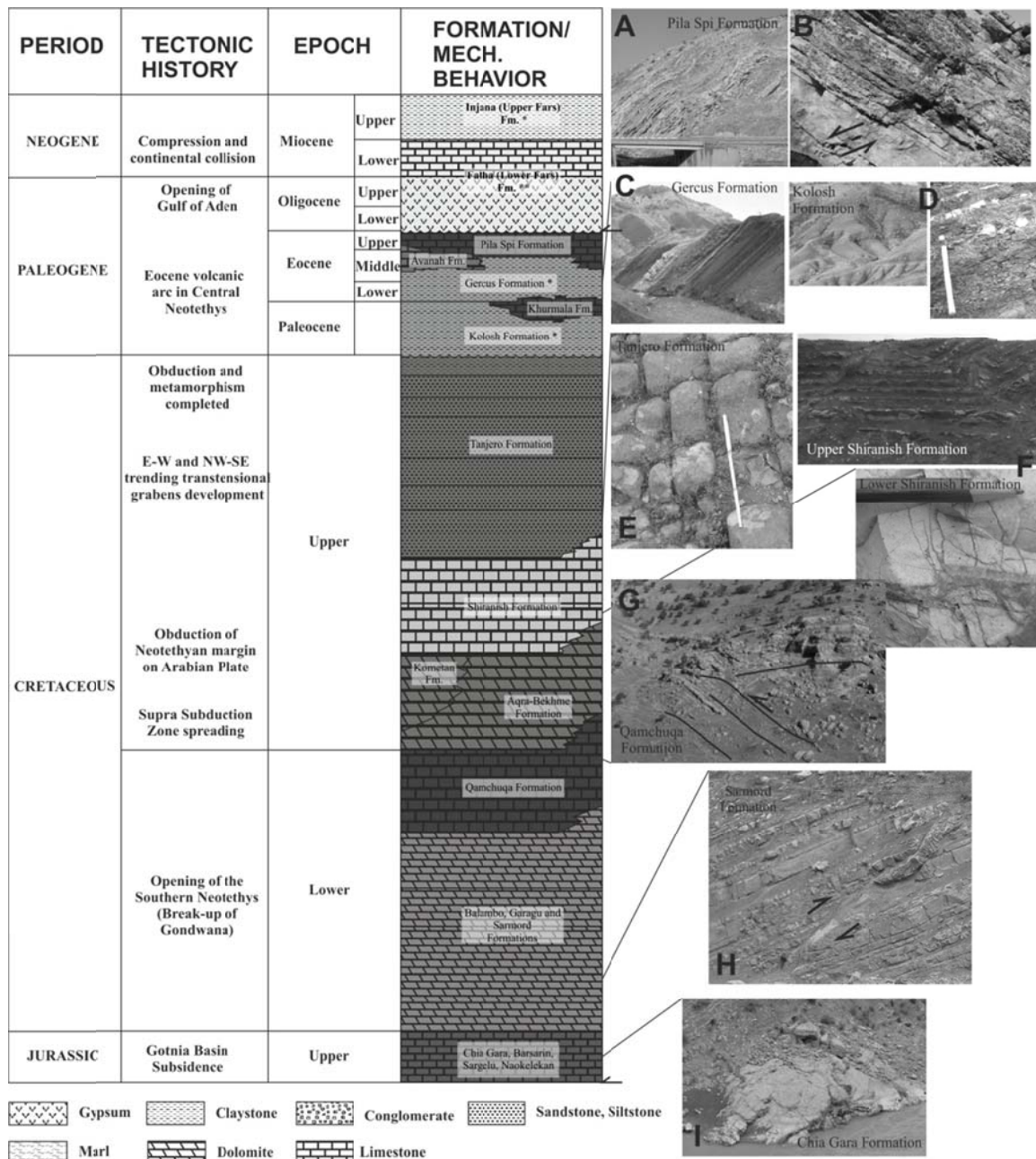


**Figure 4:** Stratigraphic column (modified from Sissakian et al., 1997) divided according to the modelled units showing the deformation style that characterizes each unit. The Lower Fars Formation on top is a possible local detachment horizon (marked with two asterisks) and was not modelled. Incompetent formations are marked with an asterisk. The black arrows denote location of possible local detachments. The photos on the right side show typical outcrops of the formations in the study area and black arrows indicate the movement direction on the faults. Coordinates of the photos (WGS1984 Zone UTM 38N): (A) Bana Bawi Anticline, E 439704 N 4014896, facing NNW; (B) Bana Bawi Anticline, E 451948 N 4009126, facing NW; (C) Safeen Anticline, E 439545 N 4029915, facing NW; (D) Bana Bawi Anticline, E 440734 N 4017745, facing NW; (E) Safeen Anticline, E 425857 N 4036266, facing NE; (F) Bana Bawi Anticline, E 434043 N 4030569, facing NW; (G) Bana Bawi Anticline, E 443959 N 4016367, facing NW; (H) Peris Anticline, E 435059 N 4060560, facing SSE; (I) Peris Anticline, E 432111 N 4058661, facing NW.

### 3.2 Construction of kinematically balanced cross-section

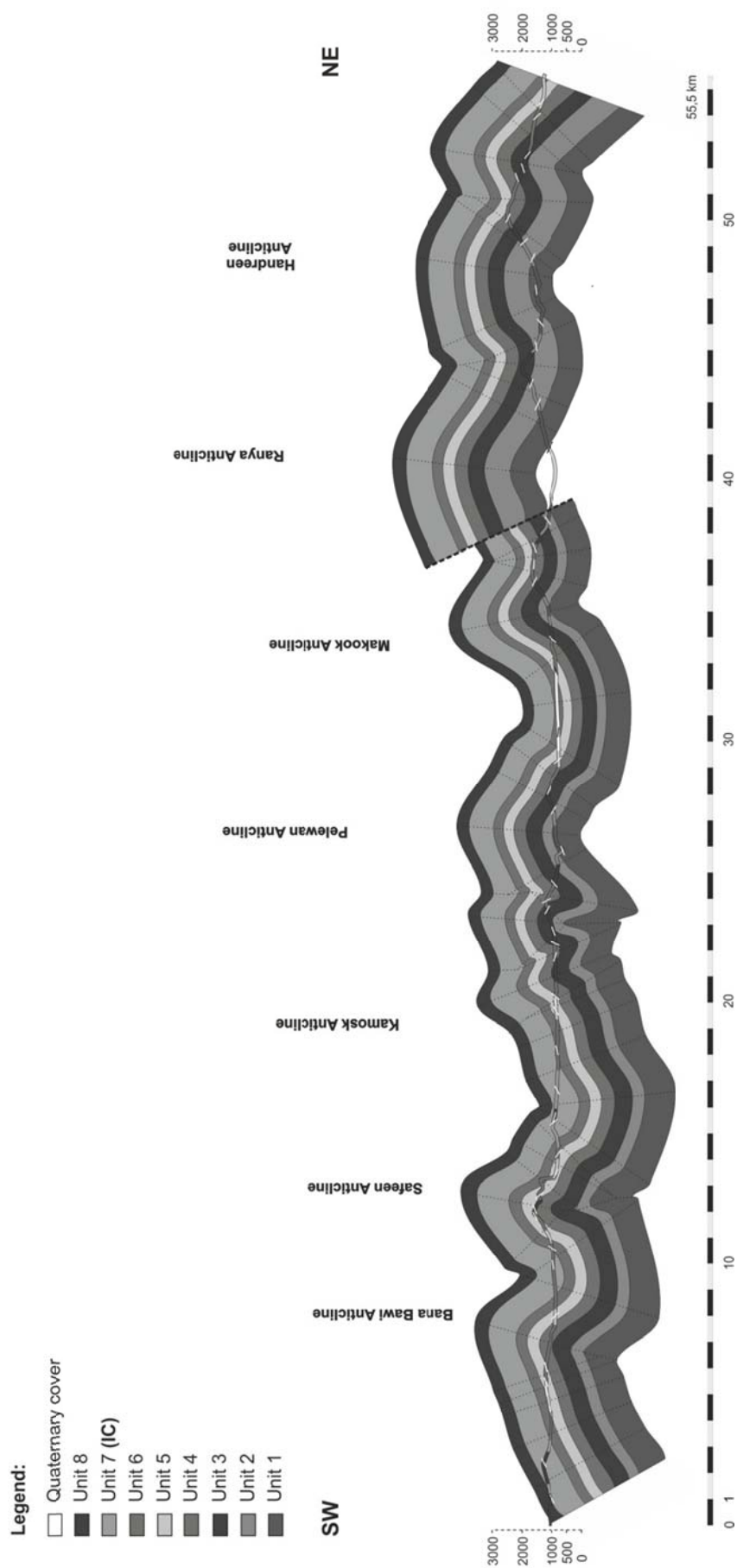
For the profile construction, the constant dip domain method was used (Tearpock and Bischke, 2003). This method separates domains of similar dip angles across a folded region with axial planes bisecting the dip angle between neighbouring domains. By including the previously mapped lithological boundaries and assuming that the surface dip of the bedding reflects also the dip of the underlying sediments, a line- and area-balanced cross section has been constructed. The thickness of the various formations (Table 1) is not very well constrained and was estimated from surface outcrops in the field, borehole information in the area, and the literature (see Jassim and Goff, 2006). The resulting bulk thickness of the cross-section is 3440 m. The cross-section contains only one major fault in the NE part of the section between the Ranya and Makook Anticlines (Figure 5). This fault is most probably a part of a NW-SE-oriented fault zone, which probably connects with the High Zagros Fault, which divides the Imbricated Zone from the High Folded Zone (Casciello et al., 2009).

In the SW of the cross-section the first major anticline emerging from the foreland is the Bana Bawi (Figure 5). The forelimb is dipping with  $\sim 25^\circ$  towards SW. According to the field measurements, the backlimb has a mean dip of  $\sim 45^\circ$  towards NE. The Bana Bawi Anticline is separated by a narrow syncline from the Safeen Anticline, whose forelimb has a mean dip of  $\sim 60^\circ$  towards SW. A broad syncline with a mean dip of both limbs of  $\sim 27^\circ$  separates the SW-verging Kamosk Anticline and the slightly NE-verging Pelewan Anticline,. Between the Pelewan Anticline and the adjacent SW-verging Makook Anticline there is again a broad syncline with  $\sim 25^\circ$  mean dip of both limbs. Between the Makook backlimb (mean dip of  $\sim 30^\circ$ ) and the Ranya Anticline a thrust marks the border between the High Folded Zone and the Imbricate Zones. The exact location, the dip angle and the offset of this NW-dipping thrust are unknown because no outcrops have been spotted in the field.

---

**Figure 5 (next page):** Balanced cross-section constructed from field and remote sensing data using the classic dip domain method. The incompetent unit is marked with “IC”. The lithology of the various units is shown in Figure 1 and Figure 4, the location of the cross-section in Figure 2. The offset of the thrust fault in the NE part of the profile is unknown.

---



#### 4. Dynamic unfolding of the cross-section

To perform dynamic unfolding-simulations several steps are necessary to transform the two-dimensional profile into a numerical model. These steps are:

1. Choose an appropriate part of the profile  
Because a continuum mechanics formulation is used in the numerical model, only the part of the profile is used that is not intersected by faults.
2. Cut profile at fold axial planes  
The numerical model uses vertical traction-free boundary conditions at both ends of the folded profile. Therefore, the profile has to be cut at positions where vertical tractions are expected to be smallest, which is along fold axial planes.
3. Assign rheology and material parameters  
This is probably the most difficult step, because the material behaviour of the modelled rock units is not known from laboratory testing. Therefore, rheological flow laws and the corresponding material parameters have to be assigned based on field observations and comparison with similar lithologies from the literature (e.g. Vanoni, 2006).

The goal of this study is to investigate first-order effects and, as suggested by Lechmann et al. (2010), to provide a guide which areas a future field campaign should focus on. Therefore, the relatively basic incompressible linear viscous rheology is used for all layers, and only two different viscosity values (herein called competent and incompetent), with a viscosity ratio of 1:100 are assigned. Based on the field investigations (Figure 4 and 5, Table 1), only layer 7 could be identified as incompetent. Two dynamic unfolding simulations were conducted: (1) with all layer interfaces perfectly welded and (2) with layer interfaces that allow for slip between the layers. This slip condition is modelled by introducing thin incompetent layers at the layer interfaces. The resulting initial model setups for the dynamic unfolding-simulations are shown in Figure 6.

As the numerical technique to solve the incompressible linear viscous force balance equations, the finite element method is used. The profile is discretized with an unstructured high-order triangular element mesh (Figure 6). The particular code used here is described in detail and applied to fold development in Frehner and Schmalholz (2006) and Frehner (2011). Extensional traction-free pure-shear boundary conditions (i.e., constant horizontal strain rate) were applied on the left and right boundaries (Figure 6) to numerically unfold the profile. At the bottom and top boundaries traction-free boundary conditions and free surface boundary conditions were applied, respectively. However, these two boundaries were set far enough away from the actual fold profile to minimize boundary effects from these two boundaries. The space above and below the fold profile was defined as incompetent (Figure 6).



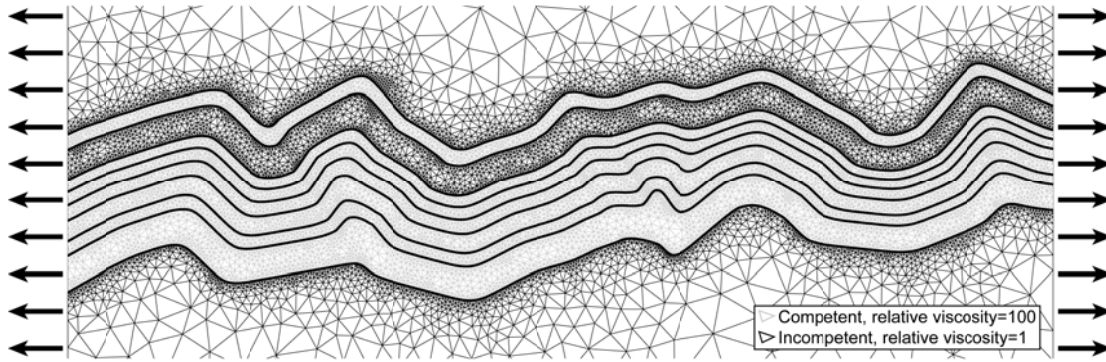


**Figure 6:** Initial model setup and triangular finite-element mesh for the two dynamic unfolding-simulations. For the first simulation, the layer interfaces are perfectly welded. For the second simulation, thin incompetent layers are introduced at the layer boundaries to simulate slip between the layers.

Prior to the dynamic unfolding-simulations the same part of the folded profile was kinematically unfolded (Figure 7). For this a constant length of the individual layer interfaces and no layer-parallel shortening or extension during folding was assumed. By comparing the original length and the unfolded length of the profile the extension of the unfolding,  $e$ , can be calculated as

$$e = (L - L_0) / L_0 . \quad (1)$$

In Equation (1)  $L$  is the unfolded length and  $L_0$  is the original length of the profile. From this value the horizontal shortening,  $s$ , can be calculated that transforms the unfolded geometry back into the folded profile, i.e.,

$$s = -(L_0 - L) / L = e / (1 + e) . \quad (2)$$

In the following, only the shortening is considered because it is geologically much more relevant than the corresponding extension of the unfolding (i.e., reverse-time) calculation. In Figure 7, the calculated shortening differs for the different layer interfaces and ranges between 8.4% and 12.3%, with an average value of 11.0%.

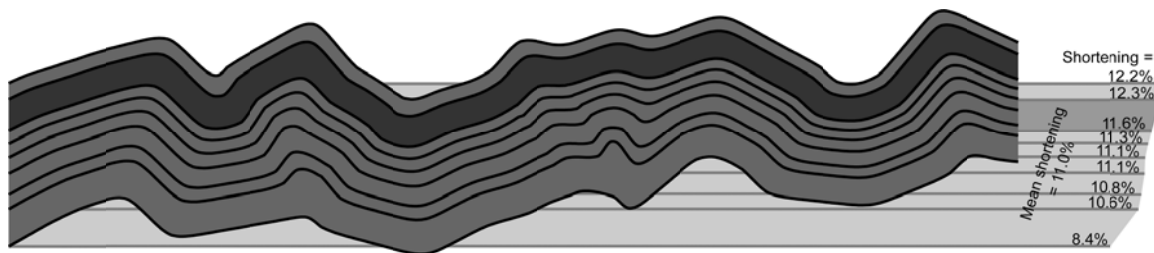


**Figure 7:** Kinematic unfolding (constant arc-length) of the part of the folded profile that is used for the dynamic unfolding-simulations.

Dynamic unfolding-simulations were performed up to a shortening of 11.0% (i.e., kinematic constant-arc-length estimate). The two different model setups (i.e., welded and slip layer interfaces), result in markedly different profile geometries (Figures 8b and c, respectively). Allowing for slip between layers (Figure 8c) leads to a much more efficient dynamic unfolding compared to the case of welded interfaces (Figure 8b), as can be seen by the flat-

lying layers in a large portion of the profile. During the dynamic unfolding-simulations the evolution of the average fold amplitude is calculated. The Mean Amplitude Decrease is defined as  $-(A-A_0)/A_0$ , where  $A$  is the unfolded average amplitude and  $A_0$  is the original average amplitude of the profile. The average amplitude is calculated as the arithmetic mean of the amplitudes of all the layer interfaces. The Mean Amplitude Decrease is 56.9% in the case of slip interfaces and only 41.9% in the case of welded interfaces, which is another expression of the more efficient dynamic unfolding in the case of slip interfaces compared to welded interfaces. As a comparison, a kinematic unfolding calculation is shown in Figure 8a assuming pure-shear deformation. This calculation is equivalent to a dynamic unfolding-simulation with zero viscosity ratio between the layers. In this case the Mean Amplitude Decrease during unfolding is always the same as the amount of shortening (i.e., 11% in Figure 8a).

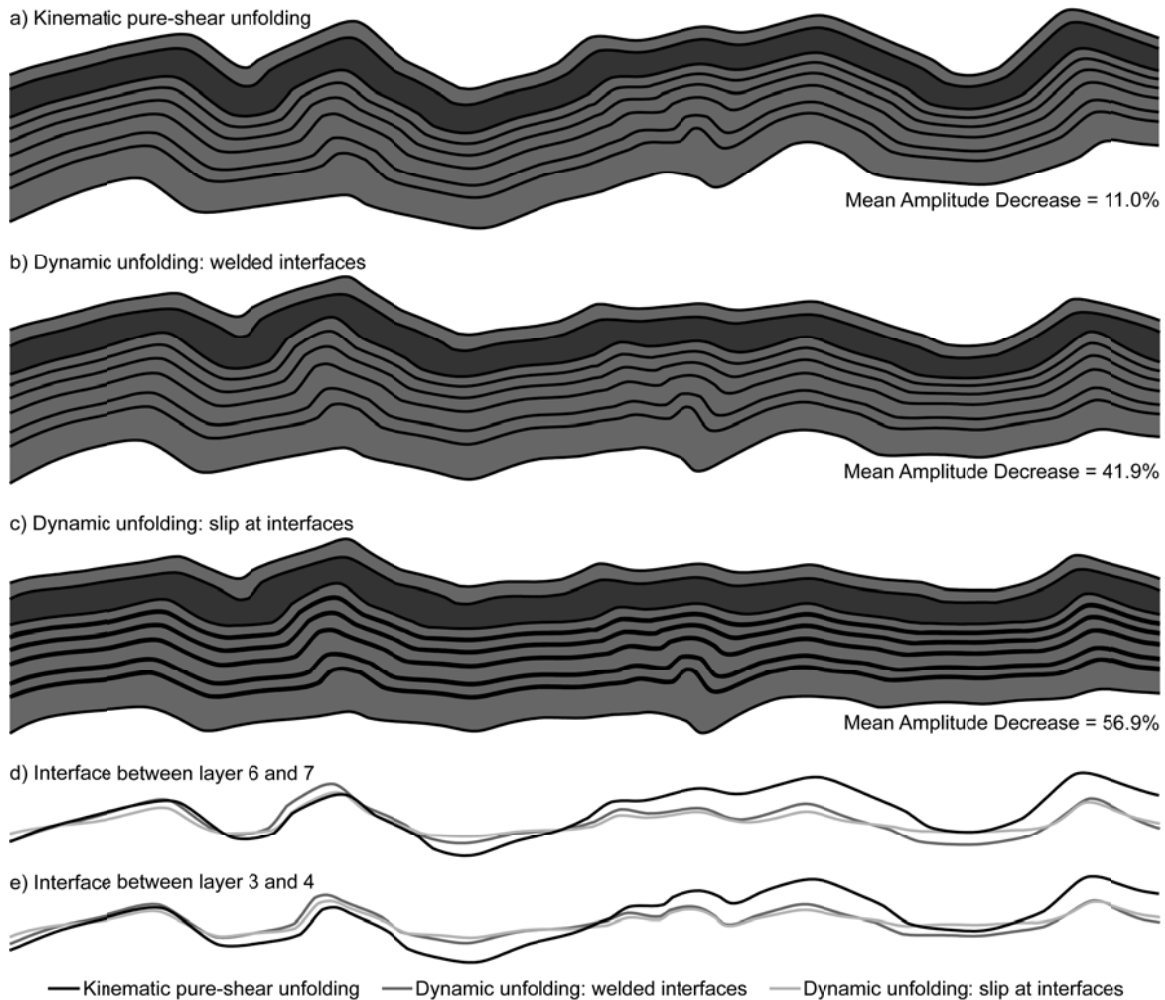


**Figure 8:** Unfolding calculations for a horizontal shortening of 11.0%. The number at the right end of each profile is the Mean Amplitude Decrease during unfolding. a) Kinematic unfolding using pure-shear deformation. b) Dynamic unfolding using perfectly welded interfaces between the layers. c) Dynamic unfolding using slipping interfaces between the layers. For a better comparison between the different calculations the interface between layer 6 and 7 and between layer 3 and 4 are overlain in d) and e), respectively.

The evolution of the Mean Amplitude Decrease during progressive unfolding is depicted in Figure 9 for the different unfolding calculations. In the initial stage, up to a shortening of about 6%, the two dynamic unfolding-simulations result in a similar fast decrease of the average amplitude. After that, the Mean Amplitude Decrease of the simulation with welded layer interfaces slows down significantly and the rate of the Mean Amplitude Decrease (i.e., slope in Figure 9) is comparable to that of the kinematic pure-shear unfolding calculation. At the same time, the rate of the Mean Amplitude Decrease of the simulation with slip layer interfaces stays high during the entire simulation. For example, a Mean Amplitude Decrease of 70% is reached already after a shortening of 16.8% while in the case of welded interfaces, this value is reached only after a shortening of 40.0%. As already noted above, Figure 9 indicates again that the dynamic unfolding is much more efficient for slip layer interfaces than for welded interfaces.

A Mean Amplitude Decrease of 70% is chosen for plotting Figure 10. Besides being a high value, this particular Mean Amplitude Decrease is arbitrarily chosen and has no special physical meaning. Figure 10 clearly shows that in the case of welded interfaces (Figure 10a) much more shortening is necessary to reach the same Mean Amplitude Decrease as in the case of slip layer interfaces (Figure 10b). However, the parts of the profile that are difficult to unfold are the same in both dynamic unfolding-simulations. These few areas still have relatively high fold amplitude while the largest part of the profile is flattened. For continuing dynamic unfolding these problematic zones remain with relatively high amplitude and never completely flatten. The same observation has been made by Lechmann et al. (2010).

## 5. Discussion

The total convergence in the Zagros fold-and-thrust Belt is  $70 \pm 20$  km, which represents 20% of the overall convergence between the Arabian and Eurasian plates (McQuarrie, 2004), and is in Iraq unevenly distributed, increasing from the Foothill Zone in the SW (~5%) through the High Folded Zone (~15%) and the Imbricate Zones (~25%) to the Zagros Suture Zone in the NE. Figure 2 shows shortening values in the Foothill Zone and the High Folded Zone estimated from short balanced cross-sections in the study area.

From kinematic fold restoration calculations in Iran it is generally believed that the Zagros Simply Folded Belt accumulated a horizontal shortening ranging from 7.5% to 17% (e.g. Sherkati, 2006; Molinaro, 2005; Mouthereau, 2007). For a shortening of 16.8%, the dynamic unfolding-simulation using slipping interfaces between the layers exhibit a substantial fold amplitude decrease of 70% (Figures 9 and 10). For the same shortening value, the fold amplitude decrease for welded layer interfaces is only around 45% (Figure 9). In other words, interlayer slip provides more realistic modelling results. A similar conclusion was drawn by Yamato et al. (2011) in the Iranian part of the Zagros fold-and-thrust belt, where a thick layer of Hormuz Salt (Kent, 1979; Bahroudi, 2003) acts as a ductile detachment below the folded sedimentary layer stack. In contrast to the dynamic unfolding-simulations used here, Yamato et al. (2011) used a numerical forward model.

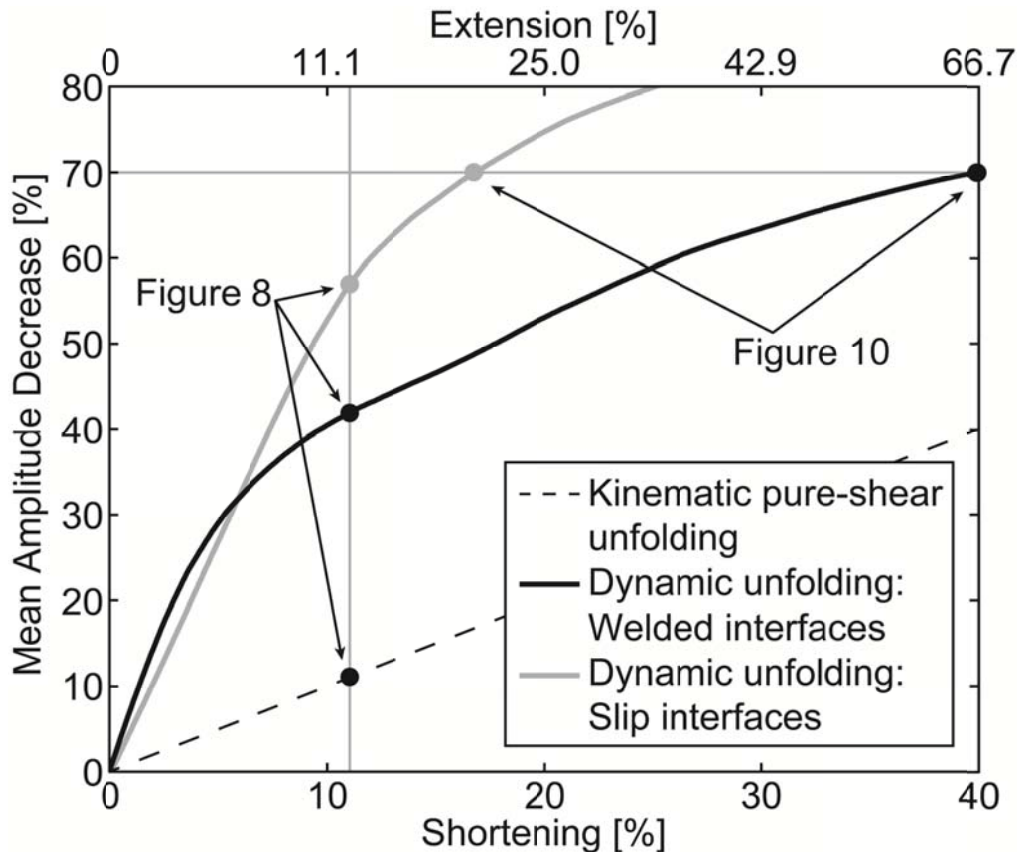


**Figure 9:** Mean Amplitude Decrease during the different progressive unfolding calculations. The dots indicate the position on these evolution-curves for which Figures 8 and 10 are plotted.

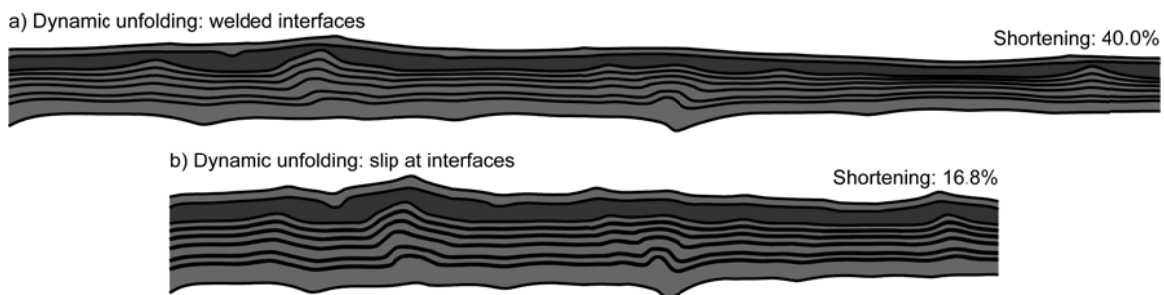


**Figure 10:** Unfolding calculations for a Mean Amplitude Decrease of 70.0%. The number at the right end of the profiles is the shortening necessary for this particular Mean Amplitude Decrease. a) Dynamic unfolding using perfectly welded interfaces between the layers. b) Dynamic unfolding using slipping interfaces between the layers.

They found that their modelled fold wavelength only agrees with the field observations when they introduce weak interlayer detachment horizons in addition to the Hormuz Salt. This observation can be understood from single-layer folding theory (Biot, 1961; Fletcher, 1977). In the presented simulations using welded layer interfaces, the six bottom layers together act as one single competent layer. For the viscosity ratio of 1:100 used in this study a wavelength-to-thickness-ratio of 16.5 is predicted by single-layer folding theory. This corresponds to a wavelength of 40–50 km, which is far off the field observation of 5–10 km. Therefore, the conclusion can be drawn that the six bottom layers together cannot act as a single competent



layer, but there must be interlayer slip that effectively separates these layers. Indeed, there is also evidence for interlayer slip in the field. Besides the already mentioned Kolosh, Upper Shiranish, and Gercus Formations in the upper part of the cross-section, also some of the Jurassic (Naokelekan, Sargelu, Chia Gara) and Cretaceous (Lower Balambo) formations contain thin-bedded shale layers, which may represent low-shear-strength surfaces separating otherwise competent lithologies and allow for interlayer slip between them. In addition, other competent units may include local thin marl or shale layers.

In general, kinematic restoration and unfolding models (e.g., Figure 6) underestimate the amount of horizontal shortening stored in a folded cross-section because they do not include layer-parallel shortening prior to folding initiation (Ghassemi et al., 2010; Lechmann et al., 2010). Dynamic unfolding does include this process. However, for natural fold profiles, dynamic unfolding is not capable of completely flatten the profile (Figures 8, 9 and 10; also Lechmann et al., 2010). Residual fold amplitude always remains, no matter how much the profile is dynamically extended. Therefore, it is necessary to choose a critical residual amplitude (or Mean Amplitude Decrease), at which the dynamic unfolding-simulation is stopped. In this study, for producing Figure 10, a critical Mean Amplitude Decrease of 70% was chosen arbitrarily. This corresponds to a fold amplification of 233% in a forward simulation. Further investigations are necessary to better define the critical residual amplitude that should be used in dynamic unfolding-simulations of natural fold profiles. Indeed, after Lechmann et al. (2010), the presented study is to our knowledge only the second that applies dynamic unfolding to a natural fold profile and the method originally proposed by Schmalholz (2008) is still under development.

Even though dynamic unfolding is not (yet) capable of fully flatten the folded profile, the simulation results are of great importance for planning future field investigations, as for example done by Lechmann et al. (2010). The areas along the profile that retain residual amplitude during dynamic unfolding-simulations behave substantially different in nature than in the numerical model. Deformation processes that may be relevant in nature, but are not included in the model, are for example non-volume-conserving processes, such as solution-precipitation processes, compaction, or dewatering. Also, three-dimensional out-of-plane processes, such as fold-axis-parallel flow, are not included in the model, but may play an important role in nature. Finally, fracturing and faulting during folding, as well as non-linear deformation behaviour may be another reason for the numerical simulation not being able to fully unfold the profile. In a future field campaign, these deformation processes should be specifically investigated in the areas that were identified by the dynamic unfolding-simulations as being difficult to unfold. Some of the above deformation processes, for example non-linear deformation behaviour or three-dimensional deformation, have been tested for their applicability in dynamic unfolding-simulations (Schmalholz, 2008; Lechmann et al., 2010); other processes, such as non-volume-conserving processes or fracturing, still need to be tested on synthetic fold profiles before they are used in dynamic unfolding-simulations of real fold profiles.

## 6. Conclusions

We used a cross-section of the Zagros Simply Folded Belt in NE Iraq constructed from field and remote sensing data for kinematical and mechanical shortening estimation. For the mechanical estimate we performed dynamical unfolding-simulations using a numerical finite element model, taking in account the different competence of the units in the model. A comparison of the results between classical length and area balanced cross-section reconstruction (11% - 15% shortening) and dynamic unfolding-simulations shows that very different shortening values can be calculated. In the kinematical estimates, the internal deformation of the units prior to folding (e.g., layer-parallel shortening, thickening and compaction) is ignored and shortening is generally underestimated. The disadvantage of dynamical unfolding is the absence of faults in the model, so the shortening caused by offset on these structures must be added to the final result. Also, other processes, such as non-volume-conserving and non-linear deformation processes, are currently not included and initially sharp hinges (from the geometric profile construction) are not possible to completely flatten. Therefore, a critical Mean Amplitude Decrease has to be defined that stops the dynamic unfolding-simulations.

We tested two different models for dynamic unfolding, one with welded interfaces between the different units and another with interlayer slip between the units. Besides the difficulties described above, the second model results in realistic shortening values in the range of the highest kinematic estimates. For example, for a critical Mean Amplitude Decrease of 70% a shortening of 16.8% is found. Not allowing for interlayer slip results in unrealistic high shortening values inconsistent with kinematic estimates. This allows concluding that interlayer slip along local detachment horizons is an important deformation mechanism in the Zagros Simply Folded Belt in NE Iraq. Indeed, such thin layers are also described in the lithology of most of the modelled units.

## Acknowledgements

We thank the OMV Exploration and Production Company, Austria, for support and ideas as well as for organising the field work, especially Herwig Peresson, Gabor Tari and Mohammad Fallah. Also many thanks to the employees of the OMV Exploration and Production Company branch office in Erbil, Iraq, for providing support, logistics and security during our stay in Erbil: Dana Mawlood, Hunaar Majeed, Faris Habib Hanna, Ashty A. Karem and many others.

## References:

- Alavi, M., 1994. Tectonics of the Zagros Orogenic Belt of Iran: new data and interpretations. *Tectonophysics*, 229(3-4): 211-238.
- Alavi, M., 2004. Regional stratigraphy of the Zagros fold-thrust belt of Iran and its proforeland evolution. *American Journal of Science*, 304(1): 1-20.
- Bahrudi, A., Koyi, H.A., 2003. Effect of spatial distribution of Hormuz salt on deformation style in the Zagros fold and thrust belt: an analogue modelling approach. *Journal of the Geological Society* 160, 719-733.

- 
- Berberian, M., 1995. Master "blind" thrust faults hidden under the Zagros folds: Active tectonics and surface morphotectonics. *Tectonophysics*, 241: 193-224.
- Biot, M.A., 1961, Theory of folding of stratified viscoelastic media and its implications in tectonics and orogenesis. *Geological Society of America Bulletin*, 72, 1595–1620.
- Burtscher, A., Frehner, M. and Grasemann, B., 2010. Tectonic geomorphological investigations of antiforms using differential geometry (Permian Anticline, Northern Iraq). *AAPG Bulletin*, accepted.
- Casciello, E., Vergés, J., Saura, E., Casini, G., Fernández, N., Blanc, E., Homke, S. and Hunt, D.W., 2009. Fold patterns and multilayer rheology of the Lurestan Province, Zagros Simply Folded Belt (Iran). *Journal of the Geological Society* 166, 947-959.
- De Vera, J., Gines, J., Oehlers, M., McClay K. and Doski, J., 2010. Structure of the Zagros fold and thrust belt in the Kurdistan Region, northern Iraq. *Trabajos de Geología*, 29.
- Emami, H., Vergés, J., Nalpas, T., Gillespie, P., Sharp, I., Karpuz, R., Blanc, E.P. and Goodarzi, M.G.H., 2010. Structure of the Mountain Front Flexure along the Anaran anticline in the Pusht-e Kuh Arc (NW Zagros, Iran): insights from sand box models. *Geological Society, London, Special Publications* 330, 155-178.
- Fletcher, R.C., 1977, Folding of a single viscous layer: Exact infinitesimal-amplitude solution. *Tectonophysics*, 39, 593–606.
- Frehner, M., 2011, The neutral line in buckle-folds. *Journal of Structural Geology*, accepted.
- Frehner, M. and Schmalholz, S. M. , 2006. Numerical simulations of parasitic folding in multilayers. *Journal of Structural Geology*, 28: 1647-1657.
- Ghassemi, M.R., Schmalholz, S.M. and Ghassemi, A.R., 2010, Kinematics of constant arc length folding for different fold shapes. *Journal of Structural Geology*, 32, 755–765.
- Hessami, K., Nilforoushan, F. and Talbot, C.J., 2006. Active deformation within the Zagros Mountains deduced from GPS measurements. *Journal of the Geological Society of London* 163, 143-148.
- Homke, S., Vergés, J., Garcés, M., Emami, H. and Karpuz, R., 2004. Magnetostratigraphy of Miocene-Pliocene Zagros foreland deposits in the front of the Push-e Kush Arc (Lurestan Province, Iran). *Earth and Planetary Science Letters*, 225(3-4): 397-410.
- Hooper, R.J., Baron, I.R., Agah, S. and Hatcher, R.D., 1995. The Cenomanian to Recent development of the southern Tethyan margin in Iran. In: M.I. Al-Husseini (Editor), *Middle East petroleum geosciences*. Gulf Petrolink, Bahrain, pp. 505-516.
- Jassim, S.Z. and Goff, J.C., 2006. *Geology of Iraq*. Dolin, Brno, Czech Republic, 352 pp.
- Kent, P.E. 1979. The emergent Hormuz salt plugs of southern Iran. *Journal of Petroleum Geology*, 2, 117–144.
- Lechmann, S.M., Schmalholz, S.M., Burg, J.-P. and Marques, F.O., 2008, Dynamic unfolding of multilayers: 2D numerical approach and application to turbidites in SW Portugal. *Tectonophysics*, 494, 64–74.
- McQuarrie, N., 2004. Crustal scale geometry of the Zagros fold-thrust belt, Iran. *Journal of Structural Geology*, 26(3): 519-535.
-

- Mouthereau, F., Tensi, J., Bellahsen, N., Lacombe, O., De Boisgrollier, T., Kargar, S., 2007. Tertiary sequence of deformation in a thin-skinned/thick-skinned collision belt: The Zagros Folded Belt (Fars, Iran). *Tectonics*, **26**, TC5006, 28 pp.
- Molinaro, M., Leturmy, P., Guezou, J.-C., Frizon De Lamotte, D. and Eshraghi, S., A., 2005. The structure and kinematics of the southeastern Zagros fold-thrust belt, Iran: from thin-skinned to thick-skinned tectonics. *Tectonics* 24, 19 pp.
- Numan, N.M.S., Hammoudi, R.A. and Chorowicz, J., 1998. Synsedimentary tectonics in the Eocene Pila Spi limestone formation in Iraq and its geodynamic implications. *Journal of African Earth Sciences*, 27(1): 141-148.
- Passchier, C.W., Trouw, R.A.J., 2005. *Microtectonics*, 2nd, Revised and Enlarged ed. Springer-Verlag, Berlin, 336 pp.
- Reif, D., Grasemann, B. and Faber, R., 2011. Quantitative structural analysis using remote sensing data: Kurdistan, Northeast Iraq. *AAPG Bulletin* 95, 941-956
- Schmalholz, S.M., 2008, 3D numerical modeling of forward folding and reverse unfolding of a viscous single-layer: Implications for the formation of folds and fold patterns. *Tectonophysics*, 446, 31–41.
- Sepehr, M., Cosgrove, J. and Moieni, M., 2006. The impact of cover rock rheology on the style of folding in the Zagros fold-thrust belt. *Tectonophysics*, 427(1-4): 265-281.
- Sherkati, S., Letouzey, J. and Frizon De Lamotte, D., 2006. The Central Zagros fold-thrust belt (Iran): new insights from seismic data, field observations and sandbox modelling. *Tectonics* 25, 27 pp.
- Sissakian, V.K., Ibrahim, E.I. and Al-Waily, I.J., 1997. Geological Map of Arbeel and Mahabad Quadrangles Sheets Nj-38-14 and Nj-38-15. In: V.K. Sissakian (Editor). State Establishment of Geological Survey and Mining, Baghdad.
- Talbot, C.J. and Alavi, M., 1996. The past of a future syntaxis across the Zagros. *Geological Society, London, Special Publications*, 100(1): 89-109.
- Tearpock, D.J. and Bischke, R.E., 2003. *Applied Subsurface Geological Mapping*, 2nd ed. Prentice Hall, New Jersey.
- Vanoni, V.A., 2006. *Sedimentation Engineering: Theory, Measurements, Modeling, and Practice*, 2nd edition ed. American Society of Civil Engineers, 424 pp.
- Yamato, P., Kaus, B.J.P., Mouthereau, F. and Castelltort S., 2011, Dynamic constraints on crustal-scale rheology from the Zagros Fold Belt, Iran. *Geology*, Vol 39. No 9. p. 815-818. doi:10.1130/G32136.1



## Appendix 3

---

***Reif, D., Decker, K., Grasemann, B. and Peresson, H., (under review). Fracture patterns in the Zagros fold-and-thrust belt, Kurdistan Region of Iraq. Tectonophysics Special Issue “Into the deformation history of the folded rocks”***

## **Fracture patterns in the Zagros fold-and-thrust belt, Kurdistan Region of Iraq.**

Daniel Reif<sup>1</sup>, Kurt Decker<sup>1</sup>, Bernhard Grasemann<sup>1</sup>, Herwig Peresson<sup>2</sup>

<sup>1</sup> University of Vienna, Department for Geodynamics and Sedimentology, 1090 Vienna, Austria

<sup>2</sup> OMV Petroleum Exploration GmbH, Erbil, Kurdistan Region of Iraq

### **1. Introduction**

#### **1.1 Scope of work**

This work extends the previous studies in the SE part of the Zagros fold-and-thrust belt and examines fracture systems developed in the lesser investigated parts of the NW Zagros, focusing on the area NE of the city of Erbil in the Kurdistan Region of Iraq (Figure 1A). The Zagros fold-and-thrust belt hosts more than 5% of the world's hydrocarbon reserves, mostly in anticlinal traps. However the Kurdish part of the Zagros is only lightly explored with many undrilled oil and gas prospects, mainly because of unstable political situation and security issues, resulting in lack of reliable geological information. In addition to that the mountainous environment may cause technical difficulties in acquiring good quality seismic data hence the outcrop studies become even more important to build a good conceptual model. The outcrops can provide information about the fracture orientation and density at deeper levels (e.g. Jurassic reservoir rocks) and thus are of a great importance. The quality of the outcrops is very good due to predominantly dry climate, lack of vegetation and incidental strong erosion. This makes the area ideal for an outcrop based fracture study as well as for the use of remote sensing methods.

#### **1.2 Previous fracture studies in the Kurdistan Region**

There are to our knowledge no published fracture studies in the Kurdistan Region in Zagros, except for Numan et al., 1998, studying the syn-sedimentary structures of the Pila Spi limestone formation (Figure 2). Therefore only the published tectonic studies from Iran can provide good analogues, ranging from older, sub-seismic fracture studies of numerous folds (McQuillan, 1973) and newer reservoir-scale fracture studies utilising also remote sensing methods (Stephenson et al., 2007) to fieldwork based fracture system studies (Lacombe et al., 2011) and single anticline studies (e.g. Tavani et al., 2011). The stratigraphic nomenclature follows the lithostratigraphic terminology used in the only available geological map of the study area (Sissakian et al., 1997).

### 1.3 The dataset

The acquired data is spread over six neighbouring anticlines (Figure 3) and comprises of joint and fault measurements from 32 outcrops and sedimentary bedding measurements from more than 100 outcrops. The presented observations of the fracture systems (both joints and faults) result from the 32 outcrops and the remote sensing (ASTER satellite images) studies covering the following anticlinal structures: Permian, Bana Bawi, Safeen, Shak Rook and Pelewan. The acquired data comes mostly from the Middle to Upper Eocene Pila Spi and Upper Cretaceous Shiranish formations (Figure 2 and 3). The faults depicted in the single available geological map (Sissakian et al., 1997) of the study area were studied as well. All presented plots are Schmidt's net, equal area, lower hemisphere projections of the data.

## 2. Geological setting and tectonic evolution of the studied area

### 2.1 Regional overview

The Zagros Mountains extend for about 1800 km in NW-SE direction and are bordered by the Central Iranian Plateau in the NE, the Taurus Mountain range in Turkey in the NW, the Oman Fault in the SE, and the Persian Gulf foreland in the SW (Talbot and Alavi, 1996), forming a major segment of the Alpine-Himalayan Orogeny. The orogeny started to form in the Upper Cretaceous, following the collision between the Arabian and Eurasian plates as a result of the closure of the Neotethys oceanic basin (Berberian, 1995; Talbot and Alavi, 1996). The shortening between the Arabian and Eurasian plates, whose horizontal velocity still reaches 2-2.5 cm/a, is partitioned into S-SW directed folding and thrusting of the Tethyan sediments and NW-SE to N-S trending dextral strike-slip faulting (McQuarrie et al., 2004).

Deposition of the approximately 10 km thick sedimentary sequence, which rests on a Precambrian polymetamorphic basement (Jassim and Goff, 2006), started in the Upper Permian to Upper Triassic, reflecting continental rifting along NW-SE striking normal faults and the opening of the Neotethyan Ocean (Alavi, 2004). During the Cretaceous, NE-directed subduction of Neotethys started, followed by SW-directed obduction of ophiolites and the uplift of the inner Zagros Orogeny (Hooper et al., 1995). As a result of an on-going subduction, the Neotethys closed in the Miocene. In the Pliocene to Pleistocene, continent-continent collision between the Arabian and Eurasian plates resulted in the main phase of the Zagros orogenic compression and the development of the fold-and-thrust belt (Homke et al., 2004). Locally, Permian to Triassic normal faults were reactivated in the basin, leading to the inversion of the overlying sedimentary cover in small basins and the formation of ejective anticlines (i.e. compressive reactivation of older faults bounding large elongated tilt blocks (e.g. Numan et al., 1998)).

In the Kurdistan Region of Iraq, the Zagros Orogeny is divided into four NW-SE striking tectonic units: The Zagros Suture, the Imbricated Zones, the High Folded Zone (equivalent to the Simply Folded Belt in the Iranian part of the Zagros,

Berberian, 1995) and finally the Foothill Zone. The boundary between the High Folded Zone and the Foothill Zone is marked by a regional morpho-tectonic feature, the Mountain Front Fault, delineated by a clustering of seismic events, which causes a sudden change in the level of exposed sedimentary layers. The Mountain Front Fault (Figure 1A) is trending parallel to the Zagros Belt and is interpreted as a result of the reactivation of Zagros basement structures (Berberian, 1995; Jassim and Goff, 2006; McQuarrie, 2004).

The fold-and-thrust belt in the Kurdistan Region of Iraq is dominated by open to gentle folding, with a characteristic wavelength of 5-10 km, therefore considerably lower than the average values of 15-25 km in the SE parts of the Zagros fold-and-thrust belt (Mouthereau et al., 2007), and amplitudes of less than 2.5 km. The two main reasons for this difference in the fold-wavelength are the absence of major faults and the absence of thick salt horizons. For example, the Neo-Proterozoic Hormuz salt overlying the crystalline basement in the SE part of the Iranian Zagros, which acts as a ductile detachment during deformation (Mouthereau et al., 2007), is absent in the NW part of the Zagros (Bahroudi and Koyi, 2003), where our study area is located.

## 2.2 Seismicity

The seismicity can be an important sign of recent activity in the above mentioned fault zones. Movement along the system of the Transversal Faults in the past could have influenced the evolution of the folds and the development of the fracture patterns as well. In the vicinity of the study area, we can divide the earthquakes in three groups according to their focal point depths. The data extracted from the USGS/NIEC database (state to 6.7.2011) show results from years 1973 to 2011 (Figure 1B). The shallowest and most common group recorded are earthquakes with hypocentre depth of 0-33 km, then the second, deeper and less common group with 33-70 km hypocentre depth and the third group with hypocentre depth of 70-150 km. Only one earthquake with hypocentre deeper than 150 km was recorded. The most earthquake magnitudes are ranging between 4 and 5. The bulk thickness of the sediments is about 8 km in the High Folded Zone (our study area) and about 12 km in the Foothill Zone (Figure 1A), which means that most of the hypocentres lie probably in the crystalline basement. Accordingly to this, the local seismic studies, which results have been summarized in Jassim and Goff, 2006, show that the maximum seismicity is distributed in the High Folded Zone and Balambo-Tanjero Zone with shallow focal depths of 30-50 km. These are exactly the areas, where the Arabian Plate is strongly tectonically deformed, being pushed to the NE directly under the Sanandaj-Sirjan Plate. This collision manifests on the surface by over-thrusting and metamorphism in the Zagros Suture Zone (Jassim and Goff, 2006) as well as by the intensified thrust faults development in the Imbricated Zone. Obviously the N- to NE-directed shortening represents the youngest, and according to the seismic activity, still active deformation in the region. Based on the focal mechanism solutions from the World Stress Map (Heidbach et al., 2008), the deformation is divided between two components, a NNW-directed dextral strike-slip component and N to NNE-directed shortening/thrust faulting component. The differential GPS deformation



pattern measurements from the Northern Zagros in Iran prove that compared to the Central Iran the strike-slip component is more important, with deformation rates of 4-6 mm yr<sup>-1</sup> (Walpersdorf, 2006).

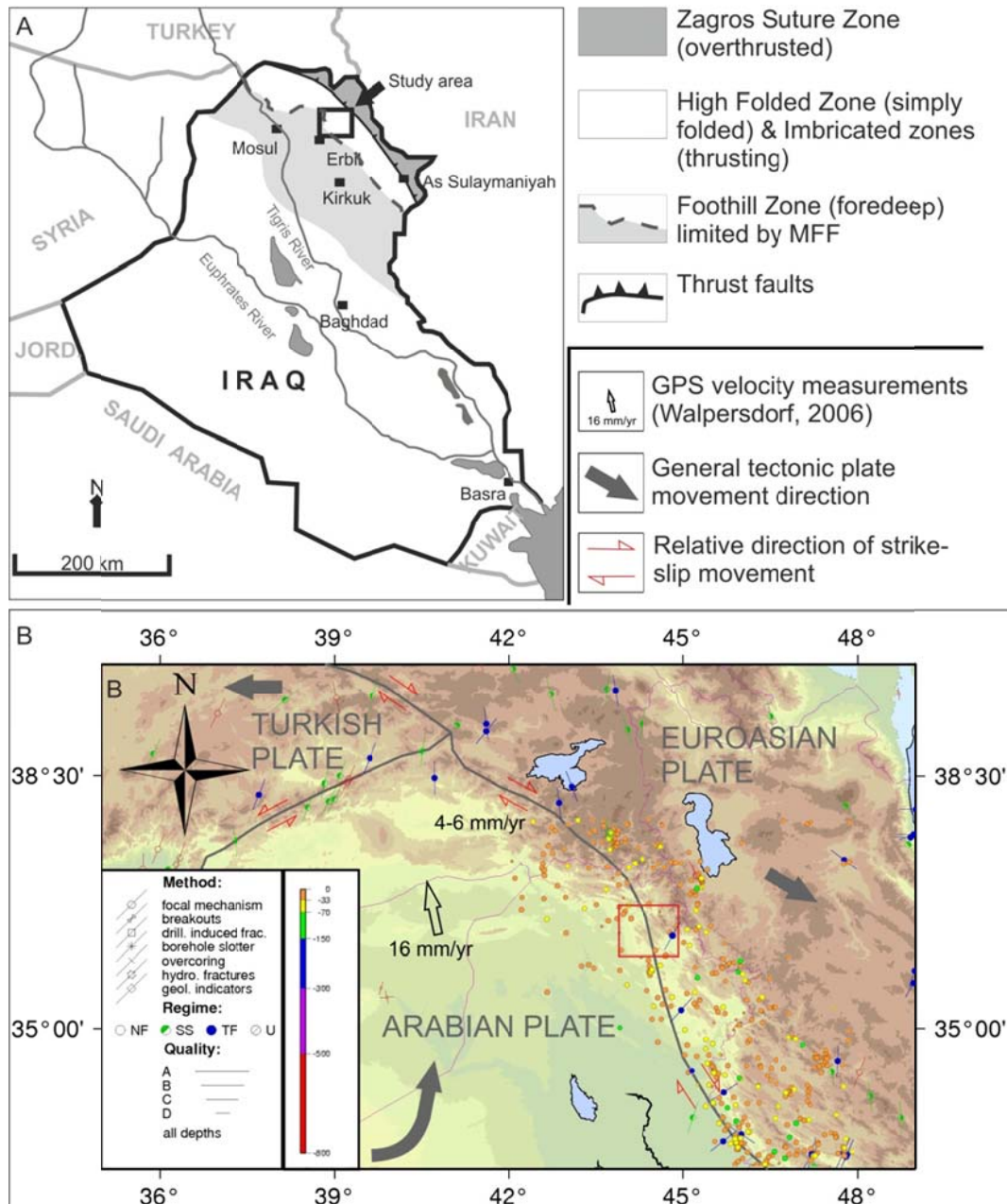


Figure 1: A) The study area (denoted by a black rectangle) is situated in the High Folded Zone of Zagros, characterised by simple folding and further to the NE increasing occurrence of thrust faulting (Imbricated Zones). B) Depth of the earthquake hypocenters (values in km, red to orange circles, USGS/NIEC database) within the study area (red rectangle), combined with the  $\sigma_{Hmax}$  data from World Stress Map (Heidbach et al., 2008) with plotted focal mechanism regimes (green, partly filled circles denote strike-slip, red empty circles normal fault and blue filled thrust fault regime) and GPS velocities (Walpersdorf et al., 2006).

## 2.3 Fault systems

The aeromagnetic surveys show that the Precambrian basement around the city of Erbil consists of amphibolite, gabbro and diorite (Jassim & Goff, 2006). The basement terrane might represent a highly imbricated ophiolitic belt with NW-SE orientation. This trend was reactivated during the Upper Tertiary (~Oligocene-Miocene) deformation. In the Precambrian (900-610 Ma) the Arabian Plate was formed during the “Pan African” orogenic cycle by oceanic accretion and micro-plate collisions in three stages (Nehling et al., 2002):

1. Oceanic accretion and subduction which led to accretion of oceanic crust and volcanic arc formation, forming thus the N-S trending Nabitah Ophiolites.
2. Collisions of accretionary units and microplates along the N-S trending Nabitah sutures. Nabitah suturing formed major molasse basins in the foredeeps within the orogenic belt. The E-W compression during this orogeny led to the formation of NW-SE trending Najd System transpressional shear zones.
3. Extension – The Amar collision was followed by destacking and crustal thinning. This resulted in development of trans-tensional basins parallel or perpendicular to the Najd shear zones.

The oldest tectonic features are the N-S trending thrusts and anticlines of the Nabitah Fault System resulting from Nabitah collision (started 680 Ma) and associated with E-W directed compression. The younger NW-SE Najd Fault System sinistral shear zones are offsetting the Nabitah faults. The trending of the system is parallel to the anticlines trending in the study area. The system developed in transpressional sinistral shear zone during the Nabitah Orogenesis. Around 670 Ma the system originated as a sinistral strike-slip faulting and resulted in the rise of gneiss domes (Nehling et al., 2002). Later (640-530 Ma) it developed as an extensional system. Najd Fault System was active during Jurassic to Quaternary time.

Upper Precambrian faults of the Transversal Fault System are trending in the NE-SW direction in the study area, sub-parallel to the main deformation direction and conjugate to the Najd Fault System (Figure 4). These faults were repeatedly reactivated since Upper Jurassic times (Jassim & Goff, 2006). The Transversal System includes both the Hadar-Bekhme and the Anah-Qalat Dizah Fault Zones. The Hadar-Bekhme Fault Zone in the vicinity of the study area strikes NE-SW and is probably active today. The fault zone is down-throwing south. The Anah-Qalat Dizah Fault Zone is an impressive transversal fault morphologically, as well as tectonically, with the Euphrates River following its course further to the SW of the study area. The Anah-Qalat Dizah and other faults of the system underwent a sinistral strike slip movement in the Quaternary. The Foothill Zone anticlines (Figure 1A) are often bent or segmented at the intersections with the faults of this system. Neotectonic activity is proven by several recorded earthquakes. The ASTER satellite image (Figure 4C) shows that on the SW end of the Bana Bawi Anticline the river network propagates along the course (adapted from Jassim and Goff, 2006) of the Anah-Qalat Dizah Fault Zone cutting through the folded sedimentary sequence. There is a sinistral strike-slip documented along the fault near Al Fathah, approximately 45 km WSW from Kirkuk, although no evidence of the movement along this fault zone was observed in our study area. From the recent seismic activity can be concluded that

both faults were active in the past and may have also influenced the formation of folded structures, other faults and also the development of fracture systems in the Kurdistan Region.

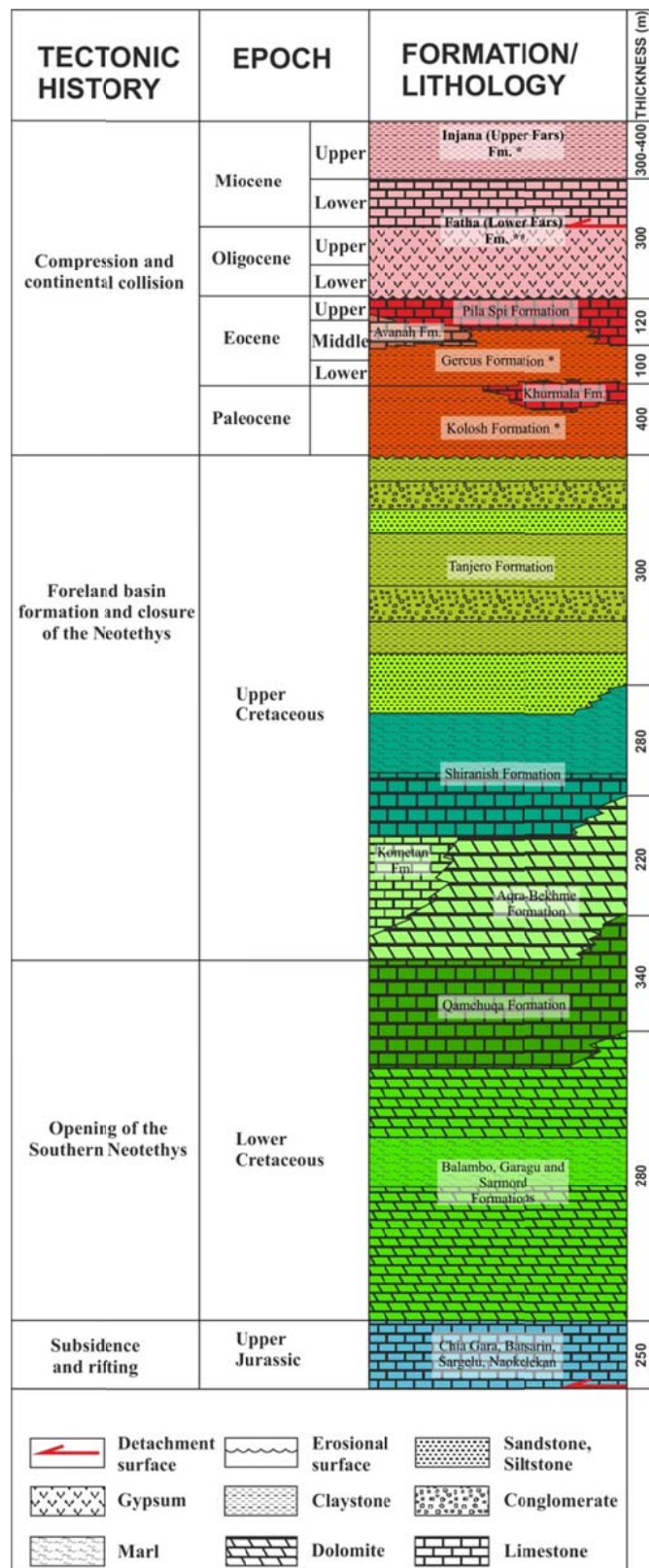


Figure 2: Overview of the formations in the study area, their age, tectonic history and lithology. The less competent formations are marked with asterisk (\*) and the arrows denote locations of possible detachment surfaces. The Lower Jurassic detachment is probably located in the Sehkanian and Sarki Formations (Sissakian et al., 1997), containing thin bedded shale.

Thrusting commenced during the compressional regime connected with the closure of the Neo-Tethys in Paleocene-Eocene as well as following Oligocene continental collision reactivated the older normal faults as thrusts and formed also new ones, which are mapped in the geologic map by Sissakian et al., 1997 (yellow lines, Figure 4C). The main trends of the faults in the geological map are (starting with the most developed) E-W, NW-SE and NE-SW. Faults located in the study area were inspected during the field work, but there is not much evidence of significant movement on most of them. Some of the faults, shown on the geological map by Sissakian et al., 1997, have not been identified in the field, while additional minor faults were described from the outcrops (see the next chapter). In summary, the major fault trends mapped in the field are roughly E-W and NW-SE (Figure 4A), which is well correlated with the trends of the large faults in the geological map, whereas the NW-SE trend was identified only locally.

### 3. Fracture data

Three major fault and fracture generations and three less developed have been identified during the field and remote sensing data studies in the studied part of the Zagros Belt. In the following subchapters we describe the exposed fractures in different positions on the anticlines (Table 1) for each geological formation separately. The formations are ordered stratigraphically from the youngest to the oldest (Figure 2). The thicknesses of the different formations are estimated from borehole data as well as from calculation of true thickness based on outcrop studies and complemented with approximate values from the literature (Jassim and Goff, 2006) in case of the Upper Fars, the Aqra-Bekhme and the Tanjero formations. The mean values of the fracture systems measured in the field were calculated and projected on the two cross-sections (for the positions see Figure 3). Because the density of the data is variable and not sufficient at places, the deformation model and the cross-sections can be improved in detail or subjected to changes in the future.

#### 3.1 The deformation model

Given the deformation history described in the published literature (Fürst, 1970; Numan et al., 1998; Alavi, 2004; Jassim and Goff, 2006 and others) the preliminary deformation model was established, summarizing main deformation events from the Mesozoic to the Recent. The faults mapped in available regional geological map (Sissakian et al., 1997) were digitized and the resulting fault trends plotted (Figure 5B). These show that the main trends are E-W and NW-SE. The smaller (2-4 km) faults trending NE-SW (Figure 4C and 5B) are less common. Similar main trends have been described also by other authors such as E-W sinistral strike-slip movement zones in the W part and NW-SE dextral strike-slip movement zones in the E part of the of the High Folded Zone respectively (Csontos et al., 2011). However, the remote sensing imagery covering the study area (ASTER 30 m with horizontal resolution) does not reveal much evidence of movement on both of the fault systems (Figure 4C). There is also number of smaller, steep, normal faults, observed in the outcrops and dipping to the NE and SW (Figure 4A and 5A), striking parallel to the NW-SE trend (Figure 5B) in the geological map (Sissakian et al., 1997) and to the D3 (folding related) fractures. These originate from the longitudinal tangential stretch in the upper layers of the folds or longitudinal tangential compression in the cores of the folds and are found in the majority of the outcrops (82%). This preliminary model was then compared with the results of the field measurements resulting in a deformation model of the evolution from Oligocene to Recent and comprising five phases. The studied formations include Pila Spi limestone which is the equivalent of the Asmari-Jahrum in Iran. Further studied are also fractures in the Shiranish (equivalent to the Gurpi Formation in Iran), Tanjero (equivalent to Maastrichtian Flysch) and Qamchuqa (equivalent of the Fahlyan Formation) Formations. All of the named equivalent formations are found in the Iranian part of the Zagros Fold-and-Thrust Belt (as described in Fürst, 1970; Kent et al., 1952; Jassim and Goff, 2006).



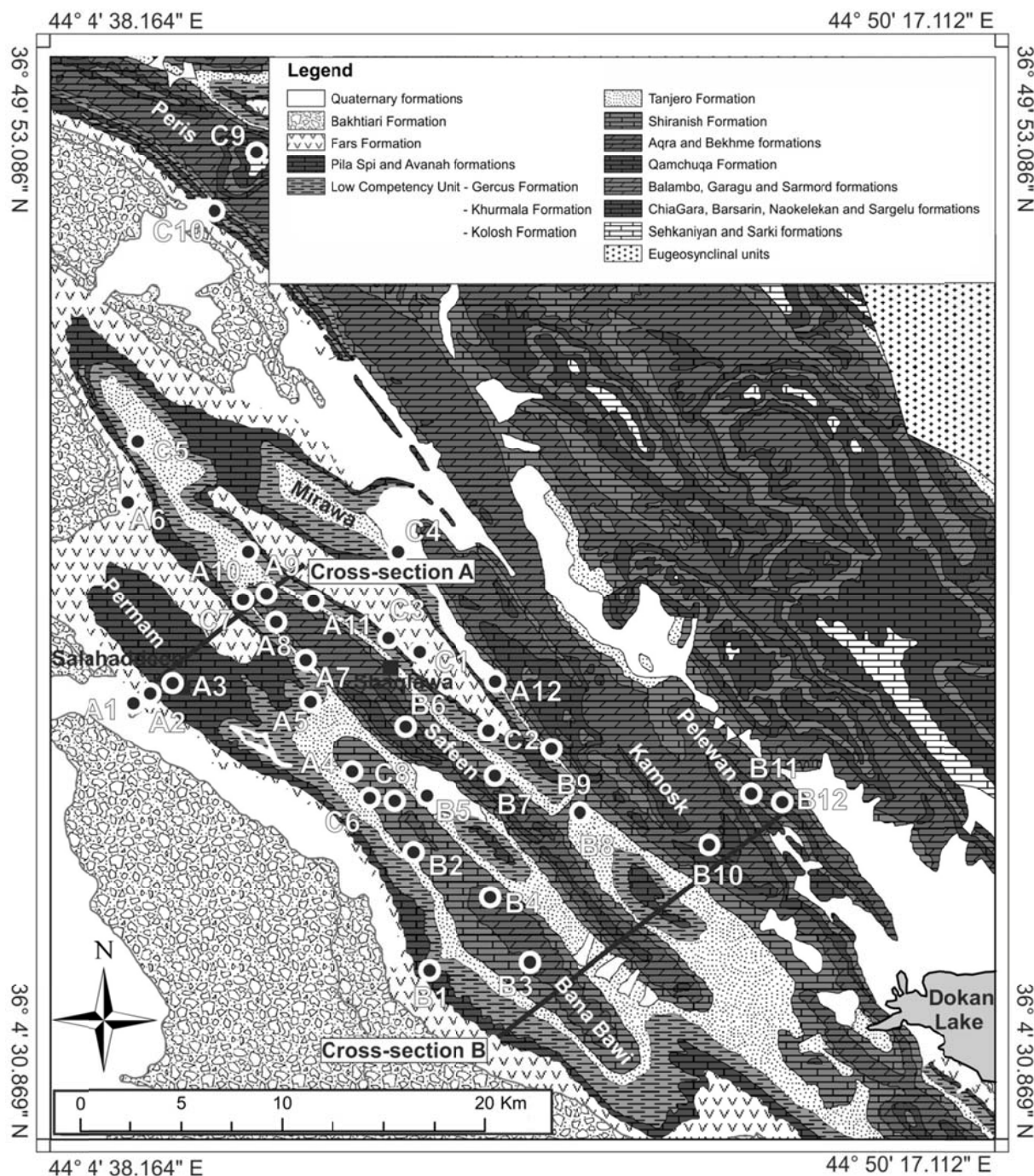


Figure 3: Simplified geological map (partly based on Sissakian et al., 1997) of the study area with marked position of the two cross-sections A and B and the according outcrops with fracture measurements (marked by black circles, labelled A1-A12, B1-B12). The position of further outcrops C1-10 is also denoted, for details on observed fracture systems see Table 1, corresponding figures and text in the section 3.

The earliest deformation D1 is according to the cross-cutting relations between the fracture systems the ESE-WNW directed extension. It was observed even in the youngest studied Oligocene Fars Formation on the forelimb of the Bana Bawi

anticline (Table 1, outcrop A2). This suggest that all the studied fracture systems are of Oligocene or younger age. The deformation was identified in 76% of the outcrops and is represented by NE- and SW-dipping normal faults, which were later reactivated by the deformation D5 as sinistral strike-slip faults and NW-SE striking tension gashes.

Deformation D2 was observed in 17% of the outcrops. It is coupled with the NE-SW directed, pre- or early-folding compressive regime and includes conjugated thrust-fault groups dipping under similar angle relative to the folded (now sub-vertical) sedimentary bedding (Figure 6C). After unfolding of the data (Figure 6D to 6F) is clear, that these thrusts predate the folding and are probably result of the same shortening direction, which caused the subsequent folding. This is also supported by findings of NW-striking sub-vertical stylolithes and NNW directed thrust faults on the forelimb of the Bana Bawi Anticline.

Fractures which are connected with the deformation D3, responsible for the folding of the formations, are divided in the two groups (D3a, D3b), distinguished by the position in the folded sedimentary succession from which these resulted. This pervasive fracture set occurs in 82% of the outcrops. The D3a deformation, representing longitudinal tangential stretch (extension), took place in the upper layers of the folded formations. The connected fractures are mainly extensional mode I joints, tension gashes and normal faults. The D3b deformation, representing longitudinal tangential compression in the cores of the folds (in the lower units) is characterized by minor, sub-seismic fore- and back-thrust fault structures (Figure 7, Sarmord and Qamchuqa Formations). The folding can be simplified by interlayer slip between the competent strata of the units, allowed by thin incompetent layers, which were recognized during the field mapping, but no offset was observed (Figure 5C). Importance of these incompetent layers is also proposed in the Iranian part of Zagros (Yamato, 2010) as an explanation for the low shortening rates resulting from the numerical models based on the data from balanced cross-sections.

The deformation D4 is E-W directed extension, comprising N-S striking, sub-vertical mode I joints and fractures. This less significant fracture set was defined on the basis of the outcrop studies and occurs in 14% of the outcrops. The fractures consists of partially calcite-filled tension gashes and normal faults, reactivating pre-existing fractures of D1 (Figure 7, outcrop C2, Pila Spi Formation).

The deformation D5, N- to NE-directed shortening comprises mainly fractures of D1 deformation reactivated by sinistral shear and few NW-striking, by dextral strike-slip reactivated fractures, originally D2. This probably reflects the dextral shear of the Zagros fold-belt under the N-S compression induced by the northward movement of the Arabian relative to the Eurasian Plate. This is well comparable to the data from the World Stress Map (Heidbach et al., 2008) database as shown in the Figure 1B.

The fracture system DX comprises sub-vertical, consistently E-W striking fractures, mainly open fractures and joints indicating extension. There is not sufficient data to



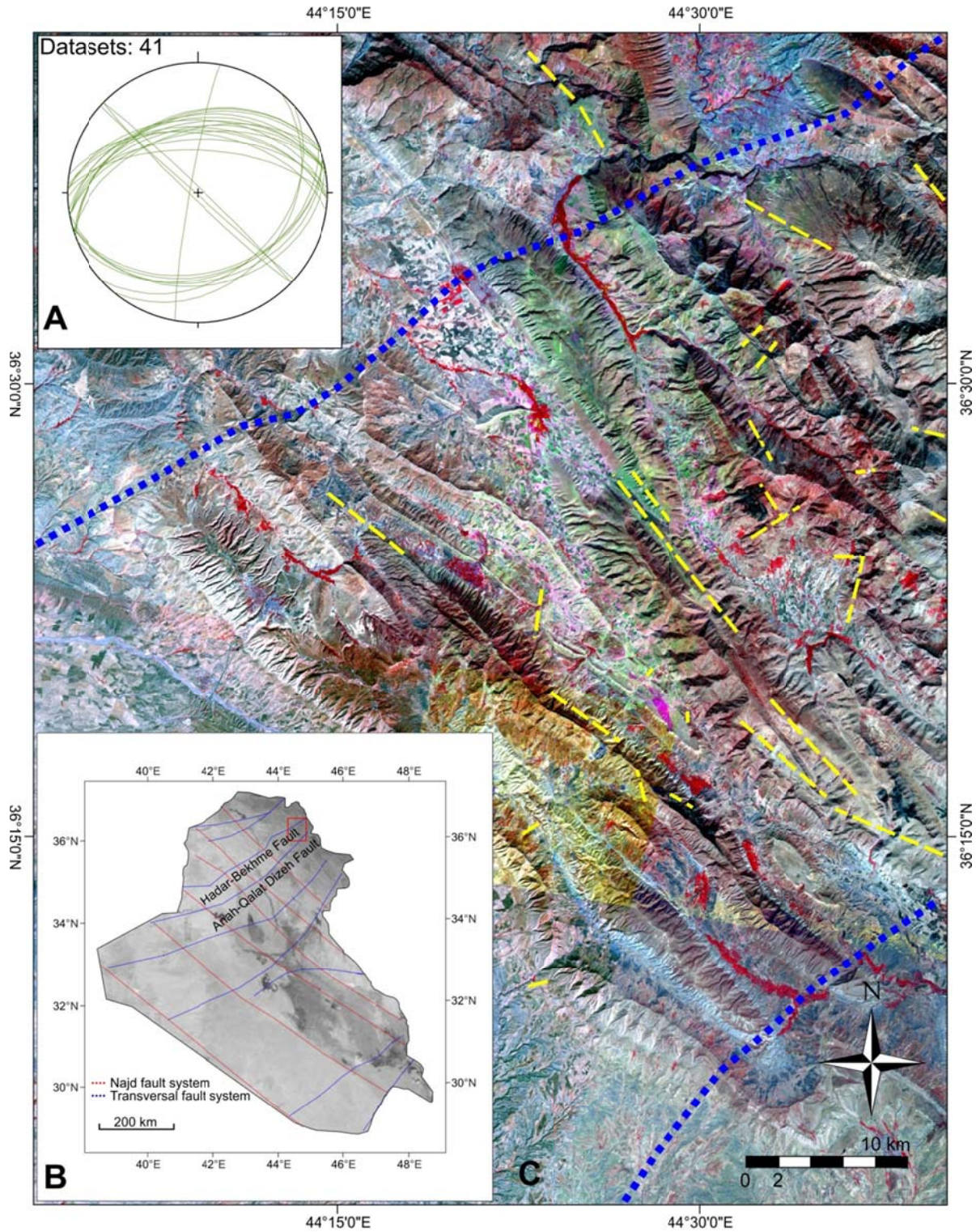


Figure 4: A) The upper small inset shows the fault plane orientations (in green) measured in the outcrops for comparison with larger faults mapped in the geological map (Sissakian et al., 1997). B) The lower small inset shows the two main fault systems in Iraq (modified after Jassim and Goff, 2006) with the two Transversal Fault Zones cutting through the study area (marked with red rectangle). C) The approximate course of the Hadar-Bekhme and Anah-Qalat Dizah Fault Zones (blue dashed lines) on ASTER satellite image of the study area surroundings. The majority of the faults (denoted by yellow dashed lines) digitized from the available geological maps (Sissakian et al., 1997) trends NNW-SSE.

determine its age relative to other fractures, because it was reliably recognised in few outcrops only on the backlimb of the Safeen Anticline and possibly in one outcrop on the backlimb of the Pelewan Anticline. The fractures show similar strike direction as the normal faults digitalized from the geological map (Sissakian et al., 1997) and are definitely younger than the fractures of the deformation D1, based on the cross-cutting relations. As the fractures were identified only on the backlimb of the two anticlines it is not possible to compare their age with the age of folding and no cross-cutting relations were observed with the fractures D3. Further investigation is necessary to resolve their age and origin.

### 3.2 Fars Formation

The 300-400 m thick Upper Miocene Upper Fars Formation (also known as Injana) is a bedded sandstone, claystone and mudstone succession which is only locally found, in the synclines, where the erosion is not as intensive. The 300 m thick Oligocene to Lower Miocene Lower Fars (also known as Fatha) Formation contains thin interbedded layers of claystone, evaporite (gypsum and anhydrite) and limestone. The observed fractures are mainly joints and normal faults associated with the folding deformation D3a (Figure 8, outcrop A6). The joints are more significant in the limestone and sandstone beds, rarely developed in the interlayering, significantly eroded claystone and mudstone successions.

### 3.3 Pila Spi Formation

The competent 120 m thick Pila Spi Formation consists of generally well bedded Mid-Upper Eocene limestone, sandwiched between the underlying Gercus and the overlying Lower Fars Formations, which are both significantly less resistant to the weathering and erosion. Therefore, the Pila Spi Formation frequently develops topographic ridges throughout the Zagros Highly Folded Zone. In the investigated area the nummulitic Eocene Avanah Formation occurs in the basal part of the Pila Spi Formation (Jassim and Goff, 2006). The mode I joints and normal faults, caused by the deformations D1, D3b are later reactivated by the E-W extension connected with the deformation D4 (Figure 8, outcrop A2, A3). The layer-parallel thin beds often contain brecciated limestone, which were already described previously (Numan, 1998) as syn-sedimentary and thus could have been probably reactivated also during the folding by interlayer slip. The D1 fractures are mostly terminated on these beds. The fractures of the deformation D2 (NE-SW compression), characterised by SW- and NE- directed thrusting were observed in the outcrop C10 (Figure 6C, for position see Figure 3). The Pila Spi Formation limestones on the forelimb of the Peris Anticline (N of the study area), showing sub-vertical sedimentary bedding with small fractures and thrust fault ramps. These are oriented symmetrically to the bedding and cored in the incorporated incompetent red claystone layers. The thrust faults as measured in the outcrop were back rotated to the position before the folding using the fold axis reconstructed from the sedimentary bedding measurements on the Peris Anticline (Reif et al., 2011). After rotating the structural inventory back to horizontal



bedding it is clear that the thrust faults are associated with the pre- or possibly early-folding deformation D2, NE-SW directed shortening.

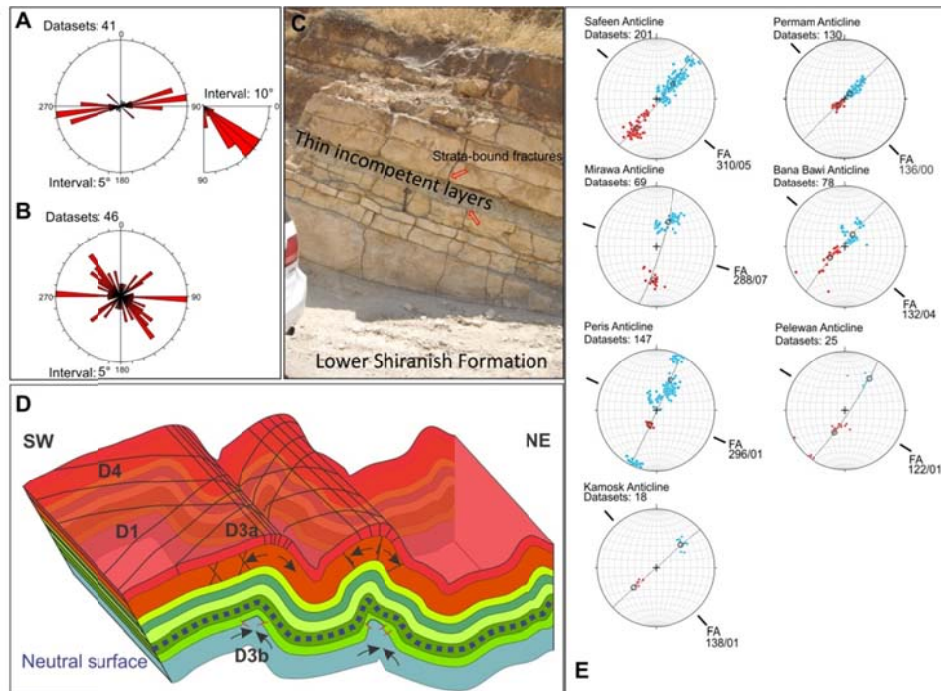


Figure 5: A) Calculated rose diagram for the strike and dip of the fault planes measured during the field work. B) Digitized fault planes from the geological map (Sissakian et al., 1997). There is no information on dip of the fault planes available. C) Strata-bound fracturing, terminated by repeated thin incompetent layers in the outcrop of the Lower Shiranish Formation. No interlayer slip observed. D) Proposed model showing characteristic fracturing, as observed in the field on the example of the first two anticlines of cross-section B (Bana Bawi and Safeen). Older pre-folding fractures belong to the deformation D1 (extension). Deformation D3, caused by the folding (D3a – fold tangential extension and D3b – fold tangential shortening). Later deformation D4 (extension) reactivates D1 tension gashes and produces N-S striking sub-vertical fractures. See text in section 3.1 for more detail and Figure 9 (cross-section B) or Figure 2 for description of the depicted sedimentary succession. E) The fold axes (FA) are modified after Reif et al. (2011), updated and complemented. Blue dots indicate sedimentary bedding measurements from the south-western forelimbs; red dots are measurements from the north-east backlimbs. The black circles show the corresponding mean values. Great circles indicate the orientation of the calculated mean  $\pi$  circle.

### 3.4 Kolosh Formation

The Kolosh Formation is of the Paleocene age and is about 400 m thick in the studied cross-sections, but only about 300 m close to the Kirkuk-117 borehole (Jassim and Goff, 2006). In the field the Kolosh Formation shows evidences of shear deformation between the underlying Cretaceous limestones and overlying competent Pila Spi limestones. This clastic formation comprises black claystone and shale with thin limestone beds occurring at the top of the formation.

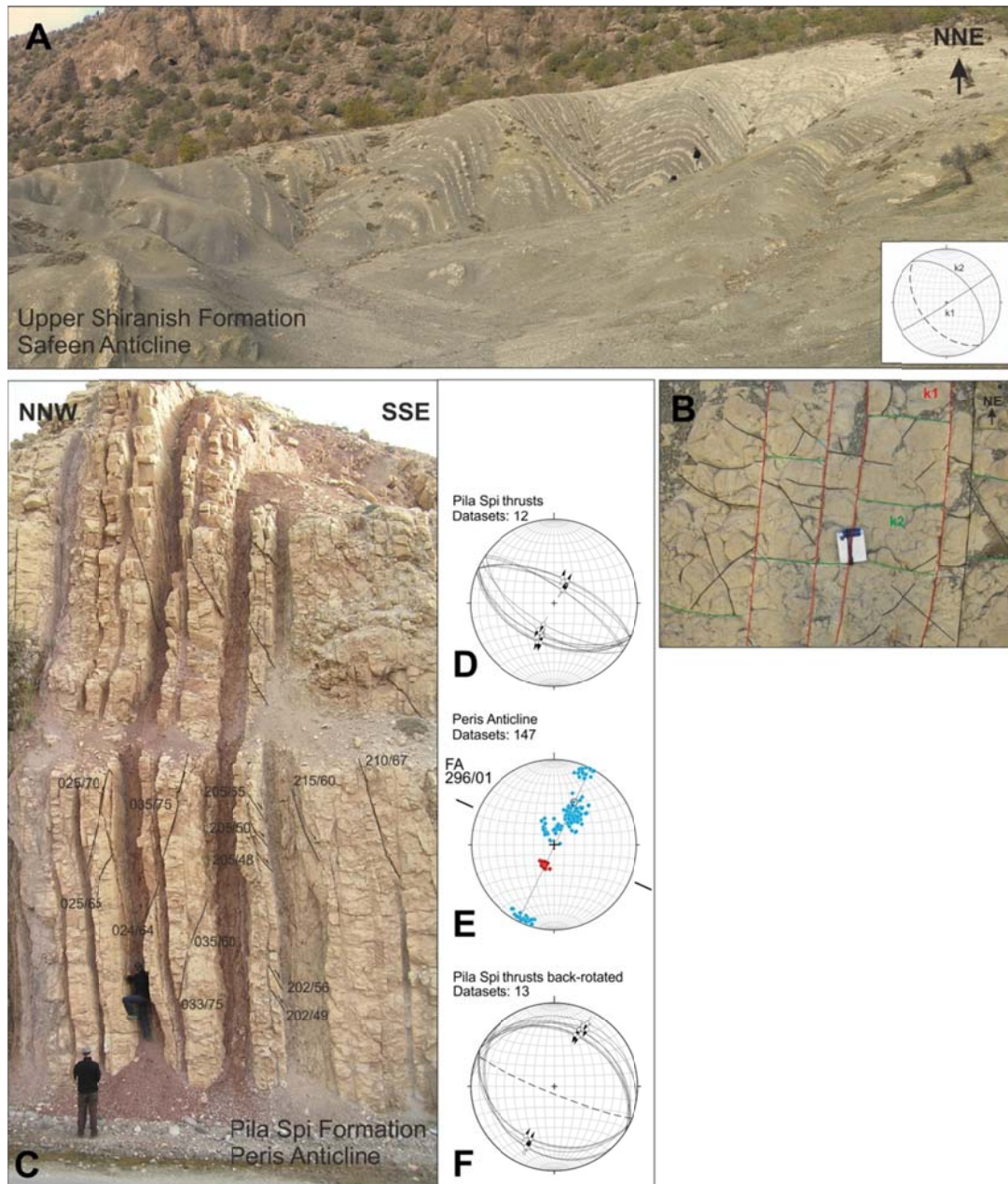


Figure 6: Deformations D1, D2 and D3a. A) Outcrop of the Upper Shiranish Formation (A7). Small inset shows orientation of the mean values of the fracture systems (full lines) and sedimentary bedding (dashed). B) Detailed view of the fractures on the same outcrop, showing abutting relationship between older k1 (red), mode I fractures (deformation D1) and younger k2 (green) mode I fractures (deformation D3a), which are terminated by k1. C) Outcrop of the Pila Spi Formation before the Peris Anticline (C10, northern part of the study area), showing sub-vertical bedding with small fractures and thrust fault ramps, oriented symmetrically to the bedding and cored in the incorporated incompetent layers. D) Schmidt's net plot with plotted thrust faults as measured in the outcrop. E) Reconstructed fold axis from measurements from the Peris Anticline (Reif et al., 2011), used for rotating the structural inventory back to horizontal bedding. F) Back-rotated thrust faults and the mean value of the observed sub-vertical sedimentary bedding (deformation D2; NE-SW directed shortening).



Locally the calcareous beds of the Paleocene Khurmala Formation are inter-fingering or overlie the Kolosh Formation. The outcrops predominantly consist of strongly shattered black shale, which is caused mainly by pressure relief in the previously over-pressurized shales at depth and sometimes by visible strong internal deformation and folding of this formation. The fracture systems (outcrop C4, for position see Figure 3) are bound on competent limestone layers. The observed deformations are similar as in the Tanjero and Pila Spi Formations (mostly D1, but D2 and D3a as well). Obtaining measurements is difficult because the outcrops are strongly eroded which is amplified by the shattered character of the complete formation.

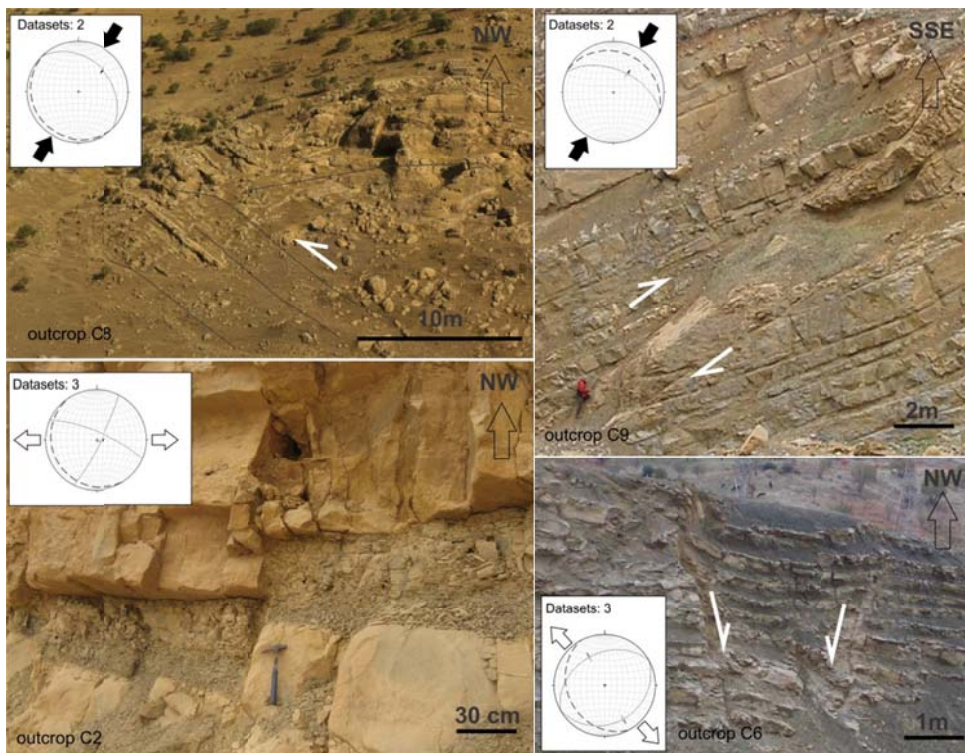


Figure 7: Deformations D3b, D1 and D4. Outcrop photos of studied formations with white arrows indicating the movement direction on the faults where unclear. Outcrops from left to right: Outcrop C8, Qamchuqa Formation with thrust faults of D3b, Bana Bawi Anticline; Outcrop C9, Sarmord Formation with thrust faults of deformation D3b, Peris Anticline; Outcrop C2, Pila Spi Formation with tension gashes of D1 later reactivated as normal faults of D4, Bana Bawi Anticline; Outcrop C6: Upper Shiranish with normal faults of D1, Bana Bawi Anticline. Insets show fault and fracture orientations (solid lines) and mean sedimentary bedding orientations (dashed lines). Note different scale of the photos.

### 3.5 Tanjero Formation

The Upper Cretaceous Tanjero Formation has been mapped in the investigated area, but was not described from the boreholes on the Bana Bawi Anticline (Herwig Peresson, OMV, 2010, personal communication). The thickness of the formation is

very variable, (locally up to thousands of meters, Jassim and Goff, 2006) and reaches 300 m in the studied cross-section over the Bana Bawi Anticline. The lower parts consist of claystone with conglomerate layers and the upper parts consist of siltstone beds. The NE-SW trending fracture system (NW-SE directed deformation D1), characterised by long extensional fractures, sub-parallel to the shortening direction, which was active in Zagros since Pliocene is found in this formation (outcrop A12, for position see Figure 3) as well as D3a fractures and less significant mode I joints of deformation D4. Additionally, the outcrop, situated in the syncline NE of the Safeen Anticline, reveals the fractures of DX (E-W striking fractures).

### 3.6 Shiranish Formation

The Upper Cretaceous Lower and Upper Shiranish Formation have a thickness of 280 m on the Bana Bawi Anticline. It comprises thin-bedded marly limestone with high pyrite content (Lower Shiranish) and blue pelagic marls (Upper Shiranish). Towards NE, this formation gradually passes into the Tanjero Formation (Jassim and Goff, 2006). The fractures are better developed in the Lower as in the Upper Shiranish Formation, which is caused by the less competent lithology of the later. Measurable fractures appear only in thin limestone beds interlayering the marls. The Lower Shiranish Formation contains also few marly beds, where the fractures are terminated (Figure 5C). The outcrops show distinctively developed fracture sets of sub-vertical, (E)NE-(W)SW directed mode I joints (D1) which are abutting younger, NW-SE trending (Figure 6A,B and Fig. 7), perpendicular to the bedding mode I joints, formed during the folding (D3a). Less developed are the roughly N-S trending, sub-vertical mode I joints, formed by deformation D4, an E-W directed extension (outcrop A11). The Shiranish Formation is strongly fractured and except of fractures of the deformation D3b, which is expected to appear at deeper levels of the folded structures, all described fracture systems were observed in the outcrops of this formation.

### 3.7 Aqra-Bekhme Formation

The 200 m thick Upper Cretaceous Aqra-Bekhme Formation, contains locally thin-bedded grey limestone with chert concretions at the base (Kometan Formation). Although elsewhere the Kometan Formation reaches a thickness of up to 500 m (Jassim and Goff, 2006), the thickness varies strongly and it is only 20 m thick on the frontlimb of Bana Bawi Anticline. The Aqra-Bekhme Formation comprises massive dolomitized limestone locally impregnated with bitumen. The bitumen inclusion are closed, partially filled with calcite and later connected with fractures. In the outcrops the layer-parallel slip on calcified planes (therefore probably formed at depth) associated with the folding (deformation D3a) was identified as well as deformation D1. On the backlimb of the Pelewan Anticline (outcrop A12) and on the Safeen Anticline (outcrop B6) the fracture system DX was also observed.



### 3.8 Qamchuqa Formation

The Lower Cretaceous Qamchuqa Formation with variable thickness between 600 and 800 m comprises detrital and argillaceous limestones, which are partly dolomitized. The thickness of the Qamchuqa Formation in the studied cross-section is approximately 340 m. The proposed neutral surface is positioned somewhere in this formation (Figure 5D). Longitudinal tangential stretch in the upper layers (outcrop B10), corresponding to the deformation D3a (outcrop B10) as well as by thrust faulting and compression characterised deformation D3b (outcrop C8) were observed in this formation. The neutral surface is to be understood in the in accordance with the definition by John Ramsey (Ramsey, 1967). We are aware of the antiquity of this simple definition and that it was later explained differently (Frehner, 2011), because the time-dependent development of the neutral surface (or neutral lines) is much more complex than it was originally assumed by Ramsey (1967). Although we believe that for the fracture studies is the use of this definition still purposeful. Other observed fractures are NNE-SSW striking, sub-vertical normal faults connected with the deformation D4 (outcrop B10).

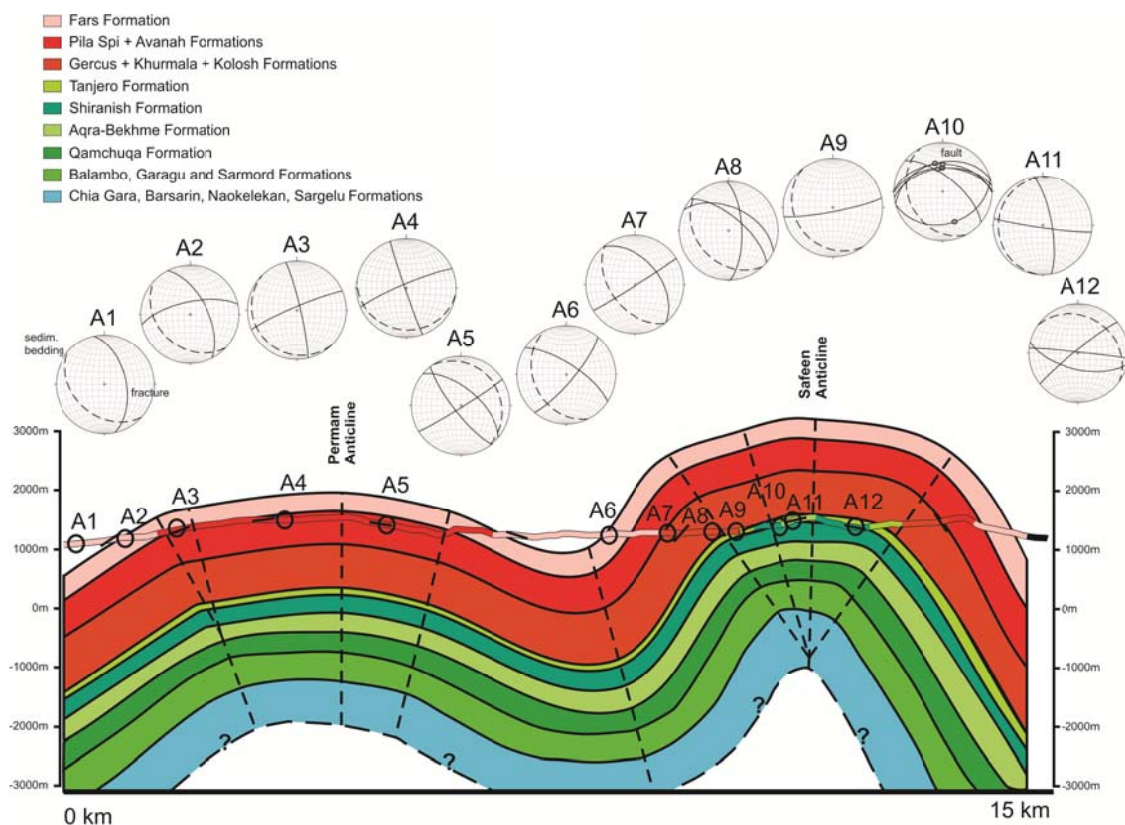


Figure 8: Cross-section A with plotted outcrops (A1-12), showing the mean orientations of the fracture systems and sedimentary bedding in the analysed outcrops. The formations are marked A-I corresponding to the depicted legend. The thin line shows the topographic surface with formation boundaries as mapped by Sissakian et al., 1997.

### 3.9 Sarmord Formation

The 100 to 250 m thick Lower Cretaceous Sarmord Formation comprises of bluish and brown marls with beds of argillaceous limestone. It was identified outcropping only in the eroded-out cores of the anticlines, exposed thanks to the extensive fracturing of the flat hinge areas of the anticlines and following erosion (Pelewan Anticline, Figure 3) or in deep river gorges such as the outcrop in the core of the Peris Anticline. Important observed deformation is the mainly N-S directed thrust faulting (D3b) in Figure 9, outcrop B11 (backlimb of the Pelewan Anticline, for position see Figure 3) and above mentioned outcrop N of the study area on the backlimb of the Peris Anticline (Figure 7, outcrop C9).

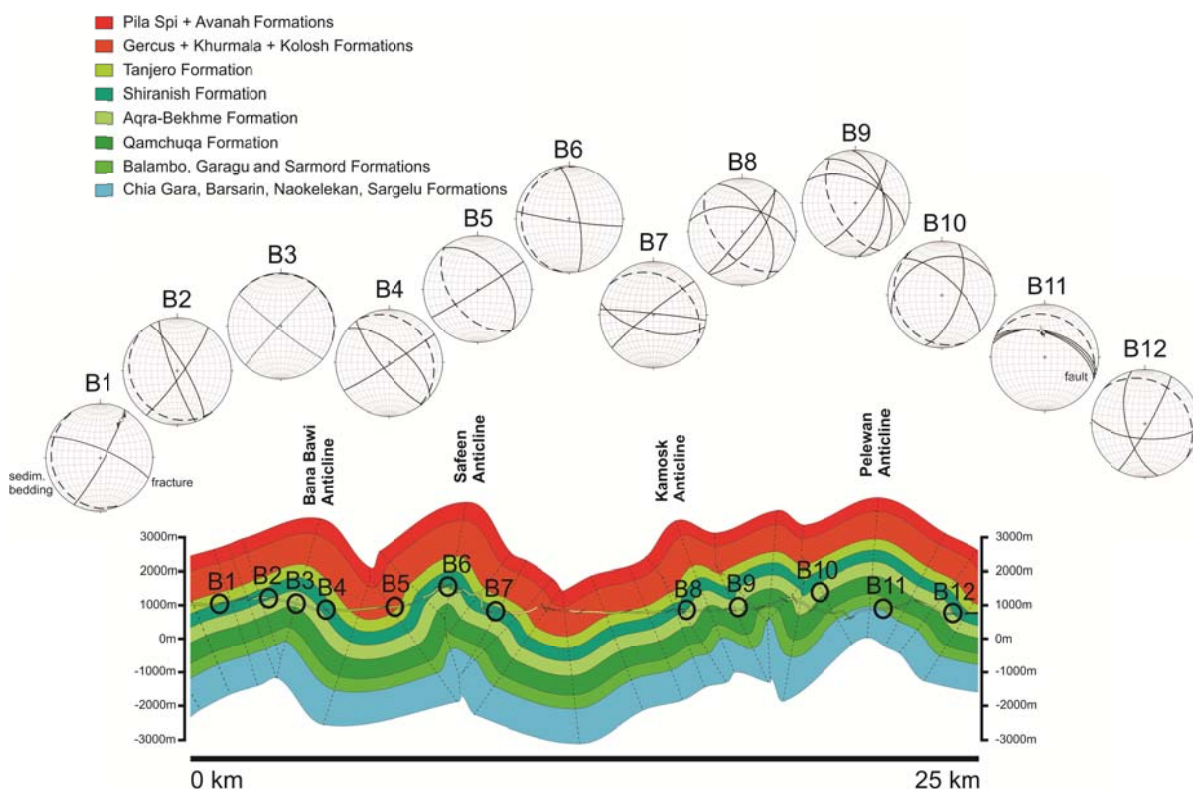
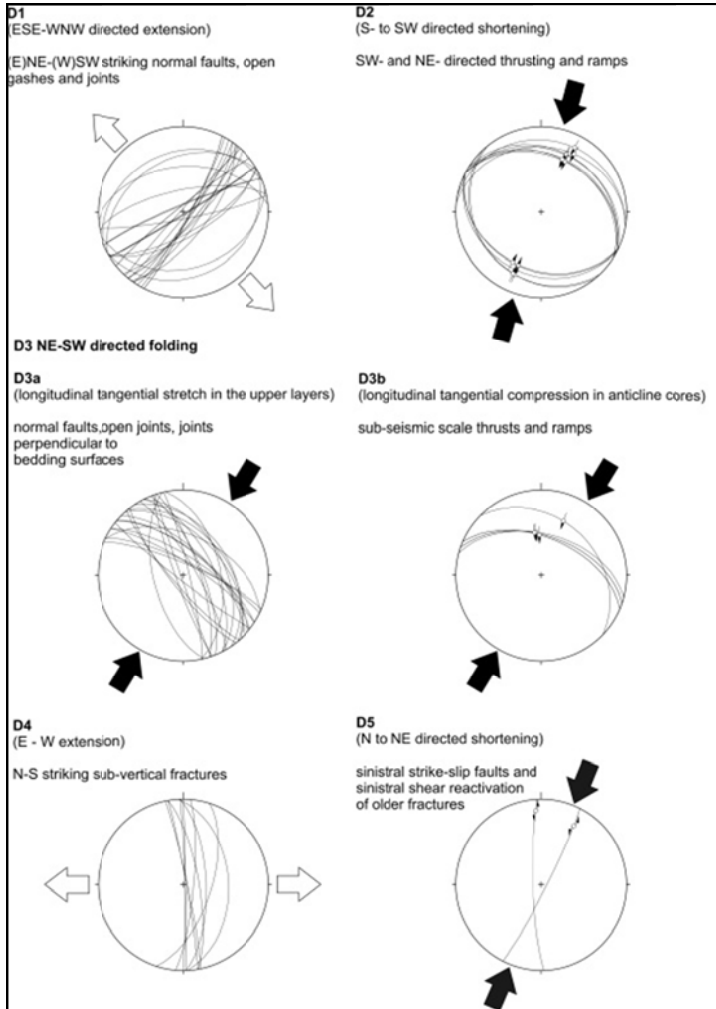


Figure 9: Cross-section B with plotted outcrops (B1-12) and corresponding mean orientations of the fracture systems and sedimentary bedding. The formations are marked B-I corresponding to the depicted legend. The thin line shows the topographic surface with formation boundaries as mapped by Sissakian et al., 1997.

The relative dating of the different fracture systems was based on the cross-cutting relations between them. The D3a fractures are being terminated at the older system D1. The clearly pre-folding D2 compression predates the formation of the D3 fractures. Both deformations D3b and D3a are formed by the fold-tangential strain related to the same folding event and thus of the same age. The younger age of the deformation D4 compared to D1 can be determined based on reactivation of existing D1 fractures by normal faulting of D4 (Figure 7, outcrop C2). The deformation D5 is

accepted as the youngest as it reactivates the older D1 by sinistral shear. The young age is also supported by the recent local stresses from World Stress Map (Figure 1B), showing mainly sinistral strike-slip and thrusting resulting from the NE-SW shortening in the area of the Zagros Orogeny.



The high mechanical anisotropy (competent limestones and sandstones, interlayered with less competent claystones, shales and marls) of the different formations controls the folding. As already mentioned, two simple balanced cross-sections cutting the study area in the NE-SW direction, parallel to the recent shortening direction, were constructed.

Figure 10: Phases (D1-D5 from old to young) of the proposed deformation model, supported by structural field data resulting from this study and in case of D5 also by the focal mechanism solutions from the World Stress Map (Heidbach et al., 2008). The black and white arrows denote compression and extension directions respectively. The D2 plot shows the data rotated back to horizontal bedding.

The first cross-section A (Figure 8) is cutting the Permian Anticline in its south-eastern part and the Safeen Anticline in its north-western part. The second cross-section B (Figure 9) is cutting the Bana Bawi, Safeen and Kamosk Anticlines in their south-eastern parts and further the Pelewan Anticline in its north-western part. The plots are showing the data in original form as measured in the field (not back-rotated).

#### 4. Discussion and conclusions

The strike of the fractures in the studied outcrops shows similar trend to the fractures mapped in the Iran (Tavani et al., 2011) and in Iraq (Numan, 1998), approximately 100 km W of our study area. Importantly the pervasive NE-SW striking D1 fractures

and N-S striking extensional fractures (D4), described in this study correlate well with published data from surrounding regions (Tavani et al., 2011; Numan, 1998). In contrast to our study Numan (1998) suggested that the N-S striking joint sets (D4) developed prior to the folding (D3), based on the restoration of the data to horizontal bedding. This was not proven in our study area, where the D4 fractures does not change their orientation across the studied cross-sections as visible in the plot, summarizing the fracture orientations (Figure 10).

Based on the filling (mainly calcite) of the different fracture assemblages, it can be estimated if the fractures were formed at depth and if they will be permeable for the fluids. This is the only criterion for the evaluation, because no borehole data and no published literature exist in the study area. To summarize our limited observations, we can say that the most of the D1 fractures were filled by calcite and thus could have been formed at depth and can be less permeable for the fluids. The D2 related fractures were formed in the complete, to-be folded sedimentary succession and are only partially filled with calcite. The fractures are thought to be formed in the early phase of the compression (the formation of thrust-ramps) and predated the actual folding (D3a, D3b). The folding related fractures of the deformation D3a are not filled and probably did not form at depth. On contrary, the fractures connected with the deformation D3b, representing the thrusting and back-thrusting in the cores of the anticlines, are bound on lower sedimentary units and therefore must have formed at significant depth. The fractures related to the later extensional regime (D4) and the fractures DX, with unclear structural interpretation are partially filled with calcite. The vertical connectivity increased during the folding (D3) due to the fracturing. The fracture system possibly controlled the hydrodynamic connectivity (fluids movement through the open fractures).

The definition of the different deformations (D1-D5) is based on very limited dataset with heterogeneous density of studied outcrops. However the fractures associated with D1 were found in 76% of the studied outcrops. The D3 associated structures, connected with the folding were identified in 82% of the outcrops. More common is the D3a, which is bound to the upper layers of the folded sedimentary succession and thus outcropping more often than the fractures of D3b, which are found only in the eroded-out cores of the anticlines. The fractures connected with the D4 (sub-vertical N-S striking mode I joints and reactivated normal faults) are found in 14% of the studied outcrops. The less significant D5 fracture system supported by the data from the World Stress Map was identified in 6% of the outcrops. The fracture system DX was observed in 18% of the outcrops, but is mainly localized on the backlimb of the Safeen Anticline (see Table 1 and for location Figure 3). Except the DX, the timing of the observed deformations seems to be sufficient, but can be improved or subjected to changes, if more data will be acquired in the future. As mentioned above, the fracture systems are developed mainly in limestone and sandstone beds. In the Iranian Zagros Stephenson (2007) described that the bedding-parallel slip, occurring predominantly in the marly layers, causes this and prevents the vertical propagation of the fracture systems. This is characteristic especially for anticline limbs with dip larger than 20 degrees. As a result, these fracture systems will be bound to one layer and thus will not be important for the production of hydrocarbons. Similarly this was proposed by the finite element models introduced for Iranian Simply Folded Belt by Yamato et al. (2011). In this study, these layers were identified



in the field but no significant kinematic indicator was found in the analysed outcrops supporting this hypothesis.

No.	Latitude	Longitude	Formation	Lithology	Age	Structure	Best fit fold axis	Bedding dip
A1	36°21'13.56"N	44°11'8.64"E	Fars	siltstone, sandstone and claystone	Miocene	Permam	136/0	222/37
A2	36°21'15.43"N	44°11'21.97"E	Fars	siltstone, sandstone and claystone	Miocene	Permam	136/0	223/34
A3	36°21'29.41"N	44°11'38.31"E	Pila Spi	well bedded limestone	Mid-Upper Eocene	Permam	136/0	225/13
A4	36°18'44.90"N	44°20'4.64"E	Shiranish	Upper: blue pelagic marls; Lower: thin-bedded marly limestone	Upper Cretaceous	Permam	136/0	188/16
A5	36°21'4.26"N	44°17'54.96"E	Pila Spi	well bedded limestone	Mid-Upper Eocene	Permam	136/0	053/19
A6	36°27'31.93"N	44°10'42.47"E	Fars	siltstone, sandstone and claystone	Miocene	Safeen	310/5	244/34
A7	36°22'23.32"N	44°18'10.67"E	Shiranish	Upper: blue pelagic marls; Lower: thin-bedded marly limestone	Upper Cretaceous	Safeen	310/5	232/49
A8	36°23'51.79"N	44°16'38.52"E	Tanjero	conglomerate, siltstone beds, claystone	Upper Cretaceous	Safeen	310/5	227/36
A9	36°25'15.05"N	44°16'15.03"E	Shiranish	Upper: blue pelagic marls; Lower: thin-bedded marly limestone	Upper Cretaceous	Safeen	310/5	233/24
A10	36°26'53.51"N	44°15'21.12"E	Shiranish	Upper: blue pelagic marl with thin limestone beds	Upper Cretaceous	Safeen	310/5	242/30
A11	36°24'43.80"N	44°18'40.65"E	Shiranish	Lower: thin-bedded marly limestone	Upper Cretaceous	Safeen	310/5	277/11
A12	36°19'12.82"N	44°29'38.38"E	Tanjero	conglomerate, siltstone beds, claystone	Upper Cretaceous	Safeen	310/5	035/27
B1	36°10'53.83"N	44°23'42.09"E	Pila Spi	well bedded limestone	Mid-Upper Eocene	Bana Bawi	132/4	241/15
B2	36°15'37.37"N	44°23'22.66"E	Shiranish	Upper: blue pelagic marls; Lower: thin-bedded marly limestone	Upper Cretaceous	Bana Bawi	132/4	230/16
B3	36°11'20.16"N	44°28'51.25"E	Aqra-Bekhme	massive dolomitized limestone, locally bitumen impregnated	Upper Cretaceous	Bana Bawi	132/4	36/02
B4	36°13'50.16"N	44°26'47.26"E	Shiranish	Lower: thin-bedded marly limestone	Upper Cretaceous	Bana Bawi	132/4	056/21
B5	36°17'30.70"N	44°23'52.36"E	Tanjero	conglomerate, siltstone beds, claystone	Upper Cretaceous	Safeen	310/5	229/51
B6	36°20'37.56"N	44°22'12.61"E	Aqra-Bekhme	massive dolomitized limestone, locally bitumen impregnated	Upper Cretaceous	Safeen	310/5	277/11
B7	36°18'35.46"N	44°26'22.71"E	Shiranish	Upper: blue pelagic marls; Lower: thin-bedded marly limestone	Upper Cretaceous	Safeen	310/5	038/30
B8	36°17'14.48"N	44°31'31.05"E	Shiranish	Upper: blue pelagic marls; Lower: thin-bedded marly limestone	Upper Cretaceous	Kamosk	138/1	227/51
B9	36°18'19.91"N	44°30'48.72"E	Shiranish	Upper: blue pelagic marls; Lower: thin-bedded marly limestone	Upper Cretaceous	Kamosk	138/1	181/03
B10	36°15'27.37"N	44°37'3.86"E	Qamchuqa	massive limestone, partly dolomitic	Lower Cretaceous	Pelewani	122/1	211/41
B11	36°17'20.35"N	44°39'6.49"E	Sarmord	bedded limestone	Lower Cretaceous	Pelewani	122/1	026/22
B12	36°17'6.65"N	44°40'30.33"E	Aqra-Bekhme	massive dolomitized limestone, locally bitumen impregnated	Upper Cretaceous	Pelewani	122/1	040/23
C1	36°24'49.29"N	44°21'9.95"E	Fars	siltstone, sandstone and claystone	Miocene	Safeen	310/5	035/30
C2	36°20'22.05"N	44°26'14.05"E	Pila Spi	well bedded limestone	Mid-Upper Eocene	Bana Bawi	132/4	238/13
C3	36°24'45.05"N	44°19'32.54"E	Gercus	red claystone, siltstone with limestone beds	Upper Eocene	Safeen	310/5	035/52
C4	36°26'18.60"N	44°22'35.57"E	Kolosh	black claystone and shale, conglomerate, thin limestone beds	Paleocene	Mirawa	288/7	224/52
C5	36°30'30.49"N	44°10'30.43"E	Tanjero	conglomerate, siltstone beds, claystone	Upper Cretaceous	Safeen	310/5	244/34
C6	36°18'10.36"N	44°20'23.61"E	Shiranish	Upper: blue pelagic marls	Upper Cretaceous	Bana Bawi	132/4	242/27
C7	36°25'4.97"N	44°15'51.43"E	Shiranish	Lower: thin-bedded marly limestone	Upper Cretaceous	Safeen	310/5	269/13
C8	36°17'26.33"N	44°22'33.27"E	Qamchuqa	massive limestone, partly dolomitic	Lower Cretaceous	Bana Bawi	132/4	234/12
C9	36°41'18.48"N	44°16'23.12"E	Sarmord	bedded limestone	Lower Cretaceous	Peris	296/1	010/33
C10	36°40'26.41"N	44°15'2.37"E	Pila Spi	well bedded limestone	Mid-Upper Eocene	Peris	296/1	202/83

Table 1: Outcrops with analysed fracture systems showing only mean values, presented in this study with coordinates, short description of lithologies, formation names and ages. The fracture systems are explained in the section 3.1, only the structural interpretation of DX remains open. The numbers correspond to the numbering of outcrops in the cross-sections (A, B) or other outcrops and figures (C). Some data from Peris Anticline, situated N of the studied area was taken in account to support the proposed deformation model (outcrops C9, C10). Explanations: **conj.** = conjugated fracture systems; **sinistr.** = sinistral; **react. (D)** = reactivation of older fracture system; **OF** = open fracture; **NF** = normal faulting, **TF** = thrust faulting (continued on the next page).

No.	Latitude	Longitude	Calculated mean values of fracture systems in the different outcrops:						
			D1	D2	D3a	D3b	D4	D5	DX
A1	36°21'13.56"N	44°11'8.64"E	X	X	078/54	X	X	X	X
A2	36°21'15.43"N	44°11'21.97"E	348/69	X	063/61	X	X	X	X
A3	36°21'29.41"N	44°11'38.31"E	337/84	X	077/84	X	X	X	X
A4	36°18'44.90"N	44°20'4.64"E	337/83	X	251/88	X	X	X	X
A5	36°21'4.26"N	44°17'54.96"E	151/85	038/59	232/78	X	X	X	X
A6	36°27'31.93"N	44°10'42.47"E	130/78	X	033/78	X	X	X	X
A7	36°22'23.32"N	44°18'10.67"E	148/88	X	050/48	X	X	X	X
A8	36°23'51.79"N	44°16'38.52"E	X	X	040/67 ; 025/51	X	088/68	X	X
A9	36°25'15.05"N	44°16'15.03"E	169/83	X	X	X	X	X	X
A10	36°26'53.51"N	44°15'21.12"E	NF: 164/34, 355/46	X	039/66	X	X	X	X
A11	36°24'43.80"N	44°18'40.65"E	X	X	068/72	X	095/80	X	188/88
A12	36°19'12.82"N	44°29'38.38"E	321/85	X	193/63	X	X	X	006/88
B1	36°10'53.83"N	44°23'42.09"E	117/85	X	23/79	X	X	react. (D1) 117/85 sinistr. shear	X
B2	36°15'37.37"N	44°23'22.66"E	125/82	X	60/78; conj. 250/83	X	X	X	X
B3	36°11'20.16"N	44°28'51.25"E	312/88	X	218/85	X	X	X	X
B4	36°13'50.16"N	44°26'47.26"E	148/87	040/62	229/80	X	X	X	X
B5	36°17'30.70"N	44°23'52.36"E	151/91	X	048/52	X	X	X	X
B6	36°20'37.56"N	44°22'12.61"E	X	X	X	X	080/75	X	188/86
B7	36°18'35.46"N	44°26'22.71"E	317/82	X	189/59	X	X	X	009/87
B8	36°17'14.48"N	44°31'31.05"E	129/86; OF: 127/66	011/53	063/50	X	X	X	X
B9	36°18'19.91"N	44°30'48.72"E	125/74	025/53	056/45	X	87/46	X	X
B10	36°15'27.37"N	44°37'3.86"E	NF: 339/30	X	044/65	X	108/63	X	X
B11	36°17'20.35"N	44°39'6.49"E	X	X	X	019/52	X	X	X
B12	36°17'6.65"N	44°40'30.33"E	119/84	X	256/62	X	X	X	184/67
C1	36°24'49.29"N	44°21'9.95"E	150/70	X	195/80	X	X	X	X
C2	36°20'22.05"N	44°26'14.05"E	121/83	X	26/77	X	react. NF: 121/83	X	X
C3	36°24'45.05"N	44°19'32.54"E	134/76	X	X	X	X	X	X
C4	36°26'18.60"N	44°22'35.57"E	122/82	39/58	X	X	X	X	X
C5	36°30'30.49"N	44°10'30.43"E	130/78	X	033/72	X	X	X	X
C6	36°18'10.36"N	44°20'23.61"E	NF: 151/25, 331/37	X	X	X	X	X	X
C7	36°25'4.97"N	44°15'51.43"E	149/66	X	072/74	X	X	X	181/76
C8	36°17'26.33"N	44°22'33.27"E	X	X	X	TF: 044/34	X	X	X
C9	36°41'18.48"N	44°16'23.12"E	X	X	X	TF: 23/54	X	X	X
C10	36°40'26.41"N	44°15'2.37"E	X	TF: 029/70; 206/55	X	X	X	268/82 sinistr. shear	X

Table 1: (continued)

In this work we have presented the results of the field work as well as remote sensing studies of the investigated area with special focus on the deformation patterns and their relationship to the evolution of the hosting structures. The deformation patterns observed can be chronologically and kinematically divided into five structural assemblages supported by surface outcrop data. The outcrop studies of the faults are further supported by the digitized and evaluated data from the available regional geological map and remote sensing studies (Figures 4 and 5B). The remote sensing study and consequent field mapping of the study area proved that the most fault structures have minimal visible horizontal offset, showing no significant displacement along the NW-SE as well as along the E-W trending faults (Figure 4). The above defined five structural assemblages and their characteristics are shortly summarized, starting from the oldest to the youngest:

The earliest is a penetrative (observed in 76% of the outcrops) sub-vertical fracture set, mainly (E)NE-striking tension gashes and NW- and SE-dipping normal faults implying NW-SE extension direction (D1). It is best developed in the limestone and dolomite (e.g. the Eocene Pila Spi Formation and the Upper Cretaceous Shiranish Formation), sandstone of the Tanjero Formation but also in the less competent lithologies like shale, marl or claystone (e.g. the Paleocene Kolosh Formation).

The deformation (D2) is characterized by roughly NE-SW directed thrusting, associated with the pre- or early-folding compressive regime. The direction slightly

changes to the W, where the N-S directed shortening (Taurus) trend becomes more significant. This includes conjugated small-scale thrust-fault groups dipping under similar angle relative to the folded (now sub-vertical) sedimentary bedding and thus predating the folding. The back-rotation of the structures to horizontal bedding position reveals that these thrusts are directed in similar shortening direction as the later folding. This is also supported by findings of NW-striking sub-vertical stylolites and NNW-directed thrust faults on the forelimb of the Bana Bawi Anticline.

Another distinct fracture set (D3) is connected with the large-scale folding event. It is oriented normal to the sedimentary bedding and striking NW-SE, parallel to the major trend of the fold axes. It can be divided in the fold tangential extension in the upper layers of the folded sedimentary succession (D3a) and in the fold tangential shortening (D3b) in the lower units, especially in the cores of the anticlines. Accordingly, deformation D3a consists of extensional mode I fractures, tension gashes and normal faults. To the contrary the D3b consists of minor fold-and-thrust structures that solve the place problems in the cores of the folds.

Deformation (D4) comprises E-W extension direction and is characterized by N-S striking mode I joints and reactivation of older normal faults, originally connected with the deformations D1 and D3a.

The last defined deformation (D5) is connected with the recent N to NE directed strike-slip shortening and includes fractures, which have a mainly NE to N trending orientation (D1) and are commonly reactivated as sinistral strike-slip faults. Also reactivation by dextral slip of the NNW-striking fractures (D2) was observed. This probably reflects the dextral shear of the Zagros fold-belt under N-S compression induced by the northward movement of the Arabian plate relative to the Eurasian Plate. Comparing the inferred palaeostrain directions with kinematics of recent GPS measurements (Figure 1B), we conclude that the N-S compression and the partitioning into NW-SE trending folds and NW to N trending strike-slip faults likely remained unchanged throughout the Neogene tectonic history of the Zagros Simply Folded Belt in Iraq.

## **Acknowledgments**

The company OMV Exploration and Production is thanked for supporting this study, for providing additional data and numerous ideas and suggestions, which helped to improve this article. Further D.R. wishes to thank Kateřina Schöpfer for providing writing assistance and proof-reading the article. Bernhard Bretis and Nikolaus Bartl are thanked for the help during the first field trip in 2008.

## **References**

Alavi, M., 2004. Regional stratigraphy of the Zagros fold-thrust belt of Iran and its proforeland evolution. *American Journal of Science*, 304(1), 1-20.

Bahroudi, A. and Koyi, H. A., 2003. Effect of spatial distribution of Hormuz salt on deformation style in the Zagros fold and thrust belt; an analogue modelling approach. *Journal of the Geological Society of London*, 160(5), 719-733.

Berberian, M., 1995. Master "blind" thrust faults hidden under the Zagros folds: Active tectonics and surface morphotectonics. *Tectonophysics*, 241, 193-224.

Csontos, L., Sasvári, Á., Pocsai, T. and László, K., 2011. Structural evolution of the north-western Zagros, Kurdistan Region, Iraq and alternative models for formation of a curved mountain chain, 73rd EAGE Conference & Exhibition, Vienna.

Earthquake Search, USGS/NIEC (PDE) database, 6.7.2011 (available online at <http://earthquake.usgs.gov/earthquakes/eqarchives/epic/>).

Frehner, M., 2011. The neutral lines in buckle folds. *Journal of Structural Geology* 33, 1501-1508. doi:10.1016/j.jsg.2011.07.005

Fürst, M. 1970. Stratigraphie und Werdegang der östlichen Zagrosketten (Iran). *Erlangen Geol. Abh.*, 80, 1-51.

Heidbach, O., Tingay, M., Barth, A., Reinecker, J., Kurfeß, D., and Müller, B. (2008). The 2008 release of the World Stress Map (available online at <http://www.world-stress-map.org>).

Homke, S., Vergés, J., Garcés, M., Emami, H. and Karpuz, R., 2004. Magnetostratigraphy of Miocene-Pliocene Zagros foreland deposits in the front of the Push-e Kush Arc (Lurestan Province, Iran). *Earth and Planetary Science Letters*, 225(3-4), 397-410.

Hooper, R. J., Baron, I. R., Agah, S. and Hatcher, R. D., 1995. The Cenomanian to Recent development of the southern Tethyan margin in Iran. In: M.I. Al-Husseini (Editor), *Middle East petroleum geosciences*. Gulf Petrolink, Bahrain, 505-516.

Jassim, S. Z. and Goff, J. C., 2006. *Geology of Iraq*. Dolin, Brno, Czech Republic, 352 pp.

Kent, P. E., Slinger, F. C. P. and Thomas, A. N., 1951. Stratigraphical exploration surveys in SW Persia. 3rd World Petroleum Congress, Proc., Section 1, 141-161.

Lacombe O., Bellahsen N. and Mouthereau F., 2011. Fracture patterns in the Zagros Simply Folded Belt (Fars, Iran): Constraints on early collisional tectonic history and role of basement faults. *Geological magazine*. doi: 10.1017/S001675681100029X.

McQuarrie, N., 2004. Crustal scale geometry of the Zagros fold-thrust belt, Iran. *Journal of Structural Geology*, 26(3), 519-535.

McQuillan, H., 1973. Small-scale fracture density in Asmari Formation of SW Iran and its relation to bed thickness and structural setting. *American Association of Petroleum Geologists Bulletin*, 57, 2367-2385.



- Mouthereau, F., Lacombe, O. and Meyer, B., 2007. Tertiary sequence of deformation in a thin-skinned/thick-skinned collision belt: The Zagros Folded Belt (Fars, Iran). *Tectonics*, 26(TC5006): 28.
- Nehling, P., Asfirane, F., Genna, A., Guerrot, C., Nicol, N., Salpeteur, I., Shanti, M. and Thiblemont, D., 2002. Aeromagnetic map constrains cratonization of the Arabian Shield. *Terra Nova*, 13, 347-353.
- Numan, N. M. S., Hammoudi, R.A. and Chorowicz, J., 1998. Synsedimentary tectonics in the Eocene Pila Spi limestone formation in Iraq and its geodynamic implications. *Journal of African Earth Sciences*, 27(1), 141-148.
- Ramsay, J. G., 1967. *Folding and fracturing of rocks*. McGraw-Hill Book Company, New York, 07-051170-5.
- Reif, D., Grasemann, B., Faber, R., 2011. Quantitative structural analysis using remote sensing data: Kurdistan, Northeast Iraq. *AAPG Bulletin* 95, 941-956.
- Sissakian, V. K., Ibrahim, E. I. and Al-Waily, I. J., 1997. Geological Map of Arbeel and Mahabad Quadrangles Sheets Nj-38-14 and Nj-38-15. In: V.K. Sissakian (Editor). State Establishment of Geological Survey and Mining, Baghdad.
- Stephenson, B. J, Koopman, A., Hillgartner, H., McQuillan, H., Bourne, S., Noad, J. J. and Rawnsley, K., 2007 Structural and stratigraphic controls on fold-related fracturing in the Zagros Mountains, Iran; implications for reservoir development (in Fractured reservoirs) *Geological Society Special Publications*, 270, 1-21.
- Talbot, C.J. and Alavi, M., 1996. The past of a future syntaxis across the Zagros. *Geological Society, London, Special Publications*, 100(1), 89-109.
- Tavani, S., Storti, F., Soleimany, B., Fallah, M., Muñoz, J. A. and Gambini, R., 2011. Geometry, kinematics and fracture pattern of the Bangestan Anticline, Zagros, SW Iran. *Geol. Mag.* 148 (5-6), 964-979. doi: 10.1017/S0016756811000197
- Walpersdorf, A., Hatzfeld, D., Nankoli, H., Tavakoli, F., Nilforoushan, F., Tatar, M., Vernant, P, Chery, J and Masson, F., 2006. Difference in the GPS deformation pattern of North and Central Zagros (Iran), *Geophy. J. Int.*, 167(3), 1077-1088.
- Yamato, P., Kaus, B. J. P., Mouthereau, F. and Castelltort, S., 2011. Dynamic constraints on the crustal-scale rheology of the Zagros fold belt, Iran. *Geology (Boulder)*, 39(9), 815-818.

## Curriculum Vitae

### Personal details

---

Name: Daniel Reif  
Date of birth: 26.6.1982  
Place of birth: Olomouc, Czech Republic  
Nationality: Czech  
Address: Technikerstrasse 2/3, A-2340 Mödling, Lower Austria  
Mobile: 0043 664 9168652  
E-mail: d.reif82@gmail.com

### Education

---

Since 2008 Doctoral degree Studies (Ph.D.): Structural geology. University of Vienna, Austria. Dissertation: Quantitative structural modelling of the Zagros fold and thrust belt in NE Iraq  
2003-2008 Diploma Studies (M. Sc.): Hydrogeology, Tectonics. University of Vienna, Austria. Diploma thesis: Hydrogeology of the Danube Basin between Bratislava and Dunajská Streda (Slovakia)  
2002-2000 Diploma Studies (M. Sc.): Hydrogeology, Tectonics. Masaryk University, Brno, Czech Republic  
2000 Language state exam – German language on State Language Institute, Olomouc, Czech Republic  
1991-2000 Tschajkovskij Gymnasium, Olomouc, Czech Republic

### Languages

---

Czech (native speaker), Slovakian (fluent), German (fluent), English (fluent), Russian (basic), Polish (basic), Spanish (beginner).

Absolved courses

---

- |      |  |
|------|--|
| 2009 | LithoTect training course – Balanced cross-sections with use of seismic and other data |
| 2008 | SeisWorks training course – Seismic interpretation, University of Vienna, Austria      |

Projects & Jobs

---

- |           |   |
|-----------|---|
| 2008-2011 | Quantitative structural modelling of the Zagros fold-and-thrust belt (Iraq). University of Vienna, Austria. Sponsored by OMV E&P, Austria ( <a href="http://www.omv.com">http://www.omv.com</a> ) |
| 2007-2008 | Geologist – Technical geology Niederbacher, Klosterneuburg ( <a href="http://www.geol.at/">http://www.geol.at/</a> )  |
| 2007      | OMV Exploration & Production: Training with focus on structural geology of Iraq ( <a href="http://www.omv.com">http://www.omv.com</a> )   |
| 2006      | Hydrogeologist - Sri Lanka (Ceylon), Geotest Brno, Czech Republic ( <a href="http://www.geotest.cz">http://www.geotest.cz</a> )   |
| 2004-2005 | Geologist - PORR Technobau und Umwelt, Pollution monitoring, Geological description of borehole cores ( <a href="http://www.porr.at">http://www.porr.at</a> )                                     |
| 2002      | Geologist - Field mapping– Map sheet: Hlinsko (1: 5000), Czech geological survey, Brno ( <a href="http://www.geology.cz">http://www.geology.cz</a> )  |
| 2001      | Digitizing of hydrogeological maps, IT department, Geotest Brno, Czech Republic ( <a href="http://www.geotest.cz">http://www.geotest.cz</a> )   |

Teaching

---

- |      |  |
|------|--|
| 2011 | Short course on use of ArcGIS and remote sensing data in geology Palacky University, Olomouc, Czech Republic |
| 2009 | Use of GIS in geology and hydrogeology for Kurdish Ministry of Water Resources, GEOTEST Brno, Czech Republic |

### Selected publications

---

**Reif, D.**, Decker, K., Grasemann, B. & Peresson, H. (under review). Fracture patterns in the Zagros fold-and-thrust belt, Kurdistan Region of Iraq. Tectonophysics Special Issue: „Into the deformation history of folded rocks“.

**Reif, D.**, Frehner, M., Grasemann, B. (under review). Mechanical versus kinematical shortening reconstructions of the Zagros High Folded Zone (Kurdistan Region of Iraq), Tectonics Journal.

**Reif, D.**, Grasemann, B. & Faber, R. H. (2011). Quantitative structural analysis using remote sensing data Kurdistan, Northeast Iraq. AAPG Journal, v. 95; no. 6; p. 941-956; DOI: 10.1306/11151010112.

### Published Abstracts and Presentations

---

**Reif, D.**, Grasemann, B. & Faber, R. H. (2011). Quantitative structural analysis using remote sensing data (Kurdistan, NE Iraq). Geophysical Research Abstracts, Vol. 13, EAGE2011-Workshop 13.

**Reif, D.**, Decker, K., Grasemann, B. & Peresson, H. (2011). Fracture patterns and generations in the simply folded part of the Zagros fold-and-thrust belt, N Iraq. Geophysical Research Abstracts, Vol. 13, EGU2011-7996.

**Reif, D.**, Grasemann, B. & Duncan Lockhart, D.A. (2010). Balancing cross-sections combining field work and remote sensing data using LithoTect software in the Zagros fold-and-thrust belt, N Iraq. Geophysical Research Abstracts, Vol. 12, EGU2010-3497.

Frehner, M., **Reif, D.** & Grasemann, B. (2010). Mechanical restoration of large-scale folded multilayers using the finite element method: Application to the Zagros Simply Folded Belt, N-Iraq. Geophysical Research Abstracts, Vol. 12, EGU2010-0.

**Reif, D.**, Grasemann, B., Faber, R. & Lockhart, D.A. (2009). Structural modelling of the Zagros fold-and-thrust belt (Iraq) combining field work and remote sensing techniques. Geophysical Research Abstracts, Vol. 11, EGU2009-7528.

**Reif, D.**, Häusler, H. & Faber, R. (2008). Hydrogeology of the Danube Basin between Bratislava and Dunajská Streda (Slovakia). , Hydrogeology (Conv. S. Birk & T. Hofmann), 20.-22. September, PANGEO Austria 2008.